Magnetization Dynamics in Hybrid Nanostructures

PROEFSCHRIFT

TER VERKRIJGING VAN DE GRAAD VAN DOCTOR
AAN DE TECHNISCHE UNIVERSITEIT DELFT,
OP GEZAG VAN DE RECTOR MAGNIFICUS
PROF. DR. IR. J. T. FOKKEMA,
VOORZITTER VAN HET COLLEGE VOOR PROMOTIES,
IN HET OPENBAAR TE VERDEDIGEN OP
WOENSDAG 22 OKTOBER 2008 OM 10.00 UUR

DOOR

Xuhui WANG
Master of Science in Physics

GEBOREN TE CHONGQING, CHINA

Dit proefschrift is goedgekeurd door de promotor:
Prof.dr.ir. G. E. W. Bauer

Samenstelling van de promotiecommissie:

Rector Magnificus,	voorzitter
Prof.dr.ir. G. E. W. Bauer	Technische Universiteit Delft, promotor
Prof.dr. T. Klapwijk,	Technische Universiteit Delft
Prof.dr. B. Koopmans,	Technische Universiteit Eindhoven
Prof.dr. S. Maekawa,	Tohoku University, Japan
Prof.dr. Y. V. Nazarov,	Technische Universiteit Delft
Prof.dr.ir. B. J. van Wees,	Rijksuniversiteit Groningen
Dr. R. A. Duine,	Utrecht Universiteit

Het onderzoek beschreven in dit proefschrift is financieel ondersteund door NanoNed.

Published by: Xuhui Wang

Casimir PhD series, Delft-Leiden 2008-06
ISBN/EAN: 978-90-8593-044-0

Cover illustration: Rutger Ockhorst (http://www.rutgerockhorst.com/)
Printed by: Sieca Repro B.V., Delft

Printed in the Netherlands

To my parents and Vera Chi Wang,
who spoil me with love.

Contents

Chapter 1

Introduction

1.1 Magnetism and electron transport

Since the discovery of the compass, as the earliest application of magnetism, by the Chinese nearly one thousand years ago [1], magnetism and magnetic materials have attracted much attention in basic and applied research. The ferromagnet, as a many-particle condensate of *angular momentum*, has a preferred direction, the orientation of the order parameter or magnetization direction [2, 3, 4]. In the presence of an external field (such as Earth's magnetic field) that is misaligned with the order parameter, the magnetization responds by minimizing its free energy, which leads to magnetization dynamics. Aided by fast developing modern nanotechnology, a ferromagnetic particle can be fabricated down to sizes at which the formation of multiple magnetic domains is energetically costly. A single domain nanoparticle can be modelled as a single macroscopic spin that describes the coherent collective precession of the magnetization.

The transport of electrons in various materials, particularly metals, has been studied for a long time as well. The electron, as an elementary particle, carries both a charge and an intrinsic angular momentum known as *spin*. Electric currents are generated by applying a voltage bias, or equivalently an electric field, over a piece of metal. Ohm's law says that the current (I) is proportional to the applied voltage (V) and inversely proportional to the resistance (R) between two measuring points, *i.e.*, $V = IR$. In the late 1980's, electron transport in a hetero-structure combining a ferromagnet (F) and an ordinary normal metal (N) was found to display a new effect called giant magneto-resistance (GMR) [5, 6], in which the magnetic configuration plays an important role in determining the resistance of the structure. It can be understood in terms of electrons of different spins, relative to the magnetization direction of the F metal, experiencing different resistances: the so-called two-channel resistor model. GMR quickly lead to innovations in data storage technologies, such as hard disk drives (HDD). Magnetic structures are usually disordered, meaning that the electrons experience many random scattering processes when passing through a device. The transport is therefore well-described by semi-classical diffusion equations [7].

1.2 Mean field theory of ferromagnetism

It is the interactions in a system that lead to the appearance of the magnetism. This section briefly describes a model of metallic ferromagnetism that serves as the basis for the development of the rest of this thesis, based on a mean field theory or Hartree-Fock approximation. The simplest picture of the *free* electron gas is said to be free, but in fact the Coulomb interaction correlates the electrons and generates new phases. The competition between the Pauli exclusion principle and the Coulomb interaction leads to the metallic ferromagnetism as desired here [8]. In many-body systems, the interactions between particles are so complicated that it is impossible to calculate every wave function associated with each particle using Schödinger's equation. In some cases, for one particle, the influence from others due to interaction can be averaged out giving rise to the so-called *mean field*, which is carefully selected in combination with symmetry considerations in order to minimize the free energy. Consequently a many-body Hamiltonian is reduced to a new effective single particle Hamiltonian, where certain operators generate non-zero expectation values with respect to the new ground-state. These operators are called order parameters [8].

The metallic ferromagnet studied in this thesis can be described by a Hamiltonian including an electron gas (free electrons) and a Coulomb repulsive interaction:

$$\mathcal{H} = \int d^3\mathbf{r} \left[\sum_\sigma \phi_\sigma^\dagger(\mathbf{r}) \left(-\frac{\hbar^2 \nabla^2}{2m} - \mu \right) \phi_\sigma(\mathbf{r}) + U \phi_\uparrow^\dagger(\mathbf{r}) \phi_\downarrow^\dagger(\mathbf{r}) \phi_\downarrow(\mathbf{r}) \phi_\uparrow(\mathbf{r}) \right], \qquad (1.1)$$

where $\phi_\sigma^\dagger$ (ϕ_σ) is the creation (annihilation) operator for an electron of spin σ. The chemical potential is introduced as μ. The first part in the Hamiltonian is the kinetic energy of the free electron gas. The second term, *i.e.* the Coulomb interaction, is chosen to be δ-function like [8]. Introducing a spinor field operator and its hermitian conjugate as

$$\phi(\mathbf{r}) = \begin{pmatrix} \phi_\uparrow(\mathbf{r}) \\ \phi_\downarrow(\mathbf{r}) \end{pmatrix}, \text{ and } \phi^\dagger(\mathbf{r}) = \left(\phi_\uparrow^\dagger(\mathbf{r}), \phi_\downarrow^\dagger(\mathbf{r})\right), \tag{1.2}$$

the interaction term can be divided into two parts [9, 10, 11]:

$$U\phi_\uparrow^\dagger(\mathbf{r})\phi_\downarrow^\dagger(\mathbf{r})\phi_\downarrow(\mathbf{r})\phi_\uparrow(\mathbf{r}) = \frac{U}{4}\left[\phi^\dagger(\mathbf{r})\phi(\mathbf{r})\right]^2 - \frac{U}{4}\left[\phi^\dagger(\mathbf{r})\boldsymbol{\sigma}\cdot\mathbf{m}\phi(\mathbf{r})\right]^2, \tag{1.3}$$

where $\boldsymbol{\sigma}$ is the Pauli matrices and the unit vector $\mathbf{m}$ describes the orientation of the magnetization. At this stage, in order to decouple the interaction Eq. 1.3, we employ the so-called Hubbard-Stratonovich transformation to introduce two dynamic fields. These are the charge density field with mean value given by $\langle n(\mathbf{r})\rangle = \langle \phi^\dagger(\mathbf{r})\phi(\mathbf{r})\rangle$, which can be absorbed into the definition of chemical potential [10], and the spin density field with mean value given by $\langle M(\mathbf{r})\mathbf{m}\rangle = \frac{U}{2}\langle \phi^\dagger(\mathbf{r})\boldsymbol{\sigma}\phi(\mathbf{r})\rangle$. This semi-classical spin density field serves the function of *order parameter*, as discussed in the beginning of this section. The appearance of non-vanishing expectation values of such order parameters is a signal that the system experiences a phase transition and therefore develops a new ground state [8]. In the current case, the new ground state is spin polarized. The magnitude of the magnetization is determined by the saddle point approximation. It is beyond the scope of this thesis to discuss the derivation of the exact values, which can be found in various references [8, 11]. In the saddle point approximation, the magnitude of the exchange interaction is given by [8, 11]:

$$M = U\int \frac{d^3\mathbf{k}}{(2\pi)^3}\left[f\left(\epsilon_\mathbf{k} - \mu - \frac{M}{2}\right) - f\left(\epsilon_\mathbf{k} - \mu + \frac{M}{2}\right)\right], \tag{1.4}$$

where $f(\epsilon)$ is the Fermi distribution function. The introduction of the spin density field yields the Stoner mean-field model for metallic ferromagnetism, which is described by an effective Hamiltonian as:

$$\mathcal{H}_{eff} = \int d^3\mathbf{r}\left[\sum_\sigma \phi_\sigma^\dagger(\mathbf{r})\left(-\frac{\hbar^2\nabla^2}{2m} - \mu\right)\phi_\sigma(\mathbf{r}) + \frac{M}{2}\sum_{\sigma\sigma'}\phi_\sigma^\dagger(\mathbf{r})\left(\mathbf{m}\cdot\boldsymbol{\sigma}\right)_{\sigma\sigma'}\phi_\sigma(\mathbf{r})\right]. \tag{1.5}$$

The mean field appears in the system as an exchange field felt by the conducting electrons. Hamiltonian Eq.1.5 is usually referred to as the well-known Stoner model, often serving as the starting point of the discussion on interaction between conducting electrons and the ferromagnet. The magnitude of the exchange interaction is proportional to the magnetization, which is usually constant at saturation magnetization (M_s). The above mean field theory does not provide information about the direction of the magnetization, since the exchange interaction exhibits rotational invariance. The direction of the magnetization is determined by various factors such as relativistic interaction (spin-orbit interactions) and external magnetic fields. The dynamics of the magnetization is likewise a large field which has beeb intensively studied for a long period. A brief discussion of dynamics is the content of the following section.

1.3 Magnetization dynamics and the Landau-Lifshitz-Gilbert equation

Suppose that a quantum spin $\hat{\mathbf{S}}$ of a particle, *e.g.* a spin-$\frac{1}{2}$ particle $\hat{\mathbf{S}} = \hbar\hat{\boldsymbol{\sigma}}/2$ (with Pauli matrix $\hat{\boldsymbol{\sigma}}$), is immersed in a magnetic field $\mathbf{B}$ and disregard the interaction of the orbital degrees of freedom with the magnetic field. Then the non-dissipative dynamics of the spin operator are governed by the Heisenberg equation of motion, determined by the Hamiltonian $\hat{H} = \mu_B\hat{\boldsymbol{\sigma}} \cdot \mathbf{B}$ (with μ_B the Bohr magneton) [12]:

$$i\hbar\frac{d\hat{\mathbf{S}}}{dt} = \left[\hat{\mathbf{S}}, \hat{H}\right] = 2i\mu_B\mathbf{B} \times \hat{\mathbf{S}}. \tag{1.6}$$

If the left-hand side of Eq. (1.6) is viewed as the rate of change of an *angular momentum*, then the right hand side can be regarded as a *torque*. The magnetic moment ($\mathbf{M}$) of an electron is proportional to its spin by a gyromagnetic ratio $\gamma < 0$, *i.e.* $\mathbf{M} = \gamma\mathbf{S}$. Therefore the equation of motion, *i.e.* Eq. (1.6), also governs the dynamics of magnetic moments of a magnetic sample. Moreover, classical objects (such as the magnetization as derived in Sec. 1.2) can also be described using Eq. (1.6) by replacing the operators with their expectation values [14].

Consider here the case that the magnetism originating from the exchange interaction, as results from the symmetry of the wave function and the electrostatic interaction of electrons, is independent of the direction of total spins. In a magnetic body at equilibrium, the *magnetization* $\mathbf{M}$, defined as the magnetic moment density, is fixed by the exchange interaction. Therefore at temperatures far below the Curie temperature, the magnitude of magnetization can be regarded as constant and is called the saturation magnetization M_s. When only the low energy excitations of the ferromagnet are concerned, the wavelength of spin waves is large compared to the size of the magnetic body (as achieved by the *status quo* fabrication techniques), and the slow motion of the magnetization can be described by the *macrospin* model. [13]. In ferromagnetic materials the magnetic moments are in contact with the environment, interacting not only with the external field, but also with the lattice, other magnetic moments, phonons, and other types of excitations. These interactions give rise to an effective field as well as dissipation. To determine the equation of motion when the dissipation is absent, in thermal equilibrium, the change of free energy $F(\mathbf{M})$ responding to an infinitesimal variation of the magnetization, at constant temperature and volume V, is found to be [13]

$$\delta F = -\int dV \mathbf{H}_{eff} \cdot \mathbf{M}, \tag{1.7}$$

(where we have used the effective field H_{eff}), which leads to the equation of motion of a magnetic moment:

$$\frac{d\mathbf{M}}{dt} = \gamma \mathbf{M} \times \mathbf{H}_{eff}. \tag{1.8}$$

In a ferromagnetic body, there also exists, in addition to the exchange interaction, the interactions of relativistic origin. These are described macroscopically as the *anisotropy energy*, which depends on the orientation of the magnetization directions [13, 4]. This anisotropy also gives rise to the effective fields appearing in the equation of motion, contributing to the magnetization dynamics. Since the magnetic moments are coupled to the environment consisting of various microscopic processes, the energy transfer from the magnetic system to the environment introduces damping to the magnetic system and guides the system to a lower energy state. The microscopic processes conducting the energy transfer between the system and the environment are complicated, and therefore a phenomenological parameter(experimentally measurable) containing all the information about dissipation processes is more convenient to describe the dynamics than the microscopic subtleties [14]. This phenomenological description of the magnetization dynamics is governed by the well-known Landau-Lifshitz-Gilbert (LLG) equation:

$$\frac{d\mathbf{M}}{dt} = \gamma \mathbf{M} \times \mathbf{H}_{eff} - \frac{\alpha}{M_s} \mathbf{M} \times \frac{d\mathbf{M}}{dt} \tag{1.9}$$

where the last term (the so-called Gilbert term) captures the damping torque originating from all possible dissipation, and the coefficient α is called the Gilbert damping parameter. This dynamic equation of magnetization was first proposed by Landau and Lifshitz in a slightly different form [13]. In order to describe a large damping, Gilbert derived the damping torque using the Lagrangian with a Rayleigh dissipation functional [14]. When the damping parameter α is small, it can be shown that the two forms of the damping torque, *i.e.* the Landau-Lifshitz and the Gilbert form, are actually equivalent [14]. For an isolated ferromagnetic metal, the damping parameter is a sample property.

As the simplest example, consider a ferromagnetic particle in a static magnetic field pointing in the z-direction: upon perturbing the magnetization direction away from the z-direction, the damping torque drags the magnetization in the direction of the external field, *i.e.* the energy minimum. In experiments such as ferromagnetic resonance (FMR), where the magnetization is resonantly excited by microwaves (an *rf*-field) to precess around a static magnetic field, the parameter α is proportional to the line-width of measurement of the intensity of microwaves. Consequently FMR is one of the standard techniques to study the damping parameter of a ferromagnet [4].

The LLG phenomenology implies that the rate of the magnetization change is caused by the torques on the magnetization. These torques, not necessarily originating from the magnetic field, can also come from other mechanisms transferring angular momentum to the magnetization, such as the so called *spin-transfer torque* discussed in the next section [17, 18]. In the presence of conduction electrons, the angular momentum transfer between two spin systems gives rise to an extra torque that appears in the LLG equation. The interplay among the field induced torque, spin-transfer torque, and the damping torque induces intriguing magnetization dynamics. The absorption of angular momentum from conducting electron can reverse the magnetization direction once the damping torque is overcome. In addition to the intrinsic damping, the loss of angular momentum or energy to the conduction electrons introduces extra damping, such as through the *spin pumping* mechanism [34].

1.4 Spin injection and non-local detection in metals

The first step towards spin manipulation in metals is spin injection. In a seminal experiment, Johnson and Silsbee investigated spin injection into a normal metal by electric means [15]. As shown in Fig. 1.1, two ferromagnets are attached to a paramagnetic metal (normal metal). The injector is biased and the detector is connected to a voltage meter. Assuming that an electric current is driven into the normal metal

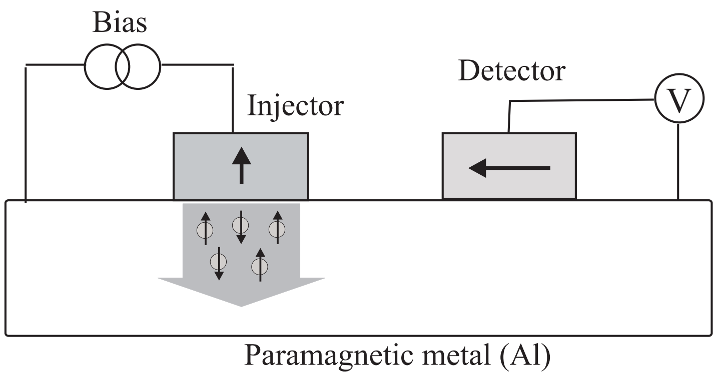

Figure 1.1: Schematic view of non-local electric spin injection and detection in metallic structures.

(Al) through the ferromagnet, at the ferromagnet-normal metal (F|N) interface, the density of states of electrons at Fermi energy is different for electrons in majority and minority spin bands. Therefore the current injected into the normal metal is spin polarized, *i.e.* there is an imbalance between the majority and minority-spin electrons, and the polarization is parallel to the magnetization direction of the injector [15]. The imbalance induced by a spin polarized current creates a non-equilibrium distribution with respect to different spins, which is usually referred to as *spin accumulation*. The spin-flip scattering in the normal metal, *e.g.* due to spin-orbit interaction or spin-dependent impurities, relaxes the spins and so diminishing the non-equilibrium spin accumulation. As long as the size of the normal metal in the transport direction is shorter than the spin flip length (l_{sf}), the spin accumulation does not, however, vanish. In this case, the spin transport can be entirely described by spin diffusion equation for the spin accumulation. The spin accumulation at the detector-normal metal interface drives spin current into the detector, and the detected voltage signal is proportional to the projection of the spin accumulation in N to the magnetization direction of the detector. Johnson and Silsbee initially proposed this method to measure the spin relaxation time in the normal metal [15], which can be well described in terms of spin diffusion equation as shown later by Jedema *et al.* in newly developed multi-terminal non-local measurements [27, 28].

1.5 Spin-transfer torque and structures

Slonczewski [17] and Berger [18] predicted the *spin transfer torques* mentioned earlier. Substantial experimental and theoretical effort has since been invested in confirming and quantifying the effect [19, 20, 21, 22, 23, 24, 25, 26]. The setup under investigation usually consists of two magnetic layers separated by a normal metal, *i.e.* a fixed layer with strong magnetization known as polarizer, and a free layer with a low coercivity field that allows relatively easy excitation of the magnetization (Fig. 1.2). In the original proposal by Slonczewski [17], the instantaneous magnetization

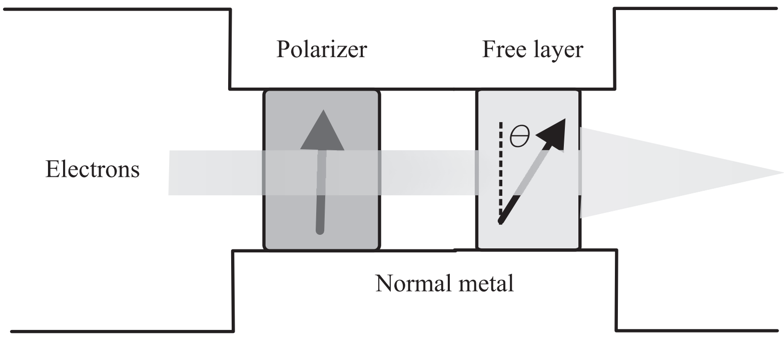

Figure 1.2: Schematic view of the multi-layer device employed to investigate the spin transfer torque, in so-called *pillar* structures. This type of device usually consists of a ferromagnetic layer with a large coercivity field serving as a *polarizer* (with magnetization $\mathbf{M}_1$), which is separated by a normal metal *spacer* from a *free layer* ferromagnet ($\mathbf{M}_2$) with lower coercivity. The two magnetization directions form an angle θ.

directions of two ferromagnets ($\mathbf{M}_1$ and $\mathbf{M}_2$) form an angle θ. If the length of the normal metal spacer at the transport direction is shorter than the spin diffusion length, the conducting electrons polarized along the magnetization direction of the fixed layer ($\mathbf{M}_1$) will be impinge on $\mathbf{M}_2$. The polarized electrons entering the free layer precess about $\mathbf{M_2}$ with a frequency governed by the exchange splitting. By consideration of angular momentum conservation, one sees that the free layer ($\mathbf{M}_2$) reacts to the conduction electrons by gaining angular momentum equal to the total inward spin flux penetrating $\mathbf{M}_2$ from both sides [17]. If the exchange interaction in $\mathbf{M}_2$ is large, it is possible for the transverse spin component of the conduction electrons to be completely absorbed by $\mathbf{M}_2$. The absorption of the transverse component by the free layer induces a torque that causes the magnetization dynamics, and the spin transfer torque is given by [17]:

$$\frac{d\mathbf{M}_2}{dt} = \frac{I}{e} g \mathbf{m}_2 \times (\mathbf{m}_1 \times \mathbf{m}_2)\,, \tag{1.10}$$

where $\mathbf{m}_{1(2)}$ is the magnetization direction of the polarizer (free layer). The coefficient g is a function of the polarization factor $P = (N_\uparrow - N_\downarrow)/(N_\uparrow + N_\downarrow)$ in terms of spin densities of majority (N_+) and minority (N_-) carriers,

$$g = \left[-4 + (1+P)^3 (3 + \mathbf{m}_1 \cdot \mathbf{m}_2)/4P^{3/2}\right]^{-1}. \tag{1.11}$$

The Landau-Lifshitz-Gilbert equation augmented by Eq. (1.10) can be used to investigate the magnetization dynamics. This model, for a single domain magnet with homogenous magnetization, is called a macro-spin model. Eq. (1.10) predicts that when $P < 1$, the spin transfer vanishes for parallel or anti-parallel magnetization configurations. The energy dissipation of this spin transfer torque mechanism scales favorably under miniaturization and is believed to be useful for the next generation of magnetic memory and storage technology.

The theoretical predictions of spin transfer torque [17, 18] were followed by significant amount of experimental studies. The experimental setups fall mainly into two categories: *pillar* structures [19, 20, 21, 22, 23, 24, 25, 26] and *lateral* structures [27, 28, 29, 30, 31, 32]. In the usual pillar structures, an electric current penetrates the magnetic layers, as schematically shown in Fig. 1.2. A typical experimental setup of pillar device is sketched in Fig. 1.3 [21]. There are two magnetic layers (such as the two Co layers in the figure), with the thicker one (Co2) acting as the polarizer and the thinner one (Co1) as the free layer. When the electrons flow from Co1 to Co2, at the interface of Co2, the reflected electrons are largely polarized antiparallel to the magnetization of Co2, since the electrons polarized parallel to Co2 can penetrate the polarizer. Consequently the reflected electrons induce a torque on the free-layer

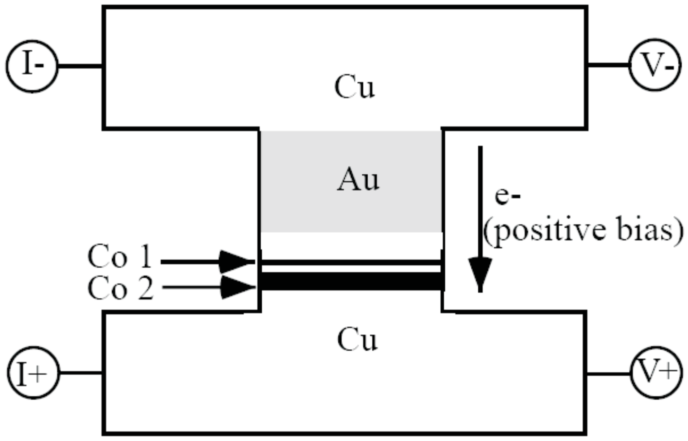

Figure 1.3: Schematic view of a pillar device with cobalt (Co) layers separated by a copper (Cu) spacer. This figure is from Ref. [21]. The *free layer* (Co1) is of thickness 25Åand the fixed layer or *polarizer* has thickness 100Å. The normal metal Cu in between two Co layer is of thickness 60Å.

which eventually switches the magnetization in Co1 to the direction antiparallel to Co2. When the transport direction of the electron flow is reversed, *i.e.* electrons flow from Co2 to Co1, the polarized current can switch the Co1 magnetization back to parallel to Co2. The signal of *switching* of magnetization is probed using the giant magneto-resistance (GMR) effect [5, 6] by measuring the *dc* resistance across the pillar. The parallel and antiparallel magnetization directions give rise to different *dc* resistances of the pillar structure: lower resistance corresponds to parallel magnetizations, while it is larger when they are antiparallel. In the experiments, an external magnetic field is applied in the plane of the magnetic films. The external field serves two purposes: to maintain the magnetization direction in the fixed layer (Co2) and to prevent the formation of domains in the magnetic films [21]. A qualitatively satisfactory explanation of the switching of free layer can be obtained by combining the Slonczewski formula for the spin-transfer torque and the Landau-Lifshitz-Gilbert equation, taking into account the anisotropy and external fields acting on the free layer.

The experiments on lateral structures do not invoke current penetrating the magnetic film but rather are *non-local* [15, 16, 27, 28, 29, 30, 31, 32]. Fig. 1.4 schematically shows a switching experiment performed on lateral structures by Kimura *et al.* [32]. The experimental setup consists two magnetic layers (permalloy films) both

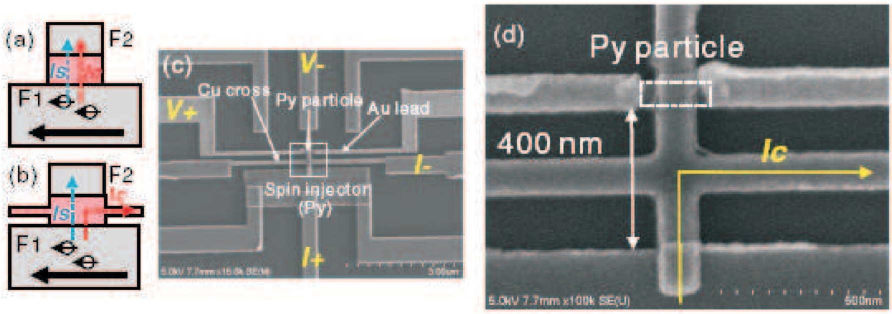

Figure 1.4: Schematic view of a lateral structure employed to investigate the spin-transfer torque effect. This figure is from Ref. [32].

deposited on the substrate, rather than on top of each other as in the pillar structures. When the electron current is applied across I_+ and I_- (as in panel (c)), the current is polarized by the spin injector (fixed layer) but there is no net charge current through the free layer. The polarized current induces spin accumulation in the central copper wire. The size of the copper wire is shorter than the spin diffusion length. As discussed in Sec. 1.4, the spin accumulation in turn drives a pure spin current that exerts a spin torque on the magnetization of the free Py layer. The experiments of Kimura *et al.* showed that the switching of the magnetization can be accomplished by the spin current alone. One of the advantages of the lateral structure is that the net charge current at the free layer-normal metal interface is zero. Since the free layer is not sandwiched by the other layers, the lateral structures also allow direct optical imaging of the magnetization dynamics, and the dipolar field generated by the dynamic magnetization can also be employed in other applications [33].

1.6 Landauer-Büttiker formalism and circuit theory

Electrons in metals do not move freely but experience scattering, *e.g.* by other electrons, impurities, phonons, or defects. The mean free path parameters indicate how far an electron can roam in the conductor [12]. When size of the conductors is much larger than the mean free path, the motion of electrons is predominantly diffuse, and the resistance is governed by the bulk scattering. In very small structures, however the resistance is determined mostly by reflections at interfaces. In that regime theoretical treatment should focus on what happens at the junctions between different materials. The well-known Landauer-Büttiker formalism systematically handles the

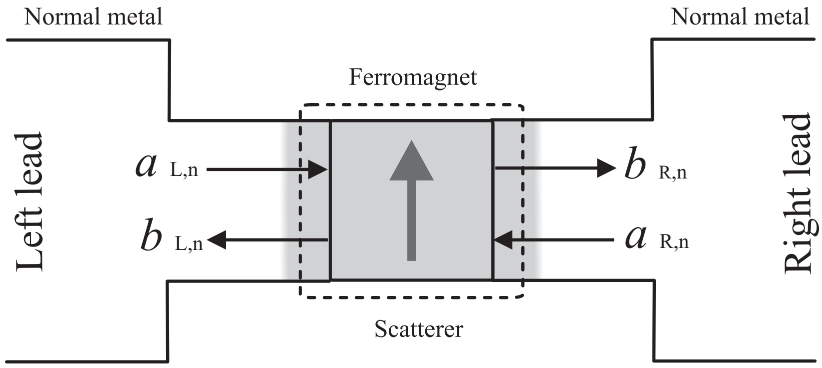

Figure 1.5: Scattering events at a ferromagnetic particle with normal metal contact. The operator $a_{L,n}$ annihilates an incident electron from the left lead(L), and $b_{L,n}$ annihilates an outgoing one in the left lead. The spin indices are suppressed for abbreviation.

electron transport in terms of the scattering processes associated with the traversal of electrons from a source contact through a sample into a drain contact. This formalism was originally proposed by Landauer on the basis of the insight that transport phenomena in solid state systems can be formulated as scattering problems [37]. Let us consider a mesoscopic scattering region in the center (not necessarily magnetic), which is connected to two reservoirs by metallic leads, as depicted in Fig. 1.5. The reservoirs are considered to be much larger than the scattering region. Transmission into, *e.g.* right reservoir from the right lead is hence reflectionless, meaning that such an electron entering the reservoir does not return on the time scale of the measurement. For each reservoir, the electrons are distributed according to the Fermi-Dirac distribution at given temperature (T) and electro-chemical potential (μ). The formalism is most straightforward when inelastic scattering processes in the conductor may be disregarded [38]. It is therefore usually assumed that the size of the scattering region is smaller than the energy relaxation length. From a quantum mechanically point of view, an electron wave incident on an interface splits into a reflected and the a transmitted contribution. At low temperature, the reflection and transmission probability amplitudes are determined by the (Fermi) energy of the incoming electron and the scattering potential, and are by definition elements of the scattering matrix [12]. The confinement potential of the leads quantizes the wave vectors perpendicular to the transport direction, giving rise to the conducting channels analogous to waveguides for classical waves [36, 38]. Generalization of the scattering approach to include spin degrees of freedom is an important ingredient in the magneto-electronic circuit theory, which is a powerful method to both qualitatively and quantitatively analyze spin and charge transport in a the ferromagnet-normal metal hybrid structure in the presence of arbitrary magnetizations [39, 40]. A detailed explanation of the method and its applications can be found in two recent comprehensive reviews [34, 35], but a brief sketch is given in the following.

Imagine a static ferromagnetic scatterer in contact with two normal metal *nodes* (or *leads*, denoted as L and R) connected to reservoirs, as sketched in Fig. 1.5. As explained above, the size of the scatterer is smaller than the energy relaxation length and the electrons originating from a given reservoir maintain their energy distribution while being scattered in the conductor. The confinement in the transverse direction defines the conducting channels described by an integer index n [38]. The total energy of the electrons can be further partitioned as $E = E_n + E_l$, where the condition that the 'longitudinal' energy $E_l > 0$ implies that only a finite number of quantum channels exist at a given energy. Away from the scattering region in the outgoing direction, channels at transverse energy E_n larger than energy E decay with vanishing amplitude. The creation and annihilation operators $\hat{a}^{\dagger}_{\alpha,n,\sigma}(E)$, $\hat{a}_{\alpha,n,\sigma}(E)$ can be introduced for an incoming electron with spin σ and *total* energy E in the transport channel n and coming from the reservoir $\alpha = L, R$. Similar notation is introduced for out-going electrons, $\hat{b}^{\dagger}_{\alpha,n,\sigma}(E)$ ($\hat{b}_{\alpha,n,\sigma}(E)$). The scattering states associated with the creation and annihilation operator in the normal metal are the eigenstates of the system (normal metal). Ref.[36] and Ref.[38] discuss spin degenerate systems in which the spin index can be omitted in favor of a factor two. For a magnetic scatterer it is essential to include the spin explicitly. It is convenient to chose the magnetization direction as the spin quantization (z)axis [39]. At an instant

t, the current operator in the leads $\alpha = L, R$ in spin space can be written as

$$I_{\alpha}^{\sigma\sigma'}(t) = \frac{e}{h}\sum_{n}\int dE\int dE' e^{i(E-E')t/\hbar}\left[\hat{a}_{\alpha,n,\sigma'}^{\dagger}(E)\hat{a}_{\alpha,n,\sigma}(E') - \hat{b}_{\alpha,n,\sigma'}^{\dagger}(E)\hat{b}_{\alpha,n,\sigma}(E')\right]. \tag{1.12}$$

The matrix current operator can be expanded into the charge current I_c and the three-component vector spin current $\mathbf{I}_s$, *i.e.* $\hat{I}_{\alpha} = (1/2)I_c - (e/\hbar)\boldsymbol{\sigma}\cdot\mathbf{I}_s$ [34, 39]. Disregarding inelastic scattering [34, 38, 39], the incoming and outgoing channels are related by the scattering matrix:

$$\hat{b}_{\alpha,n,\sigma}(E) = \sum_{m=1}^{N_{\beta}}\sum_{\beta}\sum_{\sigma'=\uparrow,\downarrow}\mathcal{S}_{\alpha\beta;nm}^{\sigma\sigma'}(E)\hat{a}_{\beta,m,\sigma'}(E). \tag{1.13}$$

With the additional assumption of the absence of spin-flip scattering by spin-orbit interaction, let us take advantage of projection matrices to split the scattering matrix into two components in spin space, *i.e.* spin-up and spin-down relative to the magnetization direction $\mathbf{m}$ that we chose parallel to the spin quantization axis [34, 35, 39]:

$$\hat{\mathcal{S}}_{\alpha\beta;nm} = \mathcal{S}_{\alpha\beta;nm}^{\uparrow}\hat{u}^{\uparrow} + \mathcal{S}_{\alpha\beta;nm}^{\downarrow}\hat{u}^{\downarrow} \tag{1.14}$$

where the projection matrices are $\hat{u}^{\uparrow(\downarrow)} = (1 \pm \boldsymbol{\sigma}\cdot\mathbf{m})/2$.

Electrons in different leads, different channels, or different energies are statistically independent[36]. Therefore the following statistical average holds:

$$\langle\hat{a}_{\alpha,n,\sigma}^{\dagger}(E)\hat{a}_{\beta,n',\sigma'}(E')\rangle = f_{\alpha}^{\sigma'\sigma}\delta_{\alpha\beta}\delta_{nn'}\delta(E-E'). \tag{1.15}$$

In contrast to conventional cases, we allow a non-equilibrium imbalance between different spin species which gives rise to the concept of a *spin accumulation*. The time-averaged charge and spin currents through a given contact, in response to the presence of a given thermodynamic imbalance, as measured at the normal metal side of an N|F contact, can then be written as [34, 39]:

$$I_c = \frac{e}{2h}\left[2(g^{\uparrow\uparrow}+g^{\downarrow\downarrow})(\mu_{c,R}-\mu_{c,L}) + (g^{\uparrow\uparrow}-g^{\downarrow\downarrow})(\boldsymbol{\mu}_R-\boldsymbol{\mu}_L)\cdot\mathbf{m}\right], \tag{1.16}$$

$$\begin{aligned}\mathbf{I}_s = &-\frac{1}{8\pi}\left[2(g^{\uparrow\uparrow}-g^{\downarrow\downarrow})(\mu_{c,R}-\mu_{c,L})\mathbf{m} + (g^{\uparrow\uparrow}+g^{\downarrow\downarrow})((\boldsymbol{\mu}_R-\boldsymbol{\mu}_L)\cdot\mathbf{m})\mathbf{m}\right.\\ &\left.+2g_r^{\uparrow\downarrow}\mathbf{m}\times\boldsymbol{\mu}_R\times\mathbf{m} + 2g_i^{\uparrow\downarrow}\boldsymbol{\mu}_R\times\mathbf{m} - 2t_r'^{\uparrow\downarrow}\mathbf{m}\times\boldsymbol{\mu}_L\times\mathbf{m} - 2t_i'^{\uparrow\downarrow}\boldsymbol{\mu}_L\times\mathbf{m}\right].\end{aligned} \tag{1.17}$$

The spin-dependent conductances can be expressed as follows by summing over all transport channels [38] at the Fermi energy:

$$g^{\sigma\sigma'} = \sum_{nn'} \left[\delta_{nn'} - r^{\sigma}_{nn'} (r^{\sigma'}_{nn'})^* \right], \tag{1.18}$$

where $r^{\sigma}_{nn'}$ is the reflection amplitude of an electron with spin σ. New here is the *mixing conductance* $g^{\uparrow\downarrow} = \sum_{nn'} \left[\delta_{nn'} - r^{\uparrow}_{nn'} (r^{\downarrow}_{nn'})^* \right]$ which governs the spin decoherence of an incoming electron with spin polarized normal to the magnetization direction, when penetrating the ferromagnet. The spin-transfer torque acting on the ferromagnetic order parameter is equal to the spin current, polarized perpendicular to the magnetization, that is absorbed by the ferromagnet. We can project out this term from Eq.(1.17) and obtain

$$\mathbf{L}_{st} = \frac{1}{4\pi} \left(g_r^{\uparrow\downarrow} \mathbf{m} \times \boldsymbol{\mu}_R \times \mathbf{m} + g_i^{\uparrow\downarrow} \boldsymbol{\mu}_R \times \mathbf{m} - {t'_r}^{\uparrow\downarrow} \mathbf{m} \times \boldsymbol{\mu}_L \times \mathbf{m} - {t'_i}^{\uparrow\downarrow} \boldsymbol{\mu}_L \times \mathbf{m} \right). \tag{1.19}$$

Allowing the thickness of the ferromagnet to be much larger than its spin coherence length, the ferromagnetic layer is effectively reduced to two single F|N contacts. In this case, the terms related to $t'^{\uparrow\downarrow}$ vanish, since due to the large exchange field inside the ferromagnet a spin accumulation can only be built up aligned with the magnetization direction. For interfaces between normal and transition metals, the imaginary part of the mixing conductance $g_i^{\uparrow\downarrow}$ is much smaller than the real part and may be usually disregarded [41]. As such we may argue that the spin torque exerted on the magnetization, to a good approximation is determined by [34]:

$$\mathbf{L}_{st} \approx \frac{1}{4\pi} g_r^{\uparrow\downarrow} \mathbf{m} \times \boldsymbol{\mu}_R \times \mathbf{m}, \tag{1.20}$$

which is clearly driven by the non-equilibrium distribution $\boldsymbol{\mu}_R$, *i.e.* the spin accumulation in the normal metal node. The spin mixing conductance is a key concept in the magneto-electronic circuit theory [39], because it not only governs the microscopic description of the spin transport in the non-collinear magnetization configurations, but also the treatment of spin-transfer torque by *ab initio* calculations [35, 41].

1.7 Spin pumping

In the previous section, the magnetization of the magnetic scatterer (or the scattering potential) was static and the scattering matrix was consequently time-independent. The scattering processes associated with the slow motion of the magnetization are equally interesting, however. Here *slow* motion means that the characteristic time scale of the magnetization dynamics is much larger than that associated with the electronic motion. Upon moving the magnetization, the scattering matrix in spin space acquires a parametric time-dependence, which induces spin currents. The charge-current response to a time-dependent internal potential in the language of the scattering matrix formalism was first discussed by Büttiker *et al.* [42]. Brouwer later developed the concept of parametric charge pumping [43] in quantum dots by time-dependent gate voltages. The mechanism of spin pumping has been proposed and investigated by Tserkovnyak *et al.* in a series of papers [44, 45], initially to explain the enhancement of the Gilbert damping parameter measured in bilayers of a ferromagnet in contact with normal metals with varying degrees of spin flip scattering [46, 47]. In the following, we explain this mechanism briefly.

Consider a setup as in Fig. 1.5 and let us assume that the magnetization is in motion, such as under ferromagnetic resonance (FMR) conditions. The magnetization can be described by a time-dependent vector parameter $\mathbf{X}(t)$ (the specific choice will be given later). The scattering matrix acquires a time-dependence through the parameter $\mathbf{X}(t)$. In general, the creation and annihilation operators satisfy

$$\hat{b}_{\alpha,n,\sigma}(E) = \sum_{m=1}^{N_\beta} \sum_{\beta} \sum_{\sigma'=\uparrow,\downarrow} \mathcal{S}^{\sigma\sigma'}_{\alpha\beta;nm}(E, E', \mathbf{X}(t)) \hat{a}_{\beta,m,\sigma'}(E'). \tag{1.21}$$

Keeping the Fourier transform of the parameter $\mathbf{X}(t)$ to first order in its frequency ω under the assumption that $\mathbf{X}(t)$ is varying slowly (adiabatically) with respect to the characteristic interaction time of electrons (*i.e.* electrons always see a static parameter $X(t)$):

$$\mathbf{X}(t) \approx \mathbf{X}(-\omega)e^{+i\omega t} + \mathbf{X}(+\omega)e^{-i\omega t}. \tag{1.22}$$

In the spirit of time-dependent perturbation theory, such an internal potential mixes the energy sub-bands of $E^{'} = E - \hbar\omega$ and $E^{'} = E + \hbar\omega$. To first order in $X(\pm\omega)$, Eq.(1.21) is expanded as

$$\hat{b}_{\alpha,n,\sigma}(E) = \sum_{m=1}^{N_\beta} \sum_{\beta} \sum_{\sigma'=\uparrow,\downarrow} \Big[\mathcal{S}^{\sigma\sigma'}_{\alpha\beta;nm}(E) \hat{a}_{\beta,m,\sigma'}(E) + \partial_X \mathcal{S}^{\sigma\sigma'}_{\alpha\beta;nm}(E, E+\hbar\omega) X(-\omega) \hat{a}_{\beta,m,\sigma'}(E+\hbar\omega) + \partial_X \mathcal{S}^{\sigma\sigma'}_{\alpha\beta;nm}(E, E-\hbar\omega) X(+\omega) \hat{a}_{\beta,m,\sigma'}(E-\hbar\omega) \Big] . \quad (1.23)$$

The above equation can be substituted back into the current operator to calculate the average current. It is found that in addition to the current corresponding to a static magnetization as discussed in the previous section, a time-dependent correction arises that is called a *pumping current*:

$$I^{(p)}_{\alpha,i}(t) = \frac{i\hbar}{8\pi} \sum_{nm,\beta} \int dE \frac{df(E)}{dE} \mathrm{Tr} \left[\hat{\sigma}_i \left(\hat{\mathcal{S}}(E) \partial_X \hat{\mathcal{S}}^\dagger(E) - \partial_X \hat{\mathcal{S}}(E) \hat{\mathcal{S}}^\dagger(E) \right) \right] \frac{dX(t)}{dt} , \quad (1.24)$$

where the trace acts in spin space (channel and lead indices of the scattering matrix $\hat{\mathcal{S}}$ are suppressed). The projection operators may again be applied in the absence of spin-flip scattering at the interface. In the case of a simple precessional motion around the z-axis, the parameter $\mathbf{X}$ can be identified to be the azimuthal angle ϕ of the magnetization direction, defined by $\mathbf{m} = (\sin\theta\cos\phi, \sin\theta\sin\phi, \cos\theta)$ [44]. After some algebra, one obtains a pumping current in terms of the mixing conductance and magnetization direction, measured at the normal metal side, as

$$\mathbf{I}^{(p)}_s = \frac{\hbar}{4\pi} \left(g^{\uparrow\downarrow}_r \mathbf{m} \times \frac{d\mathbf{m}}{dt} + g^{\uparrow\downarrow}_i \frac{d\mathbf{m}}{dt} \right) . \quad (1.25)$$

The smallness of the imaginary part of the mixing conductance compared to the real part allows us, in most situations, to discard the second term. The pumped spin current is then perpendicular to the magnetization direction and its precession rate ($\dot{\mathbf{m}}$). The above mechanism pumps only spin current but no charge current, since the latter must be conserved. The total angular momentum of the conduction electrons does not have to be conserved, since it may relax to the lattice, *e.g.* by spin-flip scattering processes. The pumping current modifies the Landau-Lifshitz-Gilbert equation since the loss of angular momentum by the pumping current is a torque acting on the magnetization. The real part of the mixing conductance contributes to the enhancement of the Gilbert damping parameter [44], as found experimentally [46, 47]. In the absence of the spin-flip scattering, the pumped spin current entering the normal metal builds up spin accumulation. A non-equilibrium spin accumulation in the normal metal, as noted in the previous section, in turn produces a *back flow* spin current that opposes the pumped one. The interplay between the pumping current and back flow led to new ideas such as *spin battery* [48], and *dc* voltage generation by spin pumping [49, 50].

1.8 This thesis

The next two chapters of this thesis, Chapter 2 and Chapter 3, describe the magnetization dynamics driven by a pure spin current as investigated in a three terminal geometry (spin-flip transistor), using magneto-electronic circuit theory and the Landau-Lifshitz-Gilbert equation augmented by the spin-transfer and pumping torques. A “spin-flip transistor” is a lateral spin valve consisting of ferromagnetic source drain contacts to a thin-film normal-metal island with an electrically floating ferromagnetic base contact on top. The charge current is sent through the source and drain contacts while at the floating contact the charge current is vanishing, but the spin current generated by the spin accumulation derived from magnetized contacts can interact with the thin film magnetization, thus producing the dynamics. The relative orientation of the anisotropy fields and the source drain magnetization direction play important roles in characterizing the dynamics.

In Chapter 2, we analyze the *dc*-current-driven magnetization dynamics of spin-flip transistors in which the source-drain contacts are magnetized perpendicularly to the device plane. Spin-flip scattering and spin pumping effects are taken into account. We find a steady-state rotation of the base magnetization at GHz frequencies that is tuneable by the source-drain bias. In Chapter 3, the source-drain magnetizations are chosen fixed and antiparallel, with all magnetizations in the device plane, while the third contact magnetization is allowed to move in a weak anisotropy field that guarantees thermal stability of the equilibrium structure at room temperature. Tunable two-state behavior of the magnetization is found.

In Chapter 4, we describe a mechanism to convert the spin signal due to spin pumping to an electric signal for a ferromagnetic (F) magnetization that is resonantly excited to a steady precession around a static applied magnetic field. The precessing magnetization pumps spin current into the adjacent normal metal (N) thereby induces a non-equilibrium spin accumulation. Diffusion processes in N average out the oscillating components of the spin current, leaving a static spin accumulation. The back-flow spin current generated by such a spin accumulation tries to penetrate F. The exchange field in F favors only the spin current component parallel to the magnetization, which leads to spin accumulation in the F side. The spin-flip scattering and the difference in conductivities for spin-up and spin-down electrons creates a potential drop across the F|N interface, which can be detected as a *dc* voltage. This mechanism shows that FMR acts not only as source of angular momentum, but also as an energy source. These theoretical predictions have been confirmed by experiments [50].

In Chapter 5, we study the damping parameter of a thin magnetic film sandwiched by normal metal from a somewhat different point of view. The spins on the thin film are coupled to the conducting electrons through s-d exchange. The conduction electrons serve as a dissipative environment for the magnetization. The imaginary-time effective action approach is adopted. To obtain the equation of motion for the magnetization, the conduction electron degrees of freedom are integrated out and what remains is an effective action of the magnetization. In the spirit of the Caldeira-Leggett formalism, the dissipation, which is responsible for the damping of the spin dynamics, is obtained by the part of the action that is non-local in time. The excitation of electron-hole pairs by the interaction with the dynamic spins is the channel for dissipation. In deriving the equation of motion for the magnetization, the Landau-Lifshitz-Gilbert equation is recovered.

Bibliography

[1] A. D. Aczel, *The Riddle of the Campass: the Invention That Changed the World* (Harvest Books, 2002).

[2] C. Kittel, *Introduction to Solid State Physics* (John Wiley and Sons, Eighth Edition, 2005).

[3] N. W. Ashcroft and N. D. Mermin, *Solid State Physics* (Saunders College Publishing, 1976).

[4] S. Chikazumi, *Physics of Ferromagnetism*, (Oxford Press, 1996).

[5] M. N. Baibich, J. M. Broto, A. Fert, F. N. V. Dau, F. Petroff, P. Etienne, G. Creuzet, A. Friedrich, and J. Chazelas, Phys. Rev. Lett. **61**, 2472 (1988).

[6] G. Binasch, P. Grunberg, F. Saurenbach, and W. Zinn, Phys. Rev. B **39**, 4282 (1989).

[7] T. Valet and A. Fert, Phys. Rev. B **48**, 7099 (1993).

[8] E. Fradkin, *Field Theories of Condensed Matter Systems*, (Westview Press, 1991).

[9] H. J. Schulz, Phys. Rev. Lett. **65**, 2462 (1990).

[10] G. Tatara and H. Fukuyama, J. Phys. Soc. Jpn. **63**, 2538 (1994).

[11] R. A. Duine, A. S. Nunez, J. Sinova, and A. H. MacDonald, Phys. Rev. B **75**, 214420 (2007).

[12] L. D. Landau and I. M. Lifshitz, *Quantum Mechanics (Non-relativistic Theory)*, (Butterworth Heinemann, 3rd Edition, 2005).

[13] E. M. Lifshitz and L. P. Pitaevskii, *Statistical Mechanics (Part 2)*, (Butterworth Heinemann, 3rd Edition, 2005).

[14] T. L. Gilbert, Phys. Rev. **100**, 1243 (1955); IEEE Trans. Magn. **40**, 3443 (2004).

[15] M. Johnson and R. H. Silsbee, Phys. Rev. Lett. **55**, 1790 (1985).

[16] M. Johnson, Phys. Rev. Lett. **70**, 2142 (1993).

[17] J. Slonczewski, J. Magn. Magn. Mater. **159**, L1 (1996); J. Magn. Magn. Mater. **195**, L261 (1999).

[18] L. Berger, Phys. Rev. B **54**, 9353 (1996).

[19] M. Tsoi, A. G. M. Jansen, J. Bass, W. C. Chiang, M. Seck, V. Tsoi, and P. Wyder, Phys. Rev. Lett. **80**, 4281 (1999).

[20] E. B. Myers, D. C. Ralph, J. A. Katine, R. N. Louie, and P. Wyder, Science **285**, 867 (1999).

[21] J. A. Katine, F. J. Albert, R. A. Buhrman, E. B. Myers, and D. C. Ralph, Phys. Rev. Lett. **84**, 3149 (2000)

[22] M. Tsoi, A. G. M. Jansen, J. Bass, W. C. Chiang, V. Tsoi, and P. Wyder, Nature (London) **406**, 46 (2000).

[23] E. B. Myers, F. J. Albert, J. C. Sankey, E. Bonet, R. A. Burhman, and D. C. Ralph, Phys. Rev. Lett. **89**, 196801 (2002).

[24] F. J. Albert, N. C. Emley, E. B. Myers, D. C. Ralph, and R. A. Buhrman, Phys. Rev. Lett. **89**, 226802 (2002).

[25] S. I. Kiselev, J. C. Sankey, I. N. Krivorotov, N. C. Emley, M. Rinkoski, C. Perez, R. A. Buhrman, and D. C. Ralph, Phys. Rev. Lett. **93**, 036601 (2004).

[26] I. N. Krivorotov, N. C. Emley, J. C. Sankey, S. I. Kiselev, D. C. Ralph, and R. A. Buhrman, Science **307**, 228 (2005).

[27] F. J. Jedema, A. T. Filip and B. J. van Wees, Nature (London) **410**, 345 (2001).

[28] F. J. Jedema, M. S. Nijboer, A. T. Filip,, and B. J. van Wees, Phys. Rev. B **67**, 085319 (2003)

[29] M. Zaffalon and B. J. van Wees Phys. Rev. B **71**, 125401 (2005)

[30] J. Hamrle, T. Kimura, Y. Otani, K. Tsukagoshi, and Y. Aoyagi, Phys. Rev. B **71**, 094402 (2005)

[31] T. Kimura, J. Hamrle, and Y. Otani, Phys. Rev. B **72**, 014461 (2005)

[32] T. Kimura, Y. Otani, and J. Hamrle, Phys. Rev. Lett. **96**, 037201 (2006)

[33] X. Wang, G. E. W. Bauer, and A. Hoffmann, Phys. Rev. B **73**, 054436 (2006).

[34] Y. Tserkovnyak, A. Brataas, G. E. W. Bauer, and B. I. Halperin, Rev. Mod. Phys. **77**, 1375 (2005).

[35] A. Brataas, G. E. W. Bauer, and P. J. Kelly, Phys. Rep. **427**, 157 (2005).

[36] M. Büttiker, Phys. Rev. B **46**, 12485 (1992).

[37] R. Landauer, IBM J. Res. Develop. **1**, 233 (1957); Phil. Mag. **21**, 863 (1970).

[38] Y. Blanter and M. Büttiker, Phys. Rep. **336**, 1 (2000).

[39] A. Brataas, Y. V. Nazarov, and G. E. W. Bauer, Phys. Rev. Lett. **84**, 2481 (2000).

[40] A. Brataas, Y. V. Nazarov, and G. E. W. Bauer, Eur. Phys. J. B **22**, 99 (2001).

[41] K. Xia, P. J. Kelly, G. E. W. Bauer, A. Brataas, and I. Turek, Phys. Rev. B **65**, 220401 (2002).

[42] M. Büttiker, H. Thomas, and A. Prtre, Z. Phys. B: Condens. Matter **94**, 133 (1994).

[43] P. W. Brouwer, Phys. Rev. B **58**, 10135 (1998).

[44] Y. Tserkovnyak, A. Brataas, and G. E. W. Bauer, Phys. Rev. Lett. **88**, 117601 (2002).

[45] Y. Tserkovnyak, A. Brataas, and G. E. W. Bauer, Phys. Rev. B **66**, 224403 (2002).

[46] S. Mizukami, Y. Ando, and T. Miyazaki, Phys. Rev. B **66**, 104413 (2002).

[47] S. Mizukami, Y. Ando, and T. Miyazaki, J. Magn. Magn. Mater. **239**, 42 (2002).

[48] A. Brataas, Y. Tserkovnyak, G. E. W. Bauer, and B. I. Halperin, Phys. Rev. B **66**, 060604 (2002).

[49] X. Wang, G. E. W. Bauer, B. J. van Wees, A. Brataas, and Y. Tserkovnyak, Phys. Rev. Lett. **97**, 216602 (2006).

[50] M. Costache, M. Sladkov, S. M. Watts, C. H. van der Wal, and B. J. van Wees, Phys. Rev. Lett. **97**, 216603 (2006).

Chapter 2

Magnetization Dynamics Induced by a Pure Spin Current

Abstract

A "spin-flip transistor" is a lateral spin valve consisting of ferromagnetic source drain contacts to a thin-film normal-metal island with an electrically floating ferromagnetic base contact on top. We analyze the dc*-current-driven magnetization dynamics of spin-flip transistors in which the source-drain contacts are magnetized perpendicularly to the device plane by magnetoelectronic circuit theory and the macrospin Landau-Lifshitz-Gilbert equation. Spin flip scattering and spin pumping effects are taken into account. We find a steady-state rotation of the base magnetization at GHz frequencies that is tuneable by the source-drain bias. We discuss the advantages of the lateral structure for high-frequency generation and actuation of nanomechanical systems over recently proposed nanopillar structures.* [1]

2.1 Introduction

Current induced magnetization excitation by spin-transfer torque [1, 2] attracts considerable attention because of potential applications for magnetoelectronic devices. The prediction of current-induced magnetization reversal has been confirmed experimentally in multilayers structured into pillars of nanometer dimensions [3, 4, 5, 6]. The devices typically consist of two ferromagnetic layers with a high (fixed layer) and a low coercivity (free layer), separated by a normal metal spacer. The applied current flows perpendicular to the interfaces. Often magnetic anisotropies force the magnetizations into the plane of the magnetic layers. Recently a number

[1]This chapter has been published as: Xuhui Wang, *et al.*, *Dynamics of Thin-Film Spin-Flip Transistors with Perpendicular Source-Drain Magnetizations,* Phys. Rev. B **73**, 054436 (2006).

of theoretical proposals pointed out interesting dynamics when the magnetization of one of the layers is oriented perpendicular to the interface planes [7, 8, 9].

Fundamental studies of charge and spin transport have also been carried out in thin-film metallic conductors structured on top of a planar substrate [7, 8, 12, 9, 10, 11]. The advantages compared to pillar structures are the flexible design and the relative ease to fabricate multi-terminal structures with additional functionalities such as the spin-torque transistor [13]. The easy accessibility to microscopic imaging of the structure and magnetization distribution should make the lateral structure especially suitable to study current-induced magnetization dynamics. Previous studies focused on the static (dc) charge transport properties, but investigations of the dynamics of laterally structured devices are underway [17, 18]. Recently, non-local magnetization switching in a lateral spin valve structure has been demonstrated [14]. In the present paper we investigate theoretically the dynamics of a lateral spin valve consisting of a normal metal film that is contacted by two magnetically hard ferromagnets. As sketched in Fig. 2.1, a (nearly) circular and magnetically soft ferromagnetic film is assumed deposited on top of the normal metal to form a spin-flip transistor [15]. We concentrate on a configuration in which the magnetization direction of the source-drain contacts lies perpendicular to the plane of the magnetization of the third (free) layer. This can be realized either by making the contacts from a material that has a strong crystalline magnetic anisotropy forcing the magnetization out of the plane, such as Co/Pt multilayers [21], or by growing the source/drain ferromagnetic contacts into deeply etched groves to realize a suitable aspect ratio. In such a geometry, the magnetization of the free layer precesses around the demagnetizing field that arises when the magnetization is forced out of the plane by the spin-transfer torque, as has been discussed in Refs. [7, 8, 9]. Therefore, as long as the out-of-plane magnetization of the free layer remains small, the free layer magnetization will always stay almost perpendicular to the source and drain magnetizations. In the present article we analyze in depth the coupled charge-spin-magnetization dynamics in such current-biased thin-film “magnetic fans” and point out the differences and advantages compared to the perpendicular pillar structures. A convenient and accurate tool to compute the dynamic properties of our device is the magneto-electronic circuit theory for charge and spin transport [15] coupled to the Landau-Lifshitz-Gilbert equation in the macrospin model. We include spin flip scattering in normal and ferromagnetic metals and the spin-pumping effect [17, 18].

The article is organized as follows: In Section 2.2, we briefly review the Landau-

Lifshitz-Gilbert equation including the current driven and spin-pumping torques that can be derived by circuit theory. In Section 2.3, the specific results for our “magnetic fan” are presented. The potential applications will be discussed in Section 2.4. Section 2.5 is devoted to the conclusion.

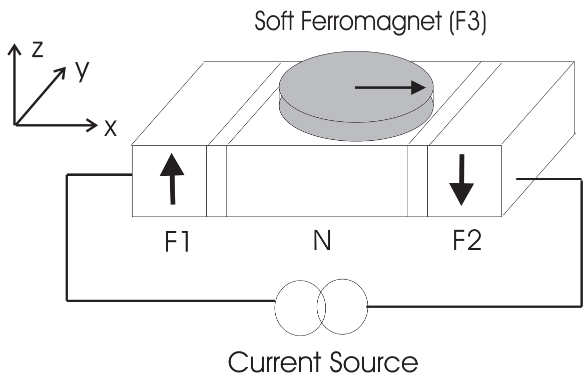

Figure 2.1: The model system consists of hard-magnetic source and drain contacts (F1 and F2) with antiparallel magnetizations perpendicular to the plane. On the top of the normal metal N, a soft ferromagnetic film (F3) is deposited with a slightly elliptical shape. The quantization direction, *i.e.*, z-axis, is chosen parallel to the magnetization of the source and the drain.

2.2 Formalism

We are interested in the magnetization dynamics of the soft ferromagnetic island (i.e., composed of permalloy) on top of the normal film as sketched in the Fig. 2.1. The Landau-Lifshitz-Gilbert (LLG) equation in the macro-spin model, in which the ferromagnetic order parameter is described by a single vector $\mathbf{M}$ with constant modulus M_s, appears to describe experiments of current-driven magnetization dynamics well [24], although some open questions remain [25]. Micromagnetic calculations of the perpendicular magnetization configuration in the pillar structure suggest a steady precession of the magnetization [8]. The LLG equation for isolated ferromagnets has to be augmented by the magnetization torque $\mathbf{L}$ that is induced by the spin accumulation in proximity of the interface as well as the spin pumping:

$$\frac{1}{\gamma}\frac{d\mathbf{m}}{dt} = -\mathbf{m}\times\mathbf{H}_{eff} + \frac{\alpha_0}{\gamma}\mathbf{m}\times\frac{d\mathbf{m}}{dt} + \frac{1}{VM_s}\mathbf{L} \tag{2.1}$$

where γ is the gyromagnetic constant, $\mathbf{m} = \mathbf{M}/M_s$ and $\mathbf{H}_{eff}$ is the magnetic field including demagnetizing, anisotropy or other external fields. α_0 is the Gilbert damping constant and V is the volume of the isolated bulk magnet.

$$\mathbf{L} = -\mathbf{m}\times\left(\mathbf{I}_s^{(p)} + \mathbf{I}_s^{(b)}\right)\times\mathbf{m},$$

where $\mathbf{I}_s^{(p)}$ and $\mathbf{I}_s^{(b)}$ denote the pumped [17] and bias-driven [1, 2] spin currents leaving the ferromagnet, respectively, and the vector products project out the components of the spin current normal to the magnetization direction.

In magnetoelectronic circuit theory a given device or circuit is split into nodes and resistors. In each node a charge potential and spin accumulation is excited by a voltage or current bias over the entire device that is connected to reservoirs at thermal equilibrium or by spin pumping. The currents are proportional to the chemical potential and spin accumulation differences over the resistors that connect the island to the nodes. The Kirchhoff rules representing spin and charge conservation close the system of equations that govern the transport. In the following we assume that the ferromagnetic layer thickness is larger than the magnetic coherence length $\lambda_c = \pi/\left|k_F^{\uparrow} - k_F^{\downarrow}\right|$ in terms of the majority and minority Fermi wave numbers that in transition metal ferromagnets is of the order of Ångströms.

Let us consider a ferromagnet-normal metal ($F|N$) interface in which the ferromagnet is at a chemical potential μ_0^F and spin accumulation $\mu_s^F\mathbf{m}$ (with magnetization direction $\mathbf{m}$), whereas the normal metal is at μ_0^N and spin accumulation $\mathbf{s}$. The charge current (in units of Ampere) and spin currents (in units of Joule), into the normal metal are [26]

$$I_c = \frac{e}{2h}[2g(\mu_0^F - \mu_0^N) + pg\mu_s^F - pg\mathbf{m}\cdot\mathbf{s}] \tag{2.2}$$

$$\begin{aligned}\mathbf{I}_s^{(b)} &= \frac{g}{8\pi}[2p(\mu_0^F - \mu_0^N) + \mu_s^F - (1-\eta_r)\mathbf{m}\cdot\mathbf{s}]\mathbf{m} \\ &\quad - \frac{g}{8\pi}\eta_r\mathbf{s} - \frac{g}{8\pi}\eta_i(\mathbf{s}\times\mathbf{m})\end{aligned} \tag{2.3}$$

where μ_0^F and μ_0^N are the chemical potentials in the ferromagnets and normal metal, respectively. $g^{\uparrow}, g^{\downarrow}$ are the dimensionless spin dependent conductances with polarization $p = (g^{\uparrow} - g^{\downarrow})/(g^{\uparrow} + g^{\downarrow})$ and total contact conductance $g = g^{\uparrow} + g^{\downarrow}$. In the Landauer-Büttiker formalism

$$g^{\uparrow(\downarrow)} = M - \sum_{nm} |r^{nm}_{\uparrow(\downarrow)}|^2 \tag{2.4}$$

where M is the total number of channels and $r^{nm}_{\uparrow(\downarrow)}$ is the reflection coefficient from mode m to mode n for spin up(down) electrons. The spin transfer torque is governed by the complex spin-mixing conductance $g^{\uparrow\downarrow}$, given by [26]

$$g^{\uparrow\downarrow} = M - \sum_{nm} r^{nm}_{\uparrow}(r^{nm}_{\downarrow})^* \,, \tag{2.5}$$

introduced in Eq. (3.1) in terms of its real and imaginary part as $\eta_r = 2\mathrm{Re}g^{\uparrow\downarrow}/g$ and $\eta_i = 2\mathrm{Im}g^{\uparrow\downarrow}/g$. All conductance parameters can be computed from first principles as well as fitted to experiments.

Slonczewski's spin transfer torque can then be written as

$$-\mathbf{m} \times \mathbf{I}^{(b)}_s \times \mathbf{m} = \frac{g}{8\pi}\eta_r[\mathbf{s} - (\mathbf{s}\cdot\mathbf{m})\mathbf{m}] + \frac{g}{8\pi}\eta_i(\mathbf{s}\times\mathbf{m}). \tag{2.6}$$

The spin-pumping current is given by [17]

$$\mathbf{I}^{(p)}_s = \frac{\hbar}{8\pi} g \left(\eta_r \mathbf{m} \times \frac{d\mathbf{m}}{dt} + \eta_i \frac{d\mathbf{m}}{dt}\right) . \tag{2.7}$$

We consider for simplicity the regime in which the spin-flip diffusion length l^N_{sf} in the normal metal node is larger than the size of the normal metal region [12]. Charge and spin currents into the normal metal node are then conserved such that [15]

$$\sum_i I_{c,i} = 0 \tag{2.8}$$

$$\sum_i \left(\mathbf{I}^{(p)}_{s,i} + \mathbf{I}^{(b)}_{s,i}\right) = \mathbf{I}^{sf}_s. \tag{2.9}$$

where we introduce a leakage current due to the spin-flip scattering $\mathbf{I}^{sf}_s = g_{sf}\mathbf{s}/4\pi$ and $g_{sf} = h\nu_{DOS}\mathrm{V}_N/\tau^N_{sf}$ is the conductance due to spin flip scattering, where ν_{DOS} is the (on-spin)density of state of the electrons in the normal metal, τ^N_{sf} is the spin flip relaxation time and V_N the volume of the normal metal node.

The polarization of the source-drain contacts is supposed to be an effective one including the magnetically active region of the bulk ferromagnet with thickness governed by the spin-flip diffusion length in the ferromagnet. For the free magnetic layer $F3$, the perpendicular component of the spin current is absorbed to generate the spin transfer torque. The collinear current has to fulfill the boundary conditions in terms of the chemical potential $\mu_s^F = \mu_\uparrow - \mu_\downarrow$ governed by the diffusion equation

$$\frac{\partial^2 \mu_s^F(z)}{\partial z^2} = \frac{\mu_s^F(z)}{\left(l_{sd}^F\right)^2}. \tag{2.10}$$

where l_{sd}^F is the spin flip diffusion length in the ferromagnet.

2.3 Spin transfer torque and steady precession of magnetization

In this Section, we solve the Landau-Lifshitz-Gilbert equation including expressions for the spin-transfer torque on the free layer according to the circuit theory sketched above.

2.3.1 Currents and spin torque

In metallic structures the imaginary part of the mixing conductance is usually very small and may be disregarded, *i.e.*, $\eta_i \simeq 0$. The source and drain contacts $F1|N$ and $F2|N$ are taken to be identical: $g_1 = g_2 = g$, $p_1 = p_2 = p$ and $\eta_{r1} = \eta_{r2} \equiv \eta_r$. For $F3|N$ we take $\eta_{r3} \equiv \eta_3$. In our device, the directions of the magnetization of the fixed magnetic leads are $\mathbf{m}_1 = (0,0,1)$ and $\mathbf{m}_2 = (0,0,-1)$. For the free layer we allow the magnetization $\mathbf{m}_3 = (m_x, m_y, m_z)$ to be arbitrary. We assume that $F3$ is a floating contact in which the the chemical potential μ_0^{F3} adjusts itself such that the net charge current through the interface $F3|N$ vanishes:

$$I_c^{(3)} = \frac{eg_3}{2h}[2(\mu_0^{F3} - \mu_0^N) + p_3\mu_s^{F3} - p_3\mathbf{s}\cdot\mathbf{m}_3] = 0. \tag{2.11}$$

Applying a bias current I_0 on the two ferromagnetic leads, $F1$ and $F2$, the conservation of charge current in the normal metal then gives $I_c^{(1)} = -I_c^{(2)} = I_0$. At the $F3|N$

interface, the continuity of the longitudinal spin current dictates

$$\sigma_\uparrow \left(\frac{\partial \mu_\uparrow}{\partial z}\right)_{z=0} - \sigma_\downarrow \left(\frac{\partial \mu_\downarrow}{\partial z}\right)_{z=0} = \frac{2e^2}{\hbar A}\mathbf{I}_{s,3} \cdot \mathbf{m}_3 \tag{2.12}$$

where $\sigma_\uparrow(\sigma_\downarrow)$ is the bulk conductivities of spin up (down) electrons in the ferromagnet and A the area of the interface. Choosing the origin of the z axis is at the $F3|N$ interface and assuming $F3$ to be of thickness d,

$$\sigma_\uparrow \left(\frac{\partial \mu_\uparrow}{\partial z}\right)_{z=d} - \sigma_\downarrow \left(\frac{\partial \mu_\downarrow}{\partial z}\right)_{z=d} = 0\,. \tag{2.13}$$

With both boundary conditions, the diffusion equation can be solved for the spin accumulation in $F3$

$$\mu_s^F(z) = \frac{\zeta_3 \cosh(\frac{z-d}{l_{sd}^F})\mathbf{s} \cdot \mathbf{m}_3}{\left[\zeta_3 + \tilde{\sigma} \tanh(\frac{d}{l_{sd}^F})\right] \cosh(\frac{d}{l_{sd}^F})} \tag{2.14}$$

where $\zeta_3 = g_3(1 - p_3^2)/4$ characterizes the contact F3|N and

$$\tilde{\sigma} = hA\sigma_\uparrow\sigma_\downarrow/(e^2 l_{sd}^F(\sigma_\uparrow + \sigma_\downarrow))$$

describes the bulk conduction properties of the free layer with arbitrary $\mathbf{m}_3$. The limit $d \ll l_{sd}^F$ corresponds to negligibly small spin-flip, which implies $\tanh(d/l_{sd}^F) \simeq 0$. Near the interface, the spin accumulation in $F3$ then reduces to

$$\mu_s^{F3} = \mathbf{s} \cdot \mathbf{m}_3\,. \tag{2.15}$$

In this limit, $\mathbf{I}_s^{(3)} \cdot \mathbf{m}_3 = 0$ the collinear component of the spin current vanishes. By solving the linear equations generated by Eqs. (2.8,2.9), we obtain the spin accumulation s in the normal metal node,

$$\mathbf{s} = \hat{\mathbf{C}} \cdot [8\pi \mathbf{I}_s^{(p)} + \mathbf{W}_b] \tag{2.16}$$

where the elements of the symmetric matrix $\hat{\mathbf{C}}$ are given in Appendix 2.6 and $\mathbf{W}_b = (0, 0, 2phI_0/e)$ is a bias-vector. Eq. (2.16) contains contribution due to bias current and spin pumping effect. The spin accumulation in the ferromagnet Eq. (2.14) should be substituted in Eq. (2.16) to give the spin accumulation in the normal metal, from which the spin transfer torque can be determined according to Eq. (2.6). For an ultrathin film, the spin transfer torque, including pumping effect and spin accumulation in the ferromagnet, reads,

$$\mathbf{L} = \frac{\eta_3 g_3}{8\pi} \hat{\mathbf{\Pi}} \cdot [8\pi \mathbf{I}_s^{(p)} + \mathbf{W}_b] \,, \tag{2.17}$$

with the elements of $\mathbf{\Pi}$ listed in Appendix.

2.3.2 Dynamics of the free layer

After the bias current is switched on, a spin accumulation builds up in the normal metal. At the beginning, the spin-transfer torque exerted on the magnetization of the free layer (F3) causes a precession out of the plane, hence generating a demagnetizing field $\mathbf{H}_A$ that is oriented perpendicular to the film plane. Subsequently the magnetization precesses around $\mathbf{H}_A$ and as long as the current I_0 continues, the rotation persists. In order to determine the dynamics of the magnetization, we apply the spin torque term $\mathbf{L}$ [Eq. (2.17)] to the Landau-Lifshitz-Gilbert (LLG) equation (2.1). Crystalline anisotropies in F3 may be disregarded for soft ferromagnets such as permalloy. The effective field in the LLG equation then reduces to

$$\mathbf{H}_A = -\mu_0 M_s (N_x m_x, N_y m_y, N_z m_z) \,, \tag{2.18}$$

where N_x, N_y and N_z are the demagnetizing factors determined by the shape of the film [19]. The anisotropy field keeps the magnetization in the plane when the torque is zero. The spin torque generated by the current bias forces the magnetization out of plane, hence triggering the nearly in-plane rotation of the magnetization. Substituting the spin-torque term Eq. (2.17) into Eq. (2.1), we obtain for the following LLG equation,

$$\frac{1}{\gamma}\frac{d\mathbf{m}}{dt} = -\mathbf{m} \times \mathbf{H}_A + \frac{1}{\gamma}\left(\alpha_0 + \overleftrightarrow{\alpha}'\right)\mathbf{m} \times \frac{d\mathbf{m}}{dt} + \mathbf{H}_{st}(I_0) \tag{2.19}$$

Here the last vector

$$\mathbf{H}_{st}(I_0) = \frac{\hbar}{2e}\Lambda_{st}\frac{I_0}{M_s V}(-m_x m_z, -m_y m_z, 1 - m_z^2) \,. \tag{2.20}$$

is the effective field induced by the spin-transfer torque that depends on the position of the magnetization and the device parameter

$$\Lambda_{st} = \frac{p\eta_3 g_3 \mathcal{G}_1}{\mathcal{G}_t \mathcal{G}_3 + 2(p^2 - 1 + \eta) g \mathcal{G}_4 (1 - m_z^2)}, \tag{2.21}$$

where $\mathcal{G}_i$'s are introduced in Appendix A. According to Eq. (2.21), we can accurately engineer the device performance by tuning the conductances and polarizations. Compared with the original LLG equation, a new dimensionless parameter entering the calculation

$$\overleftrightarrow{\alpha}' = \frac{\gamma\hbar(\mathrm{Re}g^{\uparrow\downarrow})^2}{2\pi V M_s}\hat{\mathbf{\Pi}} \tag{2.22}$$

reflects the tensor character of the pumping-induced additional Gilbert damping [28]. Choosing contact $F3|N$ to be metallic and the others to be tunneling barriers, the condition $g_3 \gg g, g_{sf}$ can be realized. In that limit $\overleftrightarrow{\alpha}'$ reduces to

$$\alpha' = \frac{\gamma\hbar}{4\pi V M_s}\,\mathrm{Re}\,g_3^{\uparrow\downarrow}\ , \tag{2.23}$$

which agrees with the enhanced Gilbert damping derived in Ref. [17]. In the following, we take $\alpha = \alpha_0 + \alpha'$ to be the enhanced Gilbert damping constant.

2.3.3 Vanishing in-plane anisotropy

Here we rewrite the free layer magnetization in two polar angles ϕ (in-plane) and θ (out-of plane) such that $\mathbf{m} = (\cos\theta\cos\phi, \cos\theta\sin\phi, \sin\theta)$ and assuming a small z-component, i.e., $m_z = \sin\theta \approx \theta$ and $\cos\theta \approx 1$. When the free layer is a round flat disk with demagnetizing factors $N_x = N_y \approx 0$ and $N_z \approx 1$, the Eqs. (2.19) reduce to:

$$\begin{aligned}\frac{d\phi}{dt} &= -\alpha\frac{d\theta}{dt} - \gamma\mu_0 M_s N_z\theta \\ \frac{d\theta}{dt} &= \alpha\frac{d\phi}{dt} + \gamma\mathcal{F}(I_0)\ ,\end{aligned} \tag{2.24}$$

introducing $\mathcal{F}(I_0) = \hbar\Lambda_{st}I_0/(2eM_sV)$. Eq. (2.24) separates the motion for the in and out-of-plane angles. We consider the dynamics of a current that is abruptly switched on to a constant value I_0 at $t = 0$, assuming that $\theta(t = 0) = 0$, *i.e.*, a magnetization that initially lies in the plane. The motion of θ for $t > 0$ is then given by

$$\begin{aligned}\theta(t) &= \frac{\omega_\phi}{\gamma\mu_0 M_s N_z}\left(1 - e^{-t/\tau}\right) \\ \frac{d\theta}{dt} &= \frac{\alpha}{1+\alpha^2}\omega_\phi e^{-t/\tau}\ .\end{aligned} \tag{2.25}$$

where we introduced the response time

$$\tau = \frac{(1+\alpha^2)}{\alpha\mu_0\gamma M_s N_z} \tag{2.26}$$

and the saturation in-plane rotation frequency

$$\omega_\phi = \frac{\gamma\mathcal{F}(I_0)}{\alpha} = \frac{\hbar}{2e}\Lambda_{st}\frac{\gamma I_0}{\alpha M_s V} \,. \tag{2.27}$$

Similarly, the in-plane rotation is governed by

$$\begin{aligned}\phi(t) &= -\omega_\phi t + \frac{\omega_\phi}{\gamma\alpha\mu_0 M_s N_z}\left(1 - e^{-t/\tau}\right) \\ \frac{d\phi}{dt} &= -\omega_\phi + \frac{\omega_\phi}{1+\alpha^2}e^{-t/\tau} \,.\end{aligned} \tag{2.28}$$

Taking the parameters from Ref. [12], *viz.* a volume of normal metal $V_n = 400^2 \times 30$ nm^3, spin flip time in the normal metal of $\tau_{sf} = 62$ ps, density of states $\nu_{\mathrm{DOS}} = 2.4 \times 10^{28}$ eV^{-1}m^{-3}, we find $e^2 g_{sf}/h = 0.3\,\Omega^{-1}$.

Let us take the thickness of the free layer $d = 5$ nm. The saturation magnetization of permalloy is $M_s = 8 \times 10^5$ A m^{-1}. The relative mixing conductance is chosen $\eta_3 \simeq \eta_r \simeq 1$ and the bulk value of the Gilbert damping constant for Py is typically $\alpha_0 = 0.006$ [17]. A metallic interface conductance (for $F3|N$) is typically 1.3fΩ m^2 [29], whereas the source/drain contacts are tunneling barriers with resistance $h/\left(e^2 g\right) = 20$ kΩ [12]. The calculated enhancement of the Gilbert damping constant is then $\alpha' = 0.004$ and the response time $\tau = 0.52$ ns. The motion of the magnetization of the free layer is depicted by Fig. 2.2 for a bias current density of $J = 10^7$ A cm^{-2} with the cross section at the electronic transport direction 400×30 nm^2 [12].

The spin pumping effect through the enhanced Gilbert damping constant reduces the saturation frequency from 2.0 to 1.2 GHz , but also the response time to reach the saturation value from 0.87 to 0.52 ns. Notice that the frequency is directly proportional to I_0 and thus in the absence of any in-plane anisotropy the frequency can be tuned continuously to zero by decreasing the bias current. The out-of-plane motion is very slow compared to the in-plane one: it decreases from 12 MHz to around 0 when the in-plane rotation approaches the saturation frequency. As shown in Fig. 2.3, within a long period the small angle approximation still holds. A larger ratio of g_3/g also gives higher frequencies. Decreasing the diameter, and thus also the volume, of the free layer gives a smaller demagnetizing factor N_z, which causes larger a response time τ according to Eq. (2.26) and increases the saturation value of the in-plane rotation frequency ω_ϕ.

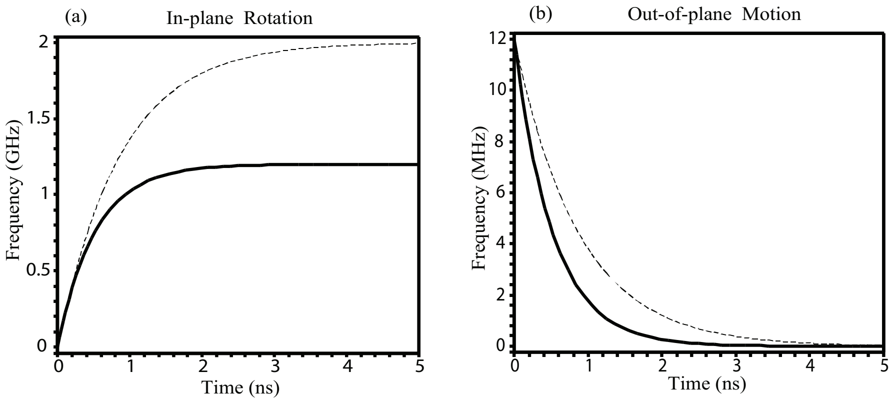

Figure 2.2: Panel (a): The in-plane rotation (in the unit of giga hertz) versus time (in nano seconds). The solid line: including spin pumping effect. The dash line: without spin pumping effect. Panel (b): The out-of-plane motion(in the unit of mega hertz) versus time (in nano seconds). The solid line: including spin pumping effect. The dash line: without spin pumping effect.

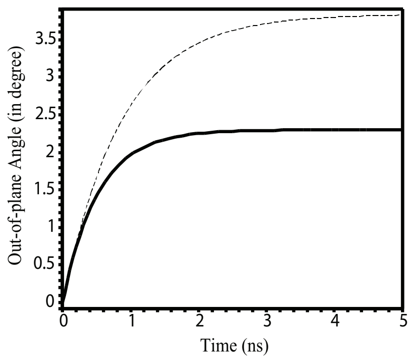

Figure 2.3: The out-plane angle θ (in degree) versus time (in nano seconds). The solid line: including spin pumping effect. The dash line: without spin pumping effect.

In-plane anisotropy

In reality, there are always residual anisotropies or pinning centers. Shape anisotropies can be introduced intentionally by fabrication of elliptic F3 discs. We consider the situation in which the free layer is slightly pinned in the plane by an anisotropy field that corresponds to an elliptic (pancake) shape of the ferromagnet. At equilibrium, the F3 magnetization is then aligned along the easy, let us say, $x-$axis. The in-plane rotation can be sustained only when the spin transfer torque overcomes the effective field generated by the shape anisotropy, hence a critical current I_c for the steady precession is expected. For an ellipse with long axis of 200 nm, thickness 5 nm and aspect ratio 0.9, the two demagnetizing factors are calculated to be $N_y = 0.0224$ and $N_x = 0.0191$. With a Gilbert damping constant $\alpha = 0.01$, the numerical simulation gives $I_c = 4.585$ mA corresponding to a current density $J_c = 3.8 \times 10^7$ A cm^{-2} (the cross section is 400×30 nm^2) [12].

These critical current densities are of the same order of magnitude as those used to excite the magnetization in spin-valve pillars. So even a relatively small anisotropy can cause a significant critical current. In order to operate the magnetic fan at small current densities, the magnetic island should be fabricated as round as possible. The magnetization responds to a current step function below the critical value by damped in-plane and out-of-plane oscillations and comes to rest at a new in-plane equilibrium angle ϕ_e with zero out-plane component (*cf.* Figs. 2.4).

At the steady state, the spin-transfer torque is balanced by the torque generated by the in-plane anisotropy, *i.e.* the angle ϕ_e is determined by

$$\sin(2\phi_e) = 2\mathcal{F}(I_0)/(\mu_0 M_s (N_y - N_x)). \tag{2.29}$$

With given bias current, smaller $|N_y - N_x|$ correspond to larger in-plane angles $|\phi_e|$. According to the theory of differential equations [22], the frequency for the damped magnetization oscillation can be found by diagonalizing the LLG equation at the "equilibrium point" given by ϕ_e, this leads to

$$\omega_\phi^< = \frac{\gamma\mu_0 M_s}{\sqrt{2}} \sqrt{(2N_z - N_x - N_y)\sqrt{\mathcal{D}(I_0)} + \mathcal{D}(I_0)}\,, \tag{2.30}$$

where

$$\mathcal{D}(I_0) = (N_y - N_x)^2 - \frac{4\mathcal{F}(I_0)^2}{\mu_0^2 M_s^2}\,. \tag{2.31}$$

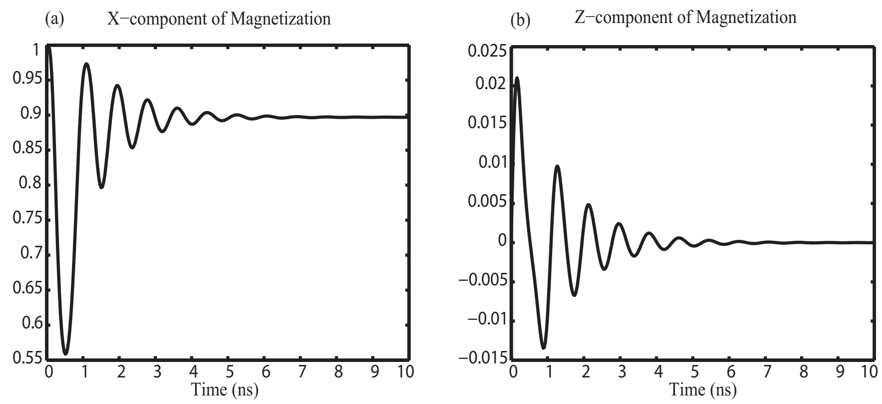

Figure 2.4: Magnetization components versus time. Panel (a): Below critical current, the x-component of magnetization versus time (in nano seconds). Panel (b): Below critical current, the z-component of magnetization versus time (in nano seconds). The bias current is 4.5 mA.

Equation (2.30) teaches us that below the critical current, decreasing the current increases the rotation frequency. Changing the damping constant does not change $\omega_\phi^<$ for a given current but only changes the response time to reach the new equilibrium.

As shown by panel (a) to (c) in Fig. 2.5 the magnetization above the critical current saturates into a steady precessional state accompanied by an oscillation of the z-component (nutation). In this situation, ϕ_e is no longer a constant of motion. Instead the new steady state is given by $m_x = m_y = 0$ and $\bar{m}_z = \mathcal{F}(I_0)/(\alpha\mu_0 M_s N_z)$. Diagonalizing the LLG around this point we derive the in-plane rotation frequency

$$\omega_\phi^> = \frac{\gamma\mathcal{F}(I_0)}{\alpha}\frac{\sqrt{(N_z - N_x)(N_z - N_y)}}{N_z}\,. \tag{2.32}$$

In the limit of vanishing in-plane anisotropy, *i.e.*, $N_x = 0$ and $N_y = 0$, we recover the previous result.

As shown by panel (d) in Fig. 2.5, the dependence of the critical current on the damping constant is different from the simple proportionality predicted for pillar structures [8]. Specifically we observe saturation of the critical current above a critical damping.

In the anisotropic case the extra power necessary for maintaining the motion generates microwaves [5, 6], which may be attractive for some applications.

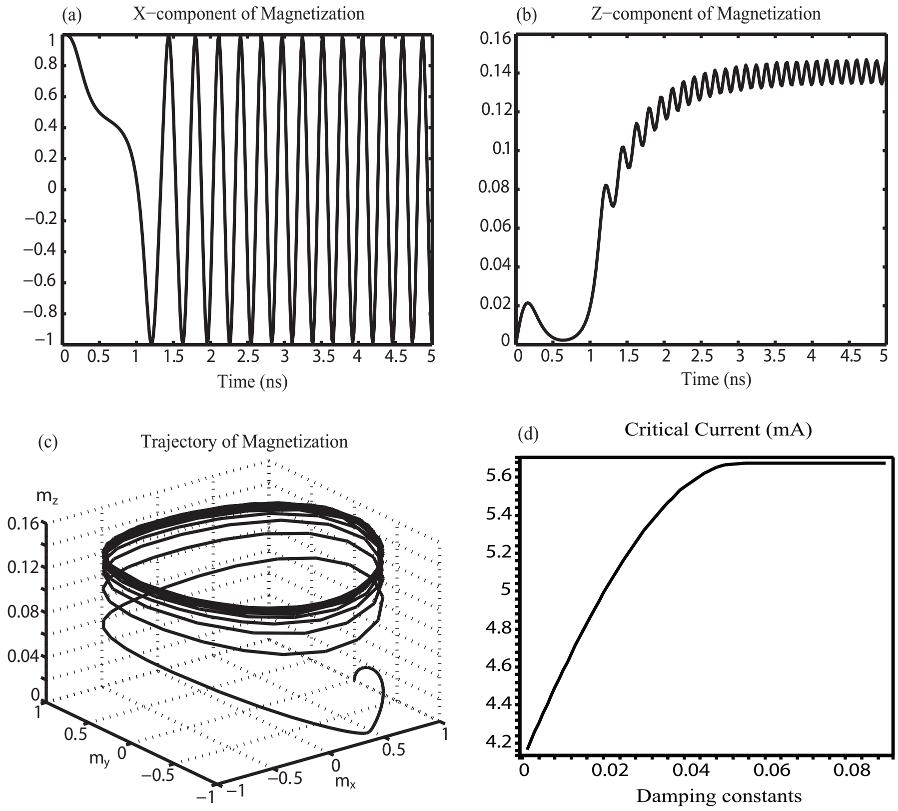

Figure 2.5: Magnetization dynamics above the critical current. (a) The x-component of magnetization versus time (in nano seconds). The bias current is 4.6 mA. The frequency is about 3.6 GHz. (b) The z-component of magnetization versus time (in nano seconds). The bias current is 4.6 mA. (c) The trajectory of magnetization within 5 nano seconds. The bias current is 4.6 mA. This picture clearly shows the steady precession of the magnetization. (d) The critical current I_c versus damping constant α. This figure shows saturation of I_c above a critical α.

2.4 Applications

Our "magnetic fan" has the advantage that the magnetization dynamics is not hidden within the structure as in the pillars, but is open to either studies of the dynamics by fast microscopy, or to the utilization of the dipolar field from the soft magnetic island. We envisage applications as magnetic actuators for nanomechanical cantilevers and nanoscale motors, as nanoscale mixers of biological or biomedical suspensions containing magnetic nanoparticles, or as magnetic resonance detectors, again possibly useful for biomedical applications.

2.4.1 Actuators

The rotating magnetization of the "magnetic fan" generates a periodic dipolar field which can be applied to actuate a nanomechanical cantilever with a (hard) ferromagnetic tip. Assuming for simplicity that the magnet F3 and the cantilever are at a sufficiently large distance the force on the cantilever magnet is given by

$$\mathbf{F} = V_c \nabla(\mathbf{M}_c \cdot \mathbf{H}_d) \,, \tag{2.33}$$

where $\mathbf{M}_c$ is the saturation magnetization and V_c is the volume of the cantilever magnet and the field $\mathbf{H}_d$ generated by a magnetic dipolar at the position $\mathbf{r}$ can be written as

$$\mathbf{H}_d = \mu_0 \frac{3(\mathbf{M} \cdot \mathbf{r})\mathbf{r} - \mathbf{M} r^2}{r^5} \,. \tag{2.34}$$

Assume a cantilever on top of the magnetic fan at a distance of 125 nm (along z-direction) [31], with beam plane parallel to the plane of the Py film F3 and magnetization along the x-axis. The saturation value of cantilever magnetization is taken as 1.27×10^6 A m^{-1}. Assuming a lateral size of the cantilever magnet [31] of 150×150 nm^2 with thickness 50 nm, the force is estimated to be

$$F = 1.1 \times 10^{-8} \cos(\omega_\phi t) \,\mathrm{N} \tag{2.35}$$

where ω_ϕ is the rotation frequency of the "magnetic fan". To efficiently generate the mechanical modes of the cantilever, the cantilever magnet should be hard enough.

Fixing other parameters, the force scales like $1/r^4$ with respect to distance r. When the two ferromagnets are closer to each other the distribution of the magnetizations increases the force over the value estimated above. We see that in the dipole-approximation, the force is already quite significant and it will be significantly larger when the the full magnetostatic energy is computed.

Generally, the torque on the cantilever may generate both flexural and torsional motion on the cantilever. The torsional motion coupled to the magnetization dynamics has been investigated for such a system [32] and the nanomechanical magnetization reversal based on the torsional modes has been proposed [33]. The coupling of a cantilever to the oscillating dipolar field will be discussed elsewhere.

2.4.2 Mixers

The dipolar field produced by our device can also be used to function as mechanical mixer for suspensions of magnetic particles. To this end we should scale down the frequency of the rotating magnetization either by decreasing the bias current or re-engineering the parameters of the device, *e.g.*, increasing the thickness of the Py film. Low saturation magnetization is detrimental in this case, since that would also reduce the usable stray fields. By these ways, one hopefully can access the kilo hertz frequency region, which is important for the hydrodynamic motion in ferrofluids [34].

2.4.3 Detectors

An external field influences the frequency of the rotation of the magnetization. Response to the change of the frequencies is the rebuilding of the spin accumulation in the normal metal hence altering the source-drain resistance R_{SD}. Due to the relation

$$\mu_0^{F1} - \mu_0^{F2} = R_{SD} I_0 \,, \tag{2.36}$$

this deviation is reflected on the source-drain voltage-current curve. This feature can be implemented as a sensor for biomedical applications in order to detect the presence of magnetic beads, which are used as labels in biosensors [35]. Furthermore, the ability to change the frequency of the "magnetic fan" should allow to measure locally the frequency dependence of the magnetic susceptibility, which offers an alternative pathway to using magnetic nanoparticles for biosensing applications [36, 37].

2.5 Conclusion

We studied the magnetization dynamics of a magnetic transistor, *i.e.*, a lateral spin valve structure with perpendicular-to-plane magnetizations and an in-plane free layer attached to the normal metal that is excited by an external current bias. By circuit theory and the Landau-Lifshitz-Gilbert equation, analytic results were obtained for the spin-transfer torque and the dynamics of the magnetization in the limit of small out-of-plane angle θ. Spin flip and spin-pumping effects were also investigated analytically and an anisotropic enhanced damping parameter in the Gilbert form was derived for the free layer magnetization. Without an externally applied magnetic field, a continuous rotation of the magnetization of the free layer at GHz frequencies can be achieved. In the lateral geometry, the free layer is no longer buried or penetrated by a dissipating charge current, thus becomes accessible for more applications. Our methods handle the microscopic details on crucial issues like spin-torque transfer efficiency, spin-flip scattering and the response time, hence offering accurate design and control. The rotation can be observed, *e.g.*, by magneto-optic methods. This new device has potential applications as high frequency generator, actuator of nanomechanical systems, biosensors, and other high-speed magnetoelectronic devices.

2.6 Appendix: Spin accumulation in a normal metal node

Here we summarize a number of complex angle dependent coefficients. The elements of the symmetric matrix $\hat{\mathbf{C}}$ in Eq.(2.16) read

$$C_{11} = \frac{\mathcal{G}_t(\mathcal{G}_1 - \mathcal{G}_4 m_x^2) - 2g(p^2 - 1 + \eta)(\mathcal{G}_t - \mathcal{G}_4 m_y^2)}{\mathcal{Q}} \tag{2.37}$$

$$C_{12} = C_{21} = \frac{\mathcal{G}_2 \mathcal{G}_4 m_x m_y}{\mathcal{Q}}, \quad \text{and} \quad C_{13} = C_{31} = \frac{\mathcal{G}_t \mathcal{G}_4 m_x m_z}{\mathcal{Q}} \tag{2.38}$$

$$C_{22} = \frac{\mathcal{G}_2(\mathcal{G}_t - \mathcal{G}_4 m_x^2) - \mathcal{G}_t \mathcal{G}_4 m_z^2}{\mathcal{Q}} \tag{2.39}$$

$$C_{23} = C_{32} = \frac{\mathcal{G}_t \mathcal{G}_4 m_y m_z}{\mathcal{Q}}, \quad \text{and} \quad C_{33} = \frac{\mathcal{G}_t(\mathcal{G}_1 + \mathcal{G}_4 m_z^2)}{\mathcal{Q}}. \tag{2.40}$$

We introduce:

$$\mathcal{G}_1 = (1 - p_3^2)(1 - \Delta_3) g_3 + 2\eta g + 2 g_{sf} \tag{2.41}$$

$$\mathcal{G}_2 = \eta_3 g_3 + 2(1 - p^2) g + 2 g_{sf} \tag{2.42}$$

$$\mathcal{G}_3 = (1 - p_3^2)(1 - \Delta_3) g_3 + 2(1 - p^2) g + 2 g_{sf} \tag{2.43}$$

$$\mathcal{G}_4 = \eta_3 g_3 - (1 - p_3^2)(1 - \Delta_3) g_3 \tag{2.44}$$

$$\mathcal{G}_t = \eta_3 g_3 + 2\eta g + 2 g_{sf} \tag{2.45}$$

$$\mathcal{Q} = \mathcal{G}_t[\mathcal{G}_t \mathcal{G}_3 + 2(p^2 - 1 + \eta) g \mathcal{G}_4 (1 - m_z^2)] \tag{2.46}$$

$$\Delta_3 = \frac{\zeta_3}{\zeta_3 + \tilde{\sigma} \tanh(d/l_{sd}^F)}\ , \tag{2.47}$$

in the limit of negligible spin flip in F, i.e., $d \ll l_{sd}^F$, then $\Delta_3 \approx 1$. The elements of the matrix in Eq.(2.17) are given by

$$\Pi_{11} = \frac{\mathcal{G}_t\mathcal{G}_3(1-m_x^2) + 2\mathcal{G}_4(p^2-1+\eta)gm_y^2}{\mathcal{Q}} \tag{2.48}$$

$$\Pi_{12} = \Pi_{21} = \frac{-\mathcal{G}_1\mathcal{G}_2 m_x m_y}{\mathcal{Q}}, \quad \text{and} \quad \Pi_{13} = \frac{-\mathcal{G}_t\mathcal{G}_1 m_x m_z}{\mathcal{Q}} \tag{2.49}$$

$$\Pi_{22} = \frac{\mathcal{G}_t\mathcal{G}_3(1-m_y^2) + 2\mathcal{G}_4(p^2-1+\eta)gm_x^2}{\mathcal{Q}} \tag{2.50}$$

$$\Pi_{23} = \frac{-\mathcal{G}_t\mathcal{G}_1 m_y m_z}{\mathcal{Q}}, \quad \text{and} \quad \Pi_{31} = \frac{-\mathcal{G}_t\mathcal{G}_3 m_x m_z}{\mathcal{Q}} \tag{2.51}$$

$$\Pi_{32} = \frac{-\mathcal{G}_t\mathcal{G}_3 m_y m_z}{\mathcal{Q}}, \quad \text{and} \quad \Pi_{33} = \frac{\mathcal{G}_t\mathcal{G}_1(1-m_z^2)}{\mathcal{Q}} \tag{2.52}$$

Bibliography

[1] J. C. Slonczewski, J. Magn. Magn. Mater. **159**, L1 (1996).

[2] L. Berger, Phys. Rev. B **54**, 9359 (1996).

[3] J. A. Katine, F. J. Albert, R. A. Buhrman, E. B. Myers, and D. C. Ralph, Phys. Rev. Lett. **84**, 3149 (2000).

[4] E. B. Myers, F. J. Albert, J. C. Sankey, E. Bonet, R. A. Buhrman, and D. C. Ralph, Phys. Rev. Lett. **89**, 196801 (2002).

[5] S. I. Kiselev, J. C. Sankey, I. N. Krivorotov, N. C. Emley, R. J. Schoelkopf, R. A. Buhrman, and D. C. Ralph, Nature (London) **425**, 380 (2003).

[6] W. H. Rippard, M. R. Pufall, S. Kaka, S. E. Russek, and T. J. Silva, Phys. Rev. Lett. **92**, 027201 (2004).

[7] A. Kent, B. Ozyilmaz, and E. del Barco, Appl. Phys. Lett. **84**, 3897 (2004).

[8] K. J. Lee, O. Redon, and B. Dieny, Appl. Phys. Lett. **86**, 022505 (2005).

[9] H. Xi, K. Z. Gao, and Y. Shi, J. Appl. Phys. **97**, 044306 (2005).

[10] F. J. Jedema, A. T. Filip, and B. J. van Wees, Nature (London) **410**, 345 (2001).

[11] F. J. Jedema, H. B. Heersche, A. T. Filip, J. J. A. Baselmans, and B. J. van Wees, Nature (London) **416**, 713 (2002).

[12] M. Zaffalon and B. J. van Wees, Phys. Rev. Lett. **91**, 186601 (2003).

[13] T. Kimura, J. Hamrle, Y. Otani, K. Tsukagoshi, and A. Aoyagi, Appl. Phys. Lett. **85**, 3501 (2004).

[14] S. O. Valenzuela and M. Tinkham, Appl. Phys. Lett. **85**, 5914 (2004).

[15] Y. Ji, A. Hoffmann, J. S. Jiang, and S. D. Bader, Appl. Phys. Lett. **85**, 6218 (2004).

[16] G. E. W. Bauer, A. Brataas, Y. Tserkovnyak, and B. J. van Wees, Appl. Phys. Lett. **82**, 3928 (2003).

[17] E. Saitoh, H. Miyajima, T. Yamaoka, and G. Tatara, Nature (London) **432**, 203 (2004).

[18] J. Grollier, M. V. Costache, C. H. van der Wal, and B. J. van Wees, J. Appl. Phys. **100**, 024316 (2006) [cond-mat/0502197].

[19] T. Kimura, Y. Otani, and J. Hamrle, Phys. Rev. Lett. **97** 037201 (2006) [cond-mat/0508559].

[20] A. Brataas, Y. V.Nazarov, and G. E. W. Bauer, Phys. Rev. Lett. **84**, 2481 (2000).

[21] P. F. Carcia, J. Appl. Phys. **63**, 5066 (1988).

[22] Y. Tserkovnyak, A. Brataas, and G. E. W. Bauer, Phys. Rev. Lett. **88**, 117601 (2002).

[23] Y. Tserkovnyak, A. Brataas, G. E. W. Bauer, and B. I. Halperin, Rev. Mod. Phys. **77** 1375 (2005) [cond-mat/0409242].

[24] I. N. Krivorotov, N. C. Emley, J. C. Sankey, S. I. Kiselev, D. C. Ralph, and R. A. Buhrman, Science **307**, 228 (2005).

[25] J. Xiao, A. Zangwill, and M. D. Stiles, Phys. Rev. B **72**, 014446 (2005).

[26] A. Brataas, Y. V. Nazarov, and G. E. W. Bauer, Eur. Phys. J. B **22**, 99 (2001).

[27] J. A. Osborn, Phys. Rev. **67**, 351 (1945).

[28] X. Wang and G. E. W. Bauer, unpublished (2004).

[29] A. Kovalev, G. E. W. Bauer, and A. Brataas, Phys. Rev. B **73**, 054407 (2006) [cond-mat/0504705].

[30] L. Perko, *Differential Equations and Dynamical Systems* (Springer, Berlin, 1996), 2nd ed.

[31] D. Rugar, R. Budakian, H. J. Mamin, and B. W. Chui, Nature(London) **430**, 329 (2004).

[32] A. A. Kovalev, G. E. W. Bauer, and A. Brataas, Appl. Phys. Lett. **83**, 1584 (2003).

[33] A. A. Kovalev, G. E. W. Bauer, and A. Brataas, Phys. Rev. Lett. **94**, 167201 (2005).

[34] M. I. Shliomis and V. I. Stepanov, Adv. Chem. Phys. **87**, 1 (1994).

[35] D. R. Baselt, G. U. Lee, M. Natesan, S. W. Metzger, P. E. Sheehan, and R. J. Colton, Biosens. Bioelectron. **13**, 731 (1998).

[36] J.Connoly and T. G. St Pierre, J. Magn. Magn. Mater. **225**, 156 (2001).

[37] S. H. Chung, A. Hoffmann, S. D. Bader, C. Liu, B.Kay, L. Makowski, and L. Chen, Appl. Phys. Lett. **85**, 2971 (2004).

Chapter 3

Controlled Magnetization Dynamics and Thermal Stability

Abstract

The current-driven magnetization dynamics of a thin-film, three-magnetic-terminal device (spin-flip transistor) is investigated theoretically. We consider a magnetization configuration in which all magnetizations are in the device plane, with source-drain magnetizations chosen fixed and antiparallel, whereas the third contact magnetization is allowed to move in a weak anisotropy field that guarantees thermal stability of the equilibrium structure at room temperature. We analyze the magnetization dynamics of the free layer under a dc source-drain bias current within the macrospin model and magneto-electronic circuit theory. A new tunable two-state behavior of the magnetization is found and the advantages of this phenomenon and potential applications are discussed. [1]

3.1 Introduction

The current induced magnetization excitation predicted by Slonczewski and Berger [1, 2] has attracted considerable attention and the prediction of current-induced magnetization reversal has been confirmed by many experiments in nano-pillar structure consisting of two ferromagnetic layers with a high ("fixed") and a low ("free") coercivity, separated by a normal metal spacer [3, 4, 5, 6]. Meanwhile, the investigations of charge and spin transport in thin-film metallic conductors structured on a planar substrate have also been carried out [7, 8, 12, 9, 10, 11]. The advantages of the planar structures are the flexible design and the relative ease to fabricate multi-terminal structures [13]. Recently, non-local magnetization switching in a lateral

[1] This chapter has been published as: Xuhui Wang, *et al.*, *Current-Controlled Magnetization Dynamics in the Spin-Flip Transistors*, Jpn. J. Appl. Phys. **45**, 3863 (2006).

spin valve structure has been demonstrated [14]. In the present chapter we present a theoretical study of the dynamics of a lateral spin-valve consisting of a normal-metal film that is contacted by two magnetically hard ferromagnets. As sketched in Fig. 2.1, a slightly elliptic and magnetically soft ferromagnetic film is assumed deposited on top of the normal metal to form a spin-flip transistor [15]. The magnetization direction of the source-drain contacts lies antiparallel to each other in the plane of the magnetization of the third (free) layer. The configuration in which the source-drain contact magnetizations are oriented perpendicular to the plane is considered elsewhere [16]. A convenient and accurate tool to study the dynamic properties of our device is the magnetoelectronic circuit theory (MECT) for charge and spin transport [15] combined with the Landau-Lifshitz-Gilbert equation in the macrospin model. The spin flip scattering in normal and ferromagnetic metals and the spin-pumping effect are also taken into account [17, 18].

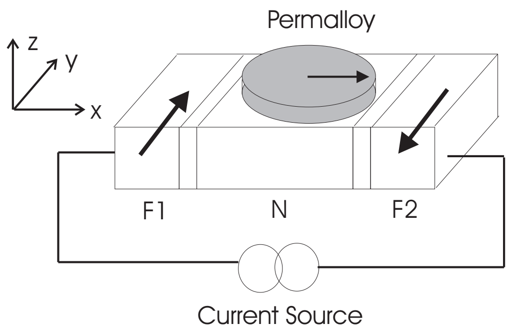

Figure 3.1: The model system contains a normal metal sandwiched by two ferromagnetic leads and a circular soft ferromagnet film (e.g., permalloy) on top of the normal metal. The magnetization unit vectors $\mathbf{m}_1$, $\mathbf{m}_2$, and $\mathbf{m}_3$ are initially aligned in the same, i.e., $x-y$ plane.

The article is organized as the follows: In Sec. 3.2, we briefly review the MECT and Landau-Lifshitz-Gilbert equation for the macrospin model. In Sec. 3.3, calculations of the spin transfer torque for our device are presented. Section 3.4 is devoted to the discussion of thermal (in)stability and in Sec. 3.5 the magnetization dynamics is treated. The conclusions are summarized in Sec. 3.6.

3.2 Magneto-electronic circuit theory

We first consider a ferromagnet-normal metal (F|N) interface at quasi-equilibrium. The ferromagnet at a chemical potential μ_0^F and spin accumulation $\mu_s^F \mathbf{m}$ aligned along the magnetization direction. The chemical potential and spin accumulation in the normal metal are denoted by μ_0^N and vector $\mathbf{S}$. The charge current I_c (in the unit of Ampere) and the spin current $\mathbf{I}_s$ (in the unit of Joule) entering the normal metal node are given by [15],

$$\begin{aligned} I_c =& \frac{e}{2h}\left[2g(\mu_0^F - \mu_0^N) + pg\mu_s^F - pg\,(\mathbf{S}\cdot\mathbf{m})\right] \\ \mathbf{I}_s =& \frac{g}{8\pi}[2p(\mu_0^F - \mu_0^N) + \mu_s^F - (1-\eta_r)(\mathbf{S}\cdot\mathbf{m})]\mathbf{m} \\ &- \frac{\eta_r g}{8\pi}\mathbf{S} - \frac{\eta_i g}{8\pi}(\mathbf{S}\times\mathbf{m})\,. \end{aligned} \tag{3.1}$$

From eq. (3.1) we may project out the component of $\mathbf{I}_s$ that is perpendicular to the magnetization direction and governs the spin transfer torque [1, 15]

$$-\mathbf{m}\times\mathbf{I}_s\times\mathbf{m} = \frac{\eta_r g}{8\pi}[\mathbf{S} - (\mathbf{S}\cdot\mathbf{m})\mathbf{m}] + \frac{\eta_i g}{8\pi}(\mathbf{S}\times\mathbf{m})\,. \tag{3.2}$$

In the above notations, the dimensionless total conductance $g = g^{\uparrow} + g^{\downarrow}$ and the mixing conductance are given by Landauer-Büttiker formulae, i.e.,

$$\begin{aligned} g^{\uparrow(\downarrow)} &= M - \sum_{nm} |r^{nm}_{\uparrow(\downarrow)}|^2\,, \\ g^{\uparrow\downarrow} &= M - \sum_{nm} r^{nm}_{\uparrow}(r^{nm}_{\downarrow})^*\,. \end{aligned} \tag{3.3}$$

where $r^{nm}_{\uparrow(\downarrow)}$ is the probability of a spin up(down) electron in mode m reflected into mode n in the normal metal and M is the total number of channels. The contact polarization is defined by $p = (g^{\uparrow} - g^{\downarrow})/(g^{\uparrow} + g^{\downarrow})$. The pumping current generated by the motion of the magnetization is [17]

$$\mathbf{I}_s^{(p)} = \frac{\hbar g}{8\pi}\left(\eta_r \mathbf{m}\times\frac{d\mathbf{m}}{dt} + \eta_i\frac{d\mathbf{m}}{dt}\right)\,. \tag{3.4}$$

We consider the situation in which the dimension of the normal metal is smaller than the spin-flip length, so that the spin accumulation does not vary spatially in the node.

$$\mathbf{I}_s^{(f)} = \frac{g_f}{4\pi}\mathbf{S} \tag{3.5}$$

where $g_f = h\nu_{DOS}\mathrm{V}_N/\tau_f^N$, ν_{DOS} and V_N are the density of states of the electrons and the volume of the normal metal, τ_f^N is the spin-flip relaxation time in the normal metal node. The charge and spin currents entering the normal metal obey the conservation laws

$$\sum_i I_{c,i} = 0, \qquad \sum_i \left(\mathbf{I}_{s,i} + \mathbf{I}_{s,i}^{(p)}\right) = \mathbf{I}_s^{(f)} . \tag{3.6}$$

3.3 Spin-transfer torque

In the structure depicted in Fig. 3.1, the source-drain magnetizations are aligned anti-parallel along the y-axis in order to inject a large spin accumulation into N, i.e., $\mathbf{m}_1 = (0, +1, 0)$ and $\mathbf{m}_2 = (0, -1, 0)$. Connecting the ferromagnets to reservoirs and applying a bias current I_0 via the two ferromagnetic leads, the conservation of charge current dictates that $I_{c,1} = I_0$ and $I_{c,2} = -I_0$ at the F1|N and F2|N interfaces, which gives

$$\mu_0^{F1} - \mu_0^N = -(\mu_0^{F2} - \mu_0^N) = \frac{I_0 h}{ge} + \frac{1}{2} p S_y . \tag{3.7}$$

The free layer is electrically floating, hence there is no net charge current flowing through F3|N interface, $I_{c,3} = 0$. The spin accumulation in the free layer $\mu_s^F = \mu_\uparrow - \mu_\downarrow$, directed along magnetization $\mathbf{m}_3$, is governed by the spin diffusion equation [11],

$$\frac{\partial^2 \mu_s^F(z)}{\partial z^2} = \frac{\mu_s^F(z)}{l_{sd}^2} \tag{3.8}$$

which satisfies the following boundary conditions. At the interface the continuity of longitudinal spin current dictates

$$\sigma_\uparrow \left(\frac{\partial \mu_\uparrow}{\partial z}\right)_{z=0} - \sigma_\downarrow \left(\frac{\partial \mu_\downarrow}{\partial z}\right)_{z=0} = \frac{2e^2}{\hbar A} \mathbf{I}_{s,3} \cdot \mathbf{m}_3 \tag{3.9}$$

and the vanishing spin current at the end of the ferromagnet implies

$$\sigma_\uparrow \left(\frac{\partial \mu_\uparrow}{\partial z}\right)_{z=d} - \sigma_\downarrow \left(\frac{\partial \mu_\downarrow}{\partial z}\right)_{z=d} = 0 . \tag{3.10}$$

The solution of eq. (3.8) reads

$$\mu_s^F(z) = \frac{\zeta_3 \cosh(\frac{z-d}{l_{sd}})\mathbf{m}_3 \cdot \mathbf{S}}{\left[\zeta_3 + \tilde{\sigma}\tanh(\frac{d}{l_{sd}})\right]\cosh(\frac{d}{l_{sd}})} \tag{3.11}$$

where $\zeta_3 = g_3(1-p_3^2)/8\pi$ characterizes the contact F3|N and $\tilde{\sigma} = \hbar A \sigma_\uparrow \sigma_\downarrow/(e^2 l_{sd}(\sigma_\uparrow + \sigma_\downarrow))$ describes the bulk properties of the free layer with arbitrary $\mathbf{m}_3$. The conservation of spin currents in eq. (3.6) generates three linear equations that determine the spin accumulation $\mathbf{S}$ in the normal metal as

$$\mathbf{S} = \hat{\mathbf{\Pi}}(g, g_3)\left(8\pi \mathbf{I}_s^{(p)} + \mathbf{W}_b\right) \tag{3.12}$$

where the vector $\mathbf{W}_b = (0, 2hpI_0/e, 0)$ is the contribution from the bias current and the elements of the symmetric matrix $\hat{\mathbf{\Pi}}(g, g_3)$ is listed in the Appendix. Equation (3.2) determines the spin transfer torque acting on the free layer magnetization, which can be arranged as

$$\mathbf{L} = \frac{\eta_3 g_3}{8\pi}\hat{\mathbf{\Gamma}}(g, g_3)\left(8\pi \mathbf{I}_s^{(p)} + \mathbf{W}_b\right) \tag{3.13}$$

and the components of the matrix $\hat{\mathbf{\Gamma}}(g, g_3)$ are listed in the Appendix.

3.4 Thermal stability

The spin transfer torque rotates the magnetization out of the equilibrium hence increasing the magneto-static energy E_{MS}. The initial magnetization is stable against thermal fluctuations when

$$\Delta E_{\mathrm{MS}} > k_B T, \tag{3.14}$$

where k_B is the Boltzmann constant and T the temperature. For an elliptic permalloy film, disregarding any residual crystalline anisotropy, the effective field due to the shape anisotropy can be written as

$$\mathbf{H}_e = -\mu_0 M_s (N_x m_x, N_y m_y, N_z m_z)\,, \tag{3.15}$$

introducing the saturation magnetization M_s and demagnetizing factors N_x, N_y and N_z [19]. When the magnetization is slightly out of plane, the difference between the magneto-static energy for magnetizations along the hard-axis and easy-axis reads $\Delta E_{\text{MS}} = \mu_0 V M_s^2 (N_y - N_x)/2$. For a very flat ellipsoid (the thickness is much smaller than the lateral dimensions) and slight ellipticity (large aspect ratio $\xi \approx 1$), we can expand the demagnetizing factors at $\xi = 1$ such that

$$N_y - N_x = \frac{\pi d}{4a} \frac{(\xi^2 + 4\xi + 1)(1 - \xi)}{\xi(\xi + 1)^2}\,, \tag{3.16}$$

where a, b and d are the lengths of easy-axis, hard axis and the thickness of the permalloy film. The aspect ratio is defined as $\xi = b/a$. The requirement $\Delta E_{\text{MS}} > k_B T$ gives

$$\frac{(\xi^2 + 4\xi + 1)(1 - \xi)}{(\xi + 1)^2} > \frac{8 k_B T}{\mu_0 M_s^2 \pi^2 a d^2}\,. \tag{3.17}$$

The saturation magnetization of permalloy is $M_s = 8 \times 10^5$ A m^{-1}. For thickness $d = 5$ nm and easy axis $a = 200$ nm [12], the right hand side of eq. (3.17) is at room temperature approximately $\epsilon = 8.36 \times 10^{-3}$ and therefore stability requires that

$$\xi \leq 1 - \frac{2}{3}\epsilon\,, \tag{3.18}$$

which suggests that even for almost circular permalloy discs, e.g., $\xi = 0.9$, thermal fluctuations around the equilibrium configuration are small.

3.5 Controlled magnetization dynamics

Here we focus on the free layer magnetization dynamics in the macrospin model. The Landau-Lifshitz-Gilbert (LLG) equation modified by the spin transfer torque [eq. (3.13)] reads

$$\frac{1}{\gamma}\frac{d\mathbf{m}}{dt} = -\mathbf{m} \times \mathbf{H}_e + \frac{\alpha_0}{\gamma}\mathbf{m} \times \frac{d\mathbf{m}}{dt} + \frac{1}{V M_s}\mathbf{L}\,. \tag{3.19}$$

Included in the torque term, i.e., Eq. (3.13), an expression

$$\overleftrightarrow{\alpha}' \equiv \frac{\gamma \hbar \eta_3^2 g_3^2}{8\pi V M_s}\hat{\mathbf{\Gamma}}(g, g_3) \tag{3.20}$$

appears as an enhancement of the Gilbert damping [17], which depends on the direction of the magnetization and shows tensor property of the pumping induced damping enhancement [21]. When the conductance at the F3|N contact is much larger than the source-drain contacts and the spin flip in the normal metal is negligible, i.e., $g_3 \gg g$ and $g_3 \gg g_{sf}$, the tensor $\overleftrightarrow{\alpha}'$ converges to [21]

$$\frac{\gamma\hbar \mathrm{Re} g_3^{\uparrow\downarrow}}{4\pi V M_s} \begin{pmatrix} 1-m_x^2 & -m_x m_y & -m_x m_z \\ -m_x m_y & 1-m_y^2 & -m_y m_z \\ -m_x m_z & -m_y m_z & 1-m_z^2 \end{pmatrix}, \tag{3.21}$$

which in the LLG equation reduces to a diagonal matrix

$$\overleftrightarrow{\alpha}' = \frac{\gamma\hbar \mathrm{Re} g_3^{\uparrow\downarrow}}{4\pi V M_s} \hat{\mathbf{1}} \tag{3.22}$$

and the coefficient in front of the matrix is exactly the value derived for the single F|N junction [17]. In the same limit, the bias-driven term of the torque reads,

$$\frac{1}{V M_s} \mathbf{L}_b = \frac{\hbar p I_0}{2 V M_s |e|} \begin{pmatrix} -m_x m_y \\ 1-m_y^2 \\ -m_y m_z \end{pmatrix}. \tag{3.23}$$

In the following discussions, we denote the enhanced Gilbert damping parameter as $\alpha = \alpha_0 + \alpha'$, where α' is the diagonal entry in Eq.(3.22). The LLG equation then reads

$$\frac{1}{\gamma}\frac{d\mathbf{m}}{dt} = -\mathbf{m} \times \mathbf{H}_e + \frac{\alpha}{\gamma}\mathbf{m} \times \frac{d\mathbf{m}}{dt} + \frac{1}{V M_s}\mathbf{L}_b\,. \tag{3.24}$$

For ultrathin permalloy films, without external field and crystalline anisotropy, the magnetization is confined in the plane by the shape anisotropy field given by Eq. (3.15). Equation (3.24) is a nonlinear differential equation that can be reformulated as

$$\frac{d\mathbf{m}}{dt} = \mathbf{f}(\mathbf{m}, I_0) \tag{3.25}$$

where $\mathbf{f}(\mathbf{m}, I_0)$ is a vector function of magnetization $\mathbf{m}$ and bias current I_0. According to the theory of differential equations [22], we find two "equilibrium points" at which $d\mathbf{m}/dt$ vanishes

$$\tilde{\mathbf{m}}_1 = (1, 0, \hbar p I_0/[2e\mu_0 V M_s^2 (N_z - N_x)])$$

and $\tilde{\mathbf{m}}_2 = (0, 1, 0)$. Expanding Eq. (3.24) at point $\tilde{\mathbf{m}}_2$ and keeping only the first-oder derivatives with respect to the magnetization, i.e.,

$$\frac{d\mathbf{m}}{dt} \approx \left(\frac{\partial \mathbf{f}}{\partial \mathbf{m}}\right)_{\tilde{\mathbf{m}}_2}, \tag{3.26}$$

where $\partial \mathbf{f}/\partial \mathbf{m}$ is a matrix with elements given by $\partial f_i/\partial m_j$. Equation (3.26) has non-zero solution when

$$\det\left[\left(\frac{\partial \mathbf{f}}{\partial \mathbf{m}}\right)_{\tilde{\mathbf{m}}_2}\right] = 0\,. \tag{3.27}$$

This determines the critical current that is necessary to obtain the maximum in-plane rotation, i.e., $\pi/2$:

$$I_c = \frac{2e\mu_0 V M_s^2 \sqrt{(N_z - N_y)(N_y - N_x)}}{\hbar p} \tag{3.28}$$

The LLG equation augmented by the spin transfer torque for the present configuration suggests a two-state behavior of the magnetization: Below the critical current I_c, the magnetization is pushed out of the initial position (easy axis), then undergoing damped precessions and finally stops along the easy axis but with a small z-component, i.e., the equilibrium given by $\tilde{\mathbf{m}}_1$. At that position, the demagnetizing field is balanced by the spin torque. Above the critical current, the magnetization precesses out of the easy axis and rotates to the hard axis without any precession.

We simulate the magnetization dynamics for a polarization $p = 0.4$ of the F3|N and a real part of the mixing conductance $\mathrm{Re}g_3^{\uparrow\downarrow}A^{-1} = 4.1 \times 10^{15}$ cm^2 [10]. The long semi-axis, short semi-axis and the thickness of the permalloy island are $a = 200$ nm, $b = 190$ nm, and $d = 5$ nm, respectively. The calculated demagnetizing factors are $N_y = 0.0224$ and $N_x = 0.0191$ [19]. The single-spin density of states in the normal metal is $\nu_{DOS} = 2.4 \times 10^{28}$ eV^{-1}m^{-3} [12]. The bulk value of the Gilbert damping parameter is $\alpha_0 = 0.006$ and the calculated enhancement of Gilbert damping is $\alpha' = 0.015$ [17]. According to Eq. (3.28), for the above dimensions, the critical current to achieve $\phi = \pi/2$ is $I_c = 139$ mA, which agrees well with the numerical results. Below the critical current, e.g., $I_0 = 30$ mA, the equilibrium z-component determined by the expression of $\tilde{\mathbf{m}}_1$is 0.0087, which also agrees with the numerical results shown in panel (b) of Fig. 3.2. The trajectory of the magnetization when suddenly switching on the bias current $I_0 = 30$ mA is depicted in panel (c) of Fig. 3.2. The magnetization starts from the easy axis (point **I** in the figure), undergoes a damped oscillation and finally stops at point **F**, where the spin transfer torque induced by the spin accumulation in the normal metal is balanced by the torque generated by the anisotropy field. The panel (f) of Fig. 3.2 shows the trajectory of the magnetization under switching on a the bias current $I_0 = 160$ mA, which is above the critical current. Panels (d) and (e) of Figures 3.2 are the time dependence of the

y and z-components of the free layer magnetization. These figures indicate that the magnetization response to a large current is close to a step function. A smaller size of the permalloy film requires a smaller critical current, as indicated by Eq. (3.28). In the above simulation, we did not take into account the effect of a finite RC time for switching on the bias current. A longer rising time of the bias current implies that it takes longer before the magnetization reaches the steady state position. But the magnitude of the critical current does not depend on how the bias current transient.

We finally note that with the dimensions chosen here, the bias currents generate a significant in-plane Ørsted field that may interfere with the spin-torque effect. It can be avoided, e.g., by spatially separating the free layer from the current path (but within the spin-flip diffusion) [14] or by generating a neutralizing Ørsted field by a neighboring circuit (suggested by Siegmann).

The advantage of the proposed device mainly comes from the two-state behavior separated by the critical current, which can be utilized as the 0 and 1 states in current controlled memory elements. We notice that after the magnetization being switched to the hard axis, only small current is needed to maintain the position stable against thermal fluctuations. Another possible application could be the implementation of such device into spin-torque transistors [13] to achieve the gain of current since the angle of the magnetization in the above device is tunable by the bias. The magnetization can be also used as a spin battery that is "charged" in the high energy state (hard axis) and relaxes a spin current into the normal metal when relaxing to the ground state (easy axis). The induced spin accumulation then creates voltage difference over the source and drain contacts.

3.6 Conclusions

In this article, the magnetization dynamics of a spin-flip transistor has been studies in the macrospin Landau-Lifshitz-Gilbert equation combined with magneto-electronic circuit theory. We found a two-state behavior of the free layer magnetization controlled by the current induced spin transfer torque and spin pumping. The two regimes are separated by a critical current, below which the magnetization undergoes a damped oscillation and stops along the easy axis with small z-component. Above the critical current, the magnetization rotates to the hard (y-) axis without precession. The critical current is found to depend on the size of the free layer, the aspect ratio of the ellipsoid, and the source-drain contact polarizations. The thermal instability analysis indicates that at room temperature the predicted effects are visible even for very large aspect ratios.

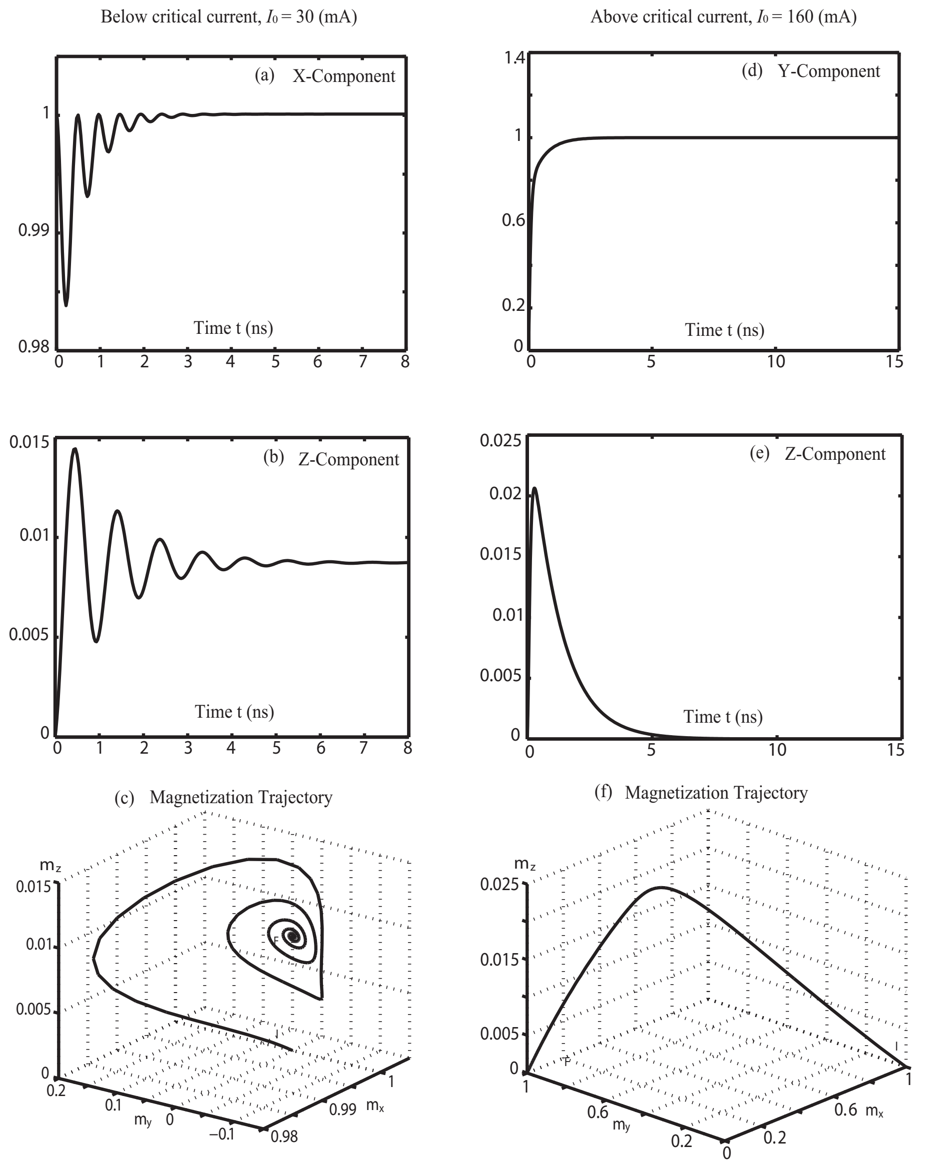

Figure 3.2: The magnetization dynamics under different bias current. Left panels (*a* to *c*): The bias current is below the critical value, *i.e.* $I_0 = 30$ mA. (*a*) The x-component of the magnetization vs time (in ns). (*b*) The z-component of the magnetization vs time (in ns). (*c*) The trajectory of the magnetization with the bias current $I_0 = 30$ mA that is below the critical current. The magnetization initially aligned along easy axis (x-axis) and after the damped oscillation it stops along the easy axis with small out-of-plane component. Right panels (*d* to *f*): The bias current is above the critical value, *i.e.* $I_0 = 160$ mA. (*d*) The y-component of the magnetization vs time. (*e*) The z-component of the magnetization vs time. (*f*) The trajectory of the magnetization under the bias above the critical current, $I_0 = 160$ mA. The magnetization initially aligned along easy axis (point **I**).

3.7 Appendix: Spin accumulation and spin transfer torque

The elements of the symmetric matrix $\hat{\mathbf{\Pi}}(g, g_3)$ in eq. (3.12) are listed in the following

$$\begin{aligned}
\mathbf{\Pi}_{11} =& [\eta_3 g_3 + 2g_{\mathrm{sf}} + 2(1-p^2)g] \\
& \times [2\eta g + \eta_3 g_3 + 2g_{\mathrm{sf}} - g_3(\eta_3 - (1-p_3^2)(1-\Delta_3))m_z^2]/\mathcal{G} \\
& - (2\eta g + \eta_3 g_3 + 2g_{\mathrm{sf}})g_3[\eta_3 - (1-p_3^2)(1-\Delta_3)]m_y^2/\mathcal{G} && (3.29) \\
\mathbf{\Pi}_{12} =& \mathbf{\Pi}_{21} = (2\eta g + \eta_3 g_3 + 2g_{\mathrm{sf}})g_3 \\
& \qquad \times [\eta_3 - (1-p_3^2)(1-\Delta_3)]m_x m_y/\mathcal{G} && (3.30) \\
\mathbf{\Pi}_{13} =& \mathbf{\Pi}_{31} = [\eta_3 g_3 + 2g_{\mathrm{sf}} + 2(1-p^2)g]g_3 \\
& \qquad \times [\eta_3 - (1-p_3^2)(1-\Delta_3)]m_x m_z/\mathcal{G} && (3.31) \\
\mathbf{\Pi}_{22} =& (2\eta g + \eta_3 g_3 + 2g_{\mathrm{sf}})\,[2\eta g + \eta_3 g_3 + 2g_{\mathrm{sf}} \\
& -g_3(\eta_3 - (1-p_3^2)(1-\Delta_3))(m_x^2 + m_z^2)\big]\,/\mathcal{G} && (3.32) \\
\mathbf{\Pi}_{23} =& \mathbf{\Pi}_{32} = (2\eta g + \eta_3 g_3 + 2g_{\mathrm{sf}})g_3 \\
& \qquad \times [\eta_3 - (1-p_3^2)(1-\Delta_3)]m_y m_z/\mathcal{G} && (3.33) \\
\mathbf{\Pi}_{33} =& [\eta_3 g_3 + 2g_{\mathrm{sf}} + 2(1-p^2)g] \\
& \times [2\eta g + \eta_3 g_3 + 2g_{\mathrm{sf}} - g_3(\eta_3 - (1-p_3^2)(1-\Delta_3))m_x^2]/\mathcal{G} \\
& - (2\eta g + \eta_3 g_3 + 2g_{\mathrm{sf}})g_3[\eta_3 - (1-p_3^2)(1-\Delta_3)]m_y^2/\mathcal{G} && (3.34)
\end{aligned}$$

where we have introduced the following notation for the common denominator

$$\begin{aligned}
\mathcal{G} =& (2\eta g + \eta_3 g_3 + 2g_{\mathrm{sf}}) \\
& \times [(\eta_3 g_3 + 2g - 2p^2 g + 2g_{\mathrm{sf}})(2\eta g + 2g_{\mathrm{sf}} + (1-p_3^2)(1-\Delta_3)g_3) \\
& + 2(p^2 - 1 + \eta)g(\eta_3 - (1-p_3^2)(1-\Delta_3))g_3 m_y^2]\,, && (3.35)
\end{aligned}$$

and $\Delta_3 = \frac{\zeta_3}{\zeta_3 + \tilde{\sigma}\tanh(d/l_{\rm sd})}$. The matrix contained in the expression of spin transfer torque eq. (3.13) has the following components

$$\begin{aligned}
\mathbf{\Gamma}_{11} = &[\eta_3 g_3 + 2g_{\rm sf} + 2(1-p^2)g] \\
&\times [2\eta g + \eta_3 g_3 + 2g_{\rm sf} - g_3(\eta_3 - (1-p_3^2)(1-\Delta_3))m_z^2]/\mathcal{G} \\
&- (2\eta g + \eta_3 g_3 + 2g_{\rm sf})\left[(\eta_3 - (1-p_3^2)(1-\Delta_3))g_3 m_y^2\right. \\
&\qquad\qquad \left. + (\eta_3 g_3 + 2g_{\rm sf} + 2(1-p^2)g)m_x^2\right]/\mathcal{G} \qquad (3.36)\\
\mathbf{\Gamma}_{12} = &-(2\eta g + \eta_3 g_3 + 2g_{\rm sf}) \\
&\times [2\eta g + 2g_{\rm sf} + (1-p_3^2)(1-\Delta_3)g_3]m_x m_y/\mathcal{G} \qquad (3.37)\\
\mathbf{\Gamma}_{13} = &-[\eta_3 g_3 + 2g_{\rm sf} + 2(1-p^2)g] \\
&\times [2\eta g + 2g_{\rm sf} + (1-p_3^2)(1-\Delta_3)g_3]m_x m_z/\mathcal{G} \qquad (3.38)\\
\mathbf{\Gamma}_{21} = &-(2\eta g + \eta_3 g_3 + 2g_{\rm sf}) \\
&\times [2g_{\rm sf} + 2(1-p^2)g + (1-p_3^2)(1-\Delta_3)g_3]m_x m_y/\mathcal{G} \qquad (3.39)\\
\mathbf{\Gamma}_{22} = &(2\eta g + \eta_3 g_3 + 2g_{\rm sf}) \\
&\times [2\eta g + 2g_{\rm sf} + (1-p_3^2)(1-\Delta_3)g_3](1-m_y^2)/\mathcal{G} \qquad (3.40)\\
\mathbf{\Gamma}_{23} = &-(2\eta g + \eta_3 g_3 + 2g_{\rm sf}) \\
&\times [2g_{\rm sf} + 2(1-p^2)g + (1-p_3^2)(1-\Delta_3)g_3]m_y m_z/\mathcal{G} \qquad (3.41)\\
\mathbf{\Gamma}_{31} = &-[\eta_3 g_3 + 2g_{\rm sf} + 2(1-p^2)g] \\
&\times [2\eta g + 2g_{\rm sf} + (1-p_3^2)(1-\Delta_3)g_3]m_x m_z/\mathcal{G} \qquad (3.42)\\
\mathbf{\Gamma}_{32} = &-(2\eta g + \eta_3 g_3 + 2g_{\rm sf}) \\
&\times [2\eta g + 2g_{\rm sf} + (1-p_3^2)(1-\Delta_3)g_3]m_y m_z/\mathcal{G} \qquad (3.43)\\
\mathbf{\Gamma}_{33} = &[\eta_3 g_3 + 2g_{\rm sf} + 2(1-p^2)g] \\
&\times [2\eta g + \eta_3 g_3 + 2g_{\rm sf} - g_3(\eta_3 - (1-p_3^2)(1-\Delta_3))m_x^2]/\mathcal{G} \qquad (3.44)\\
&- (2\eta g + \eta_3 g_3 + 2g_{\rm sf})\left[(\eta_3 - (1-p_3^2)(1-\Delta_3))g_3 m_y^2\right. \\
&\qquad\qquad \left. + (\eta_3 g_3 + 2g_{\rm sf} + 2(1-p^2)g)m_z^2\right]/\mathcal{G}\,. \qquad (3.45)
\end{aligned}$$

Bibliography

[1] J. C. Slonczewski, J. Magn. Magn. Mater. **159** L1 (1996).

[2] L. Berger, Phys. Rev. B **54** 9359 (1996).

[3] J. A. Katine, F. J. Albert, R. A. Buhrman, E. R. Myers, and D. C. Ralph, Phys. Rev. Lett. **84** 3149 (2000).

[4] E. B. Myers, F. J. Albert, J. C. Sankey, E. Bonet, R. A. Buhrman, and D. C. Ralph, Phys. Rev. Lett. **89** 195801 (2000).

[5] S. I. Kiselev, J. C. Sankey, I. N. Krivorotov, N. C. Emley, R. J. Schoelkopf, R. A. Buhrman, and D. C. Ralph, Nature **425** 380 (2003).

[6] W. H. Rippard, M. R. Pufall, S. Kaka, S. E. Russek, and T. J. Silva, Phys. Rev. Lett. **92** 027201 (2004).

[7] F. J. Jedema, A. T. Filip, and B. J. van Wees, Nature **410** 345 (2001).

[8] F. J. Jedema, H. B. Heersche, A. T. Filip, J. J. A. Baselmans, and B. J. van Wees, Nature **416** 713 (2002).

[9] T. Kimura, J. Hamrle, Y. Otani, K. Tsukagoshi, and A. Aoyagi, Appl. Phys. Lett. **85** 3501 (2004).

[10] S. O. Valenzuela and M. Tinkham, Appl. Phys. Lett. **85** 5914 (2004).

[11] Y. Ji, A. Hoffmann, J. S. Jiang, and S. D. Bader, Appl. Phys. Lett. **85** 6218 (2004).

[12] M. Zaffalon and B. J. van Wees, Phys. Rev. Lett. **91** 186601 (2003).

[13] G. E. W. Bauer, A. Brataas, Y. Tserkovnyak, and B. J. van Wees, Appl. Phys. Lett. **82** 3928 (2003).

[14] T. Kimura, Y. Otani, and J. Hamrle, Phys. Rev. Lett. **97** 037201 (2006) [cond-mat/0508559].

[15] A. Brataas, Y. V. Nazarov, and G. E. W. Bauer, Phys. Rev. Lett. **84** 2481 (2000).

[16] X. Wang, G. E. W. Bauer, and A. Hoffmann, Phys. Rev. B **73**, 054436 (2006).

[17] Y. Tserkovnyak, A. Brataas, and G. E. W. Bauer, Phys. Rev. Lett. **88** 117601 (2002).

[18] Y. Tserkovnyak, A. Brataas, G. E. W. Bauer, and B. I. Halperin, Rev. Mod. Phys. **77** 1375 (2005).

[19] J. A. Osborn, Phys. Rev. **67** 351 (1945) .

[20] M. Johnson and R. H. Silsbee, Phys. Rev. B **37** 5312 (1988) .

[21] X. Wang, G. E. W. Bauer, Y. Tserkovnyak and A. Brataas, unpublished.

[22] L. Perko, *Differential Equations and Dyanmical Systems*, (Springer, Berlin, 1996), 2nd ed.

[23] K. Xia, P. J. Kelly, G. E. W. Bauer, A. Brataas, and I. Turek, Phys. Rev. B **65** 220401 (2002) .

Chapter 4

Voltage Generation by Ferromagnetic Resonance

Abstract

A ferromagnet can resonantly absorbs rf radiation to sustain a steady precession of the magnetization around an internal or applied magnetic field. We show that under these ferromagnetic resonance (FMR) conditions, a dc voltage is generated at a normal-metal electric contact to a ferromagnet with spin-flip scattering. This mechanism allows an easy electric detection of magnetization dynamics. [1]

4.1 Introduction

The field of magnetoelectronics utilizes the electronic spin degrees of freedom to achieve new functionalities in circuits and devices made from ferromagnetic and normal conductors. The modulation of the DC electrical resistance by means of the relative orientation of the magnetizations of individual ferromagnetic elements ("giant magnetoresistance") is by now well-established. Dynamic effects, such as the current-induced magnetization reversal, are still subject of cutting edge research activities. Here we concentrate on an application of the concept of spin-pumping, *i.e.* the emission of a spin current from a moving magnetization of a ferromagnet (F) in electrical contact with a normal conductor (N) [1, 2], *viz.* the "spin battery"[3]. In this device a ferromagnet that precesses under ferromagnetic resonance (FMR) conditions pumps a spin current into an attached normal metal that may serve as a source of a constant spin accumulation (see also Ref. [4]). In this chapter we report that spin-flip scattering in the ferromagnet translates the pumped spin accumulation into a charge voltage over an F|N junction. Due to the spin-flip scattering in F,

[1]This chapter has been published as: Xuhui Wang, *et al*, *Voltage Generation by Ferromagnetic Resonance at a Nonmagnet to Ferromagnet Contact*, Phys. Rev. Lett. **97**, 216602 (2006).

a back-flow spin current collinear to the magnetization is partially absorbed in the ferromagnet. Since the interface and bulk conductances are spin-dependent, this leads to a net charging of the ferromagnet, which thus serves as a source as well as electric analyzer of the spin pumping current. We note the analogy to the voltage in excited F|N|F spin valves predicted by Berger [5] and recently analyzed by Kupferschmidt *et al.* [6]. Since the spin-flip scattering in conventional magnets such as permalloy is very strong, this effect provides a handle to experimentally identify the FMR induced spin accumulation in the simplest setup [7]. A detailed experimental test of our predictions is in progress [8].

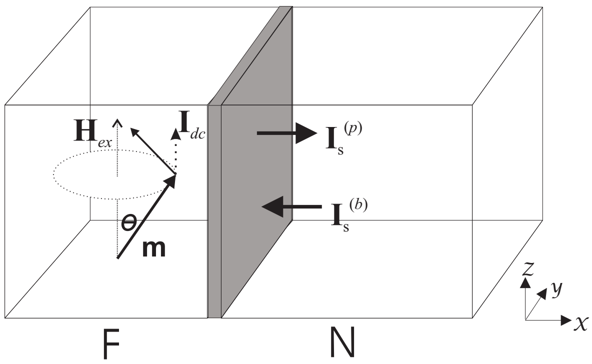

Figure 4.1: Schematic view of spin battery operated by ferromagnetic resonance. The dotted line $\mathbf{I}_{dc}$ represents the dc component of pumping current.

4.2 Spin and charge currents

The "spin battery" operated by ferromagnetic resonance has been proposed by Brataas *et al.* [3] in the limit of weak spin flip scattering in the ferromagnet. It is based on the spin current pumped into a normal metal by a moving magnetization (F|N) [1]

$$\mathbf{I}_s^{(p)} = \frac{\hbar}{4\pi}\left(\mathrm{Re}\, g^{\uparrow\downarrow}\mathbf{m}\times\frac{d\mathbf{m}}{dt} + \mathrm{Im}\, g^{\uparrow\downarrow}\frac{d\mathbf{m}}{dt}\right) , \tag{4.1}$$

where $\mathbf{m}$ is the unit vector of magnetization. $\mathrm{Re}\, g^{\uparrow\downarrow}$ and $\mathrm{Im}\, g^{\uparrow\downarrow}$ are the real and imaginary parts of the (dimensionless) spin-mixing conductance $g^{\uparrow\downarrow}$ [9]. This spin current creates a spin accumulation $\mathbf{s}$ in the normal metal, which induces a back flow of spins, and, as we will see, charges the ferromagnet. According to magnetoelectronic circuit theory [9] the charge and spin currents flowing through the F|N interface (into N) in the presence of non-equilibrium charge and spin accumulations μ_0^N, s in N and μ_0^F, $\mu_s^F \mathbf{m}$ in F, read [9]

$$\begin{aligned} I_c &= \frac{eg}{2h}\left[2(\mu_0^F - \mu_0^N) + p\mu_s^F - p(\mathbf{m}\cdot\mathbf{s})\right] \\ \mathbf{I}_s^{(b)} &= \frac{g}{8\pi}\left[2p(\mu_0^F - \mu_0^N) + \mu_s^F - (1 - 2\,\mathrm{Re}\,g^{\uparrow\downarrow}/g)\mathbf{m}\cdot\mathbf{s}\right]\mathbf{m} \\ &\quad - \frac{\mathrm{Re}g^{\uparrow\downarrow}}{4\pi}\mathbf{s} - \frac{\mathrm{Im}g^{\uparrow\downarrow}}{4\pi}(\mathbf{s}\times\mathbf{m})\,, \end{aligned} \tag{4.2}$$

where $g = g^{\uparrow} + g^{\downarrow}$ is the total interface conductance of spin-up and spin-down electrons, p is the contact polarization given by $p = (g^{\uparrow} - g^{\downarrow})/(g^{\uparrow} + g^{\downarrow})$. For typical metallic interfaces, the imaginary part of the mixing conductance is quite small [10], hence discarded in the following discussion . We choose the transport direction along the x-axis that is perpendicular to the interface at the origin. $\mathbf{H}_{ex}$, the sum of DC external and uniaxial anisotropy magnetic fields, points in the z-direction, which is also the chosen spin quantization axis in the normal metal. At the ferromagnetic resonance, the magnetization precesses steadily around the z-axis with azimuthal angle θ (see Fig. 4.1) that is tunable by the intensity of an AC magnetic field. The thickness of the normal and ferromagnetic metal films are d_N and d_F, respectively. s (x,t) is determined by the spin-diffusion equation [11]

$$\frac{\partial \mathbf{s}}{\partial t} = D_N \frac{\partial^2 \mathbf{s}}{\partial x^2} - \frac{\mathbf{s}}{\tau_{sf}^N}\,, \tag{4.3}$$

where τ_{sf}^N is the spin-flip relaxation time and D_N the diffusion constant in the normal metal. Assuming that the magnetization precesses around the z-axis with angular velocity ω, we consider the limit where the spin-diffusion length in the normal metal is much larger than the transverse spin-averaging length $l_\omega \equiv \sqrt{D_N/\omega}$, *i.e.*, $\lambda_{sd}^N \gg l_\omega$, or equivalently $\omega\tau_{sf}^N \gg 1$. We can then distinguish two regimes. When the thickness of the normal metal $d_N \gg l_\omega$, which is equivalent to the Thouless energy $\hbar D_N/d_N^2 \ll \hbar\omega$, the oscillating transverse component of the induced spin accumulation vanishes inside the normal metal, and one is left with a time-dependent spin accumulation along z-axis decaying away from the interface on the scale λ_{sd}^N. The back flow due to the steady state spin accumulation aligned along the z-axis cancels the same component of the pumping current. The former acquires the universal value $\hbar\omega$ when the spin-flip scattering is sufficiently weak [3]. The opposite regime of ultrathin or ultra clean normal metal films in which $\hbar D_N/d_N^2 \gg \hbar\omega$ the spin accumulation s is governed by a Bloch equation and will be discussed elsewhere [12].

4.3 Spin diffusion and the dc voltage

Continuity of the total spin current into the normal metal at the interface

$$\mathbf{I}_s = \mathbf{I}_s^{(p)} + \mathbf{I}_s^{(b)} \tag{4.4}$$

is the first boundary condition for the diffusion equation,

$$\partial \mathbf{s}/\partial x|_{x=0} = -2\mathbf{I}_s/(\hbar\nu_{\rm dos} A D_N), \tag{4.5}$$

where $\nu_{\rm dos}$ is the one-spin density of states and A the area of the interface, and the second is its vanishing at the sample edge $\partial \mathbf{s}/\partial x|_{x=d_N} = 0$. The time-averaged solution of Eq. (4.3) reads $\langle \mathbf{s} \rangle_t = s_z \hat{\mathbf{z}}$ with

$$s_z = \frac{\cosh\left(x - d_N\right)/\lambda_{sd}^N}{\sinh d_N/\lambda_{sd}^N} \frac{2\lambda_{sd}^N}{\hbar\nu_{\rm dos} A D_N} I_{s,z} \,. \tag{4.6}$$

The component of the spin accumulation parallel to the magnetization is a constant for the precessional motion considered here. It can penetrate the ferromagnet, hence building up a spin accumulation $\mu_s^F = \mu_\uparrow^F - \mu_\downarrow^F$ in F, which obeys the spin diffusion equation [11]

$$\frac{\partial^2 \mu_s^F(x)}{\partial x^2} = \frac{\mu_s^F(x)}{\left(\lambda_{sd}^F\right)^2} \,, \tag{4.7}$$

where λ_{sd}^F is the spin-flip diffusion length in the ferromagnet. The boundary conditions are given by the continuity of the longitudinal spin current at the interface

$$\sigma_\uparrow \left(\frac{\partial \mu_\uparrow^F}{\partial x}\right)_{x=0} - \sigma_\downarrow \left(\frac{\partial \mu_\downarrow^F}{\partial x}\right)_{x=0} = -\frac{2e^2}{\hbar A} I_{s,z} \cos\theta \tag{4.8}$$

and a vanishing spin current at the outer boundary

$$\sigma_\uparrow \left(\frac{\partial \mu_\uparrow^F}{\partial x}\right)_{x=-d_F} - \sigma_\downarrow \left(\frac{\partial \mu_\downarrow^F}{\partial x}\right)_{x=-d_F} = 0 \,, \tag{4.9}$$

where $\sigma_{\uparrow(\downarrow)}$ is the conductivity of spin up (down) electrons in the ferromagnet [13]. In the steady state there can be no net charge flow. From $I_c = 0$ follows that a charge chemical potential difference $\mu_0^F - \mu_0^N = p[s_z \cos\theta - \mu_s^F]_{x=0}/2$ builds up across the contact. At the interface on the F side, the longitudinal component of the total spin current leaving the ferromagnet then reads

$$I_{s,z}\cos\theta = \frac{(1-p^2)g}{8\pi}[\mu_s^F - s_z\cos\theta]_{x=0} \,. \tag{4.10}$$

The interface resistance is in series with a resistance $\rho_\omega = l_\omega/(h\nu_{\mathrm{dos}}AD_N)$ of the bulk normal metal of thickness l_ω that accounts for the averaging of the transverse spin current components. This reduces the interface conductances for spin-up (down) electrons to $g_\omega^{\uparrow(\downarrow)} = g^{\uparrow(\downarrow)}/(1+\rho_\omega g^{\uparrow(\downarrow)})$ and the spin-mixing conductance $g_\omega^{\uparrow\downarrow} = \mathrm{Re}\, g^{\uparrow\downarrow}/(1+\rho_\omega \,\mathrm{Re}\, g^{\uparrow\downarrow})$. We also introduce

$$g_\omega = g_\omega^\uparrow + g_\omega^\downarrow, \quad p_\omega = \frac{g_\omega^\uparrow - g_\omega^\downarrow}{g_\omega^\uparrow + g_\omega^\downarrow} \,. \tag{4.11}$$

Solving Eq. (4.7) under the above boundary conditions gives

$$\mu_s^F(x) = \frac{\tilde{g}\cosh\left[(x+d_F)/\lambda_{sd}^F\right]\cos\theta}{\left[\tilde{g} + g_F\tanh\left(d_F/\lambda_{sd}^F\right)\right]\cosh\left(d_F/\lambda_{sd}^F\right)} s_z|_{x=0} \tag{4.12}$$

where $\tilde{g} = (1-p_\omega^2)g_\omega$ and $g_F = 4hA\sigma_\uparrow\sigma_\downarrow/[e^2\lambda_{sd}^F(\sigma_\uparrow+\sigma_\downarrow)]$ is a parametrizes the properties of the bulk ferromagnet [13]. When the spin-flip in F is negligible, *i.e.*, $d_F \ll \lambda_{sd}^F$, then $\mu_s^F|_{x=0} = s_z|_{x=0}\cos\theta$ and consequently the longitudinal spin current vanishes. In the present limit, $\omega\tau_{sf}^N \gg 1$, the time-averaged pumping current Eq. (4.4) reads $I_{s,z}^{(p)} = \hbar\omega \mathrm{Re} g^{\uparrow\downarrow}\sin^2\theta/4\pi$ and the spin accumulation in N at distance l_ω near the interface becomes

$$s_z = \frac{\hbar\omega\sin^2\theta}{\eta_N(\omega) + \sin^2\theta + \frac{(1-p_\omega^2)\eta_F^{\uparrow\downarrow}}{1-p_\omega^2+\eta_F}\cos^2\theta} \tag{4.13}$$

where we have introduced the reduction factors for N and F:

$$\eta_N(\omega) = \frac{g_N}{g_\omega^{\uparrow\downarrow}}\tanh\frac{d_N}{\lambda_{sd}^N}, \quad \eta_F^{\uparrow\downarrow} = \frac{g_F}{g_\omega^{\uparrow\downarrow}}\tanh\frac{d_F}{\lambda_{sd}^F} \,, \tag{4.14}$$

where $g_N = h\nu_{\mathrm{dos}}AD_N/\lambda_{sd}^N$ and $\eta_F = g_\omega^{\uparrow\downarrow}\eta_F^{\uparrow\downarrow}/g_\omega$. With weak spin-flip in F, *i.e.*, $d_F \ll \lambda_{sd}^F$, $\eta_F^{\uparrow\downarrow} \approx 0$ and Eq. (4.13) reduces to $s_z = \hbar\omega\sin^2\theta/(\eta_N(\omega)+\sin^2\theta)$ [3].

Increasing the spin flip in F or the ratio d_F/λ_{sd}^F, the factor $\eta_F^{\uparrow\downarrow}$ gets larger and the spin accumulation signal decreases accordingly. More interesting is the chemical potential bias $\Delta\mu_0 = \mu_0^F - \mu_0^N$ that builds up across the interface, for which we find

$$\Delta\mu_0 = \frac{\hbar\omega p_\omega\,(\eta_F/2)\sin^2\theta\cos\theta}{\alpha_F\left(\eta_N(\omega)+\sin^2\theta\right)+(1-p_\omega^2)\eta_F^{\uparrow\downarrow}\cos^2\theta}\,. \tag{4.15}$$

where $\alpha_F = 1 - p_\omega^2 + \eta_F$. We now estimate the magnitude of s_z and $\Delta\mu_0$ for the typical systems Py|Al [14]. In Al the spin diffusion length is $\lambda_{sd}^N = 500$ nm, the spin-flip time $\tau_{sf}^N = 100$ ps (at low temperature) and the density of states of Al is $\nu_{\mathrm{dos}} = 1.5\times10^{47}\ \mathrm{J}^{-1}\ \mathrm{m}^{-3}$. The mixing conductance of the Py|Al interface in a diffuse environment can be estimated as twice the Sharvin conductance of Al [16] to be $\mathrm{Re}g_{\uparrow\downarrow}/A \approx 20\times10^{19}\ \mathrm{m}^{-2}$. The bare contact polarization is taken as $p = 0.4$. The spin-flip length in Py is very short, around $\lambda_{sf}^F = 5$ nm [15] and $(\sigma_\uparrow + \sigma_\downarrow)/\sigma_\uparrow\sigma_\downarrow$ is about $6.36\times10^{-7}\ \Omega\,\mathrm{m}$ [17]. Assuming a magnetization precession cone of $\theta = 5°$, the voltage $\Delta\mu_0/e$ of Py|Al interface as a function of the FMR frequency is plotted in Fig. 4.2. The induced spin accumulation in the normal metal and the voltages across the interface as a function of d_F are plotted in Fig. 4.3. The voltage bias across the interface, for given bulk properties of the normal metal, is seen to saturate at large spin-flip scatterings on the F side $d_F \gg \lambda_{sd}^F$. Spin-flip in the normal metal is detrimental to both spin accumulation and voltage generation. On the other hand, a transparency of the contact reduced from the Sharvin value increases the polarization p_ω up to its bare interface value and with it the voltage signal (up to a maximum value governed by the reduction factor η_N that wins in the limit of very low transparency).

The angle dependence of the voltage across the interface is plotted in the inset of Fig. 4.2 in the limit of large spin flip in F $d_F \gg \lambda_{sd}^F$. When $d_N \ll \lambda_{sd}^N$ (but still $d_N \gg l_\omega$) we obtain the maximum value:

$$\Delta\mu_0 = \frac{\hbar\omega p_\omega\,(g_F/2g_\omega)\sin^2\theta\cos\theta}{\alpha_F\sin^2\theta + (1-p_\omega^2)g_F\cos^2\theta/g_\omega^{\uparrow\downarrow}} \tag{4.16}$$

given $\alpha_F \to 1 - p_\omega^2 + g_F/g_\omega$. At small angle of the magnetization precession θ

$$\Delta\mu_0 \overset{\theta\to0}{=} \frac{p_\omega g_\omega^{\uparrow\downarrow}\theta^2}{2(1-p_\omega^2)g_\omega}\hbar\omega\,. \tag{4.17}$$

In the opposite limit, $d_N \gg \lambda_{sd}^N$ (but $\lambda_{sd}^N \gg l_\omega$) the voltage drop becomes

$$\Delta\mu_0 = \frac{\hbar\omega p_\omega\,(g_F/2g_\omega)\sin^2\theta\cos\theta}{\alpha_F\left(g_N/g_\omega^{\uparrow\downarrow}+\sin^2\theta\right)+(1-p_\omega^2)g_F\cos^2\theta/g_\omega^{\uparrow\downarrow}}\,, \tag{4.18}$$

which in the limit of small angle reduces to

$$\Delta\mu_0 \to p_\omega g_\omega^{\uparrow\downarrow}\theta^2\hbar\omega/[2(1+g_N/g_F)(1-p_\omega^2)g_\omega+2g_N]. \tag{4.19}$$

In both limits at small precession angles, the voltages are proportional to θ^2, *i.e.*, increases linearly with power intensity of the AC field. Eqs. (4.16) and (4.18) as function of FMR frequency are depicted in Fig. 4.2 as solid and dashed lines.

In contrast to Berger [5], who predicted voltage generation in spin valves, *viz.* that dynamics of one ferromagnet causes a voltage when analyzed by a second ferromagnet through a normal metal spacer, we consider here a simple bilayer. The single ferromagnetic layer here serves simultaneously as a source and detector of the spin accumulation in the normal metal layer. The presence of spin-flip scattering that allows the back-flow of a parallel spin current is essential, and permalloy is ideal for this purpose. The voltage bias under FMR conditions can be measured simply by separate electrical contacts to the F and N layers. It can be detected even on a single ferromagnetic film with normal metal contacts [7], provided that the two contacts are not equivalent.

We can also study the FMR generated bias in a controlled way in the $N_1|F\,|N_2$ trilayers in which the F layer is sandwiched by two normal metal layers. The magnetization of the ferromagnet again precesses around the z-axis. The thicknesses of N1, F and N2 in the transport direction are d_{N1}, d_F and d_{N2}, respectively. The spin diffusion length in normal metal node *i* is λ_i. With weak spin flip in the sandwiched ferromagnetic layer, $d_F \ll \lambda_{sd}^F$, the spin accumulation of F at both interfaces are the same. We find that the values of μ_s^F near the interfaces are mixtures of the interface values of the spin accumulations in the normal metals. In other words, the two normal metals talk to each other through F by the back-flow and the generated voltages across the interfaces are different given different contacts. In the opposite limit with massive spin flip in F, $d_F \gg \lambda_{sd}^F$, the strong spin flip scattering eventually separates the spin accumulation in the two normal metal nodes such that the "exchange" between the two normal metals is suppressed. We then recover Eq. (4.12).

According to Eq. (4.15) the voltage drops across the interfaces, $\Delta\mu_0^{(1)} \equiv \mu_0^F - \mu_0^{N1}$ and $\Delta\mu_0^{(2)} \equiv \mu_0^F - \mu_0^{N2}$ are different for different spin-diffusion lengths in the normal

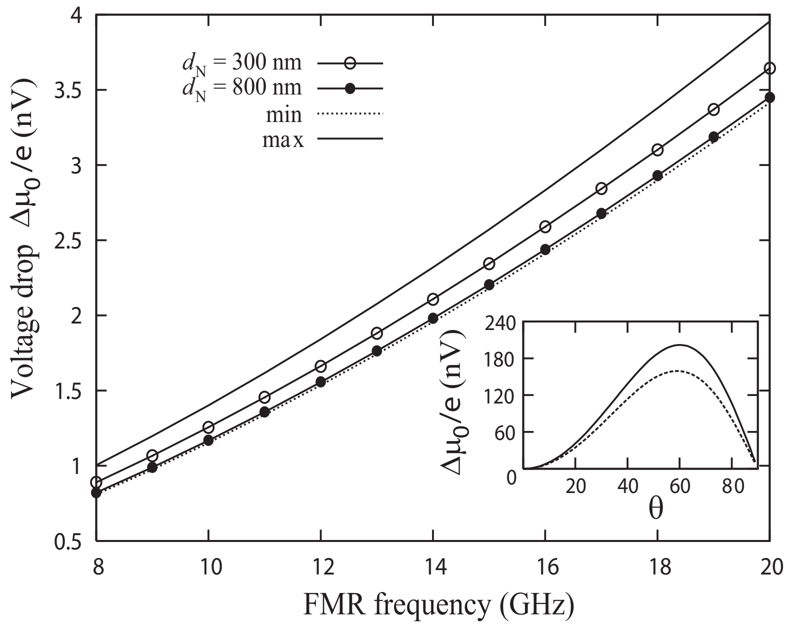

Figure 4.2: The voltage drop $\Delta\mu_0/e$ (in the unit nV) as function of FMR frequency (in GHz) for Py|Al interface. The line with circles denotes the situations when $d_N = 300$ nm (empty symbols) and $d_N = 800$ nm (filled symbols) when the thickness of ferromagnet is taken as $d_F = 14$ nm. The solid and dashed lines refer to the limits as indicated by Eq. (4.16) and Eq. (4.18). These curves indicate that due to averaging of the transverse spin components inside the normal metal, the voltage is not linear with FMR frequency. The precession angle of magnetization is taken as $\theta = 5^\circ$. The inset shows the angle dependence of the voltage at fixed frequency $15.5\,\mathrm{GHz}$. At small angle, the voltage drop is proportional to θ^2.

metals (λ_i) or different conductances ($\mathrm{Re}\, g^{\uparrow\downarrow}$). For example, taking identical normal metals but different contacts, *e.g.*, a clean and a dirty one, $\Delta\mu_0^{(1)}$ and $\Delta\mu_0^{(2)}$ will be different due to different spin-mixing conductances.

In conclusion, we report a unified description for spin pumping in F|N structure and analyze the spin accumulation in the normal metal induced by a spin-pumping current. We predict generation of a DC voltage over a single F|N junction. The Py|Al system should be an ideal candidate to electrically detect magnetization dynamics in this way.

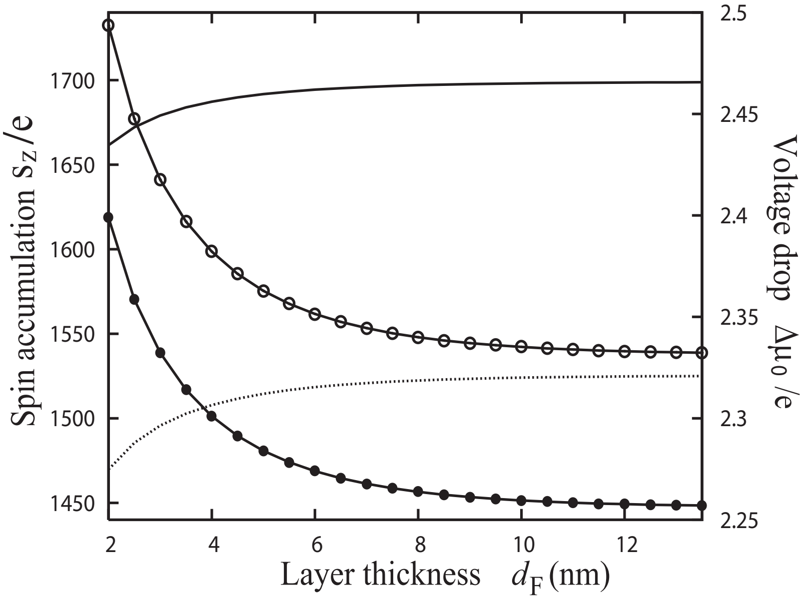

Figure 4.3: Lines with circles are the spin-pumping induced accumulation s_z/e (in unit of nV) in Al near the interface to permalloy as a function of the Py layer thickness d_F and two Al layer thicknesses, *i.e.*, $d_N = 300\,\mathrm{nm}$ (empty symbols) and $d_N = 800\,\mathrm{nm}$ (filled symbols). Solid($d_N = 300\,\mathrm{nm}$)and dotted($d_N = 800\,\mathrm{nm}$) lines are the chemical potential discontinuity across the interface $\Delta\mu_0/e$ (in units of nV), as a function of the Py layer thickness d_F. The FMR frequency is 15.5 GHz.

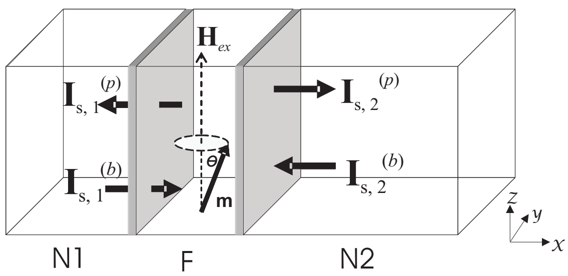

Figure 4.4: The $N_1|F|N_2$ system in which the sandwiched F layer precesses around the z-axis under FMR condition. The origin of the x-axis is located at the $F|N_2$ interface.

Bibliography

[1] Y. Tserkovnyak, A. Brataas, and G. E. W. Bauer, Phys. Rev. Lett. **88**, 117601 (2002).

[2] Y. Tserkovnyak, A. Brataas, G. E. W. Bauer, and B. Halperin, Rev. Mod. Phys. **77**, 1375 (2005).

[3] A. Brataas, Y. Tserkovnyak, G. E. W. Bauer, and B. I. Halperin, Phys. Rev. B **66**, 060404 (2002).

[4] S. M. Watts, J. Grollier, C. H. van der Wal, and B. J. van Wees, Phys. Rev. Lett. **96**, 077201 (2006).

[5] L. Berger, Phys. Rev. B **59**, 11465 (1999).

[6] J. N. Kupferschmidt, S. Adam, and P. W. Brouwer, Phys. Rev. B. **74**, 134416 (2006) [cond-mat/0607145].

[7] A. Azevedo, L. H. V. Leao, R. L. Rodriguez-Suarez, A. B. Oliveira, and S. M. Rezende, J. Appl. Phys. **97**, 10C715 (2005); E. Saitoh, M. Ueda, M. Miyajima, and G. Tatara, Appl. Phys. Lett. **88**, 182509 (2006).

[8] M.V. Costache, M. Sladkov, C.H. van der Wal, and B.J. van Wees, Phys. Rev. Lett. **97**, 216603 (2006) [cond-mat/0609089]

[9] A. Brataas, Y. V. Nazarov, and G. E. W. Bauer, Phys. Rev. Lett. **84**, 2481 (2000); Eur. Phys. J. B **22**, 99 (2001).

[10] K. Xia, P. J. Kelly, G. E. W. Bauer, A. Brataas, and I. Turek, Phys. Rev. B **65**, 220401 (2002); A. Brataas, G. E. W. Bauer, and P. J. Kelly, Phys. Rep. **427**, 157 (2006).

[11] M. Johnson and R. H. Silsbee, Phys. Rev. B **37**, 5312 (1988).

[12] X. Wang, G. E. W. Bauer, A. Brataas, and Y.Tserkovnyak, unpublished (2006).

[13] Y. Tserkovnyak, A. Brataas, and G. E. W. Bauer, Phys. Rev. B **67**, 140404 (2003).

[14] F. J. Jedema, H. B. Heersche, A. T. Filip, J. J. A. Baselmans, and B. J. van Wees, Nature, **416**, 713 (2002); M. Zaffalon and B. J. van Wees, Phys. Rev. Lett. **91**, 186601 (2003).

[15] J. Bass and W. P. Pratt, J. Magn. Magn. Mater. **200**, 274 (1999).

[16] G. E. W. Bauer, Y. Tserkovnyak, D. Huertas-Hernando, and A. Brataas, Phys. Rev. B **67**, 094421 (2003).

[17] A. Fert and L. Piraux, J. Magn. Magn. Mater. **200**, 338 (1999).

Chapter 5

Effective Action Approach to the Damping of Magnetization Dynamics

Abstract

We investigate the damping of magnetization dynamics in a magnetic film that is sandwiched by conducting material (host material), in the absence of bias. The magnetization is coupled to the spins of conducting electrons by $s-d$ exchange interaction. The damping is obtained by deriving the equation of motion of the magnetiztion from an effective action. In the case of aa normal-metal host, we obtain a Landau-Lifshitz-Gilbert equation with damping described by a single parameter, which compares favorablly to earlier results by others. When the host is magnetic, the damping takes a tensor form, and we also discuss the half-metallic limit.

5.1 Introduction

The damping of magnetization dynamics is a subtle and important issue attracting much attention from both theoretical and experimental perspectives. For an isolated ferromagnetic particle, the Landau-Lifshitz-Gilbert equation qualitatively and quantitatively describes both the non-dissipative and dissipative (damping) dynamics of the magnetization [1, 2]. When in contact with paramagnetic metals, the interactions between the magnetization and the conduction-electron spins give rise to enhancement of the damping parameter, as measured in FMR experiments on ferromagnet -normal metal (F—N) heterostructures [3]. The enhancement of damping can be interpreted via a mechanism called spin pumping, where by interacting with the conducting electrons, the precessing magnetization losses angular momentum to the adjacent normal metal [4, 5]. The scattering approach describes this phenomenon well in terms of a *mixing conductance*, invented as a key ingredient in the magnetoelectronic theory [6], in the framework of Landauer-Büttiker formalism

[7] and parametric pumping [5, 8]. The damping of magnetization dynamics in the presence of conduction electrons can be understood in different languages, such as its relation to the susceptibilities of the conduction electrons [9], or to the time lag in the RKKY oscillations [10]. Meanwhile, some heavy machinery such as the Keldysh formalism has been employed to investigate the magnetization dynamics in both equilibrium and current-driven cases [11]. In this chapter, we present an investigation into the damping of the magnetization dynamics in the bath of conduction electrons, using the effective action approach [12] and Caldeira-Leggett formalism [13] to study the dissipation. The latter handles the dissipation of a system in contact with environment as the *non-local-in-time* contribution to the effective action of the system, when the influence of the environment is properly accounted for.

This chapter is arranged as follows: In the imaginary-time path-integral formulation, Sec. 5.2 develops the total action of a magnetization film sandwiched by normal metals, which with the spins of the conduction electrons through an s-d exchange interaction. In Sec. 5.3 the effective action of magnetization is obtained by removing the electronic degrees of freedom, and considering only the elastic scattering of the electrons by the spins in the ferromagnetic film. The action that is nonlocal in time is derived by perturbation theory. Section 5.4 outlines the derivation of equation of motion, using the principle of least action, yielding a Landau-Lifshitz-Gilbert form, from which we identify the damping parameter. The damping parameter obtained from this straightforward approach agrees favorably with earlier results.

5.2 The action of coupled systems

The system under investigation consists of a thin magnetic film sandwiched by normal metal hosts. The interaction between the magnetization and the spins of the conduction electrons can be well described by an s-d exchange model [9, 10]. In the absence of a bias over the system, the damping of the magnetization can be expressed in terms of the imaginary part of the dynamic spin- susceptibility function of the conduction electrons [9]. This section demonstrates the connection between the effective-action approach and the direct calculation of the dynamical spin susceptibility of the conduction electrons in the normal metal host.

The conduction electrons in the host metal are coupled to the sandwiched magnetic layer by the exchange interaction. In this case the dynamics of the magnetization excites electron-hole pairs of the conduction electron Fermi sea. Energy and momentum are carried away by these excitations, which leads to a *damping* of the magnetization motion, which is associated with the imaginary part of the dynamical spin susceptibilities. The setup is depicted in Fig. 5.1. We assume that the system is

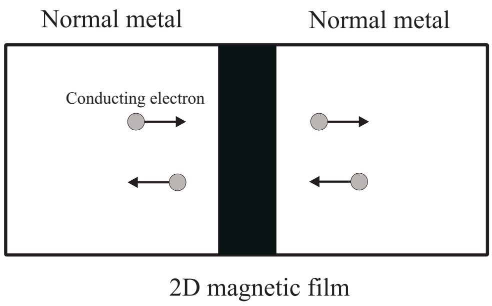

Figure 5.1: A two-dimensional magnetic film is embedded in the normal metal host.

not biased. In terms of the s-d exchange model between localized spins ($\mathbf{S}_i$ on site-i) in the film and the conduction electrons ($\phi_\sigma(r)$), the Hamiltonian of the conduction electrons and its coupling to magnetization is given by

$$\mathcal{H} = \mathcal{H}_0 - \frac{J\hbar}{V}\sum_i \sum_{\sigma,\sigma'} \int d^3\mathbf{r}\, \phi_\sigma^\dagger(\mathbf{r}) \left(\boldsymbol{\sigma}\cdot\mathbf{S}(\mathbf{r}_i,t)\right)_{\sigma\sigma'} \phi_{\sigma'}(\mathbf{r})\delta(\mathbf{r}-\mathbf{r}_i)\,. \tag{5.1}$$

where the spins are related to the magnetization $\mathbf{M}(\mathbf{r}_i,t)$ by $\mathbf{S}(\mathbf{r}_i,t) = (\mathcal{V}/\gamma)\mathbf{M}(\mathbf{r}_i,t)$, with $\mathcal{V}$ the volume of the unit cell, and $\gamma = -g\mu_B/\hbar$ the gyromagnetic ratio. Pauli matrix $\boldsymbol{\sigma}$ describes the spins of conduction electrons. The dimensionless field operators can be Fourier expanded as $\phi_\sigma(r) = \sum_{\mathbf{k}} \phi_{\mathbf{k},\sigma} e^{i\mathbf{k}\cdot\mathbf{r}}$, such that the total Hamiltonian reads

$$\mathcal{H} = \sum_{\mathbf{k},\sigma} \xi_{\mathbf{k},\sigma}\phi^\dagger_{\mathbf{k},\sigma}\phi_{\mathbf{k},\sigma} - \frac{N_s J\hbar}{V}\sum_{\mathbf{k},\mathbf{k}'}\sum_{\sigma,\sigma'} \phi^\dagger_{\mathbf{k},\sigma}\mathbf{S}_{\mathbf{k}\mathbf{k}'}(t)\cdot\boldsymbol{\sigma}_{\sigma\sigma'}\phi_{\mathbf{k}',\sigma'}. \tag{5.2}$$

Here V is the total volume of the normal metal host, and N_s the total number of spins of the magnetic film. We have used the definition $\xi_{\mathbf{k},\uparrow(\downarrow)} = \epsilon_{\mathbf{k}} - \mu - (+)\Delta$ given single particle energy $\epsilon_{\mathbf{k}} = \hbar^2\mathbf{k}^2/2m$ and Δ coming from magnetic field or exchange splitting (such as the one to be discussed in the magnetic host situation).

In the imaginary time formalism, the total action is given by

$$\mathcal{S} = \mathcal{S}_{WZNW} + \mathcal{S}_{con} + \int_0^{\hbar\beta} d\tau \sum_{k,\sigma} \phi^\dagger_{\mathbf{k},\sigma}(\tau)\hbar\frac{\partial}{\partial\tau}\phi_{\mathbf{k},\sigma}(\tau) + \int_0^{\hbar\beta} d\tau\mathcal{H}(\tau), \tag{5.3}$$

where the geometric Wess-Zumino-Novikov-Witten (or Berry phase) term has been introduced as [14, 15]:

$$\mathcal{S}_{WZNW} = -i\mathcal{N}_s S\int_0^{\hbar\beta} d\tau\ \mathbf{A}(\mathbf{n})\cdot\dot{\mathbf{n}}, \tag{5.4}$$

where $\mathbf{S} = S\mathbf{n}$ and the vector potential $\mathbf{A}(\mathbf{n})$ satisfies Stokes theorem, *i.e.*

$$\boldsymbol{\nabla}\times\mathbf{A}\cdot\mathbf{n} = \epsilon^{ijk}\frac{\partial A^j}{\partial n^i}n^k = 1, \text{ and } i,j,k = \{x,y,z\}. \tag{5.5}$$

Tensor ϵ^{ijk} is fully antisymmetric. The action $\mathcal{S}_{WZNW}$ is required to recover the classical equation of motion from the principle of least action. In Eq. (5.4), S is the magnitude of each spin on the lattice of the ferromagnet film. An applied external field ($\mathbf{H}_{ex}$) enters the action through $\mathcal{S}_{con}$, where the subscript denotes the conservative part of the action:

$$\mathcal{S}_{con} = \gamma\mathcal{N}_s\int_0^{\hbar\beta} d\tau\mathbf{S}(\tau)\cdot\mathbf{H}_{ex}. \tag{5.6}$$

In the following we show that applying the Euler-Lagrange principle on the spin action $\mathcal{S}_{spin} \equiv \mathcal{S}_{WZNW} + \mathcal{S}_{con}$ yield the correct classical equation of motion for the spins. The variation of the WZNW action is given by

$$\begin{aligned}\delta\mathcal{S}_{WZNW} &= -i\mathcal{N}_s S\int_0^{\hbar\beta} d\tau\left[\frac{\partial A^i}{\partial n^j}\left(\delta n^j\dot{n}^i - \dot{n}^j\delta n^i\right) + A^i\frac{d}{d\tau}\delta n^i + \frac{\partial A^i}{\partial n^j}\dot{n}^j\delta n^i\right]\\ &= -i\mathcal{N}_s S\int_0^{\hbar\beta} d\tau\frac{\partial A^i}{\partial n^j}\epsilon^{ijk}\left(\dot{\mathbf{n}}\times\delta\mathbf{n}\right)_k\\ &= -i\mathcal{N}_s S\int_0^{\hbar\beta} d\tau\mathbf{n}\cdot\left(\dot{\mathbf{n}}\times\delta\mathbf{n}\right).\end{aligned} \tag{5.7}$$

The variation of the magnetic field related action is relatively simple, it reads

$$\delta\mathcal{S}_{con} = \gamma\mathcal{N}_s S\int_0^{\hbar\beta} d\tau\delta\mathbf{n}\cdot\mathbf{H}_{ex} \tag{5.8}$$

and with $\delta\mathcal{S}_{spin} = 0$ we immediately have the following equation of motion (a Wick rotation has been performed to real time *i.e.* $\tau \to it$)

$$\frac{d\mathbf{S}}{dt} = -\gamma\mathbf{S} \times \mathbf{H}_{es}, \tag{5.9}$$

which is the classical equation of motion of a spin or magnetization in the presence of a magnetic field, as derived in Chapter 1.

The Fourier series in the imaginary-time domain of the fermionic field operators are given by:

$$\phi_{\mathbf{k},\sigma}(\tau) = \frac{1}{\sqrt{\hbar\beta}}\sum_n \phi_{\mathbf{k},\sigma,n}e^{-i\omega_n\tau}, \quad \phi_{\mathbf{k},\sigma,n} = \frac{1}{\sqrt{\hbar\beta}}\int_0^{\hbar\beta} d\tau\phi_{\mathbf{k}\sigma}(\tau)e^{i\omega_n\tau}, \tag{5.10}$$

where the Matsubara frequencies are $\omega_n = (2n+1)\pi/\hbar\beta$ and $\beta = 1/k_BT$, with k_B the Boltzmann constant and T the absolute temperature. The Matsubara-frequency expansion for the spin variable is bosonic, *i.e.* $\omega_n = 2n\pi/\hbar\beta$, since spin operators are bilinear in terms of fermionic operator [14]. Hence

$$\mathbf{S}_{\mathbf{k}\mathbf{k}'}(\tau) = \frac{1}{\sqrt{\hbar\beta}}\sum_n \mathbf{S}_{\mathbf{k}\mathbf{k}',n}e^{-i\omega_n\tau}, \quad \mathbf{S}_{\mathbf{k}\mathbf{k}',n} = \frac{1}{\sqrt{\hbar\beta}}\int_0^{\hbar\beta} d\tau\mathbf{S}_{\mathbf{k}\mathbf{k}'}(\tau)e^{i\omega_n\tau}. \tag{5.11}$$

The total action in the explicit form in spin space can be written as

$$\begin{aligned}\mathcal{S} =& \mathcal{S}_{WZNW} \\ &+ \sum_{n,n'}\sum_{\mathbf{k},\mathbf{k}'}\left(\phi^\dagger_{\mathbf{k}n\uparrow}, \phi^\dagger_{\mathbf{k}n\downarrow}\right)\left[\begin{pmatrix} -i\hbar\omega_n + \xi_{\mathbf{k}\uparrow} & 0 \\ 0 & -i\hbar\omega_n + \xi_{\mathbf{k}\downarrow}\end{pmatrix}\delta_{kk'}\delta_{nn'}\right. \\ &\qquad\left. - \frac{N_sJ\hbar}{V\sqrt{\hbar\beta}}\begin{pmatrix} S_z & S_- \\ S_+ & -S_z\end{pmatrix}_{\mathbf{k},\mathbf{k}';n,n'}\right]\begin{pmatrix}\phi_{\mathbf{k}'n'\uparrow} \\ \phi_{\mathbf{k}'n'\downarrow}\end{pmatrix},\end{aligned} \tag{5.12}$$

where the definitions $S_\pm = S_x \pm iS_y$ have been introduced linking two of the three components of $\mathbf{S} = (S_x, S_y, S_z)$.

5.3 Effective action of magnetization

We now wish to integrate out the conduction electrons, thus removing the fastest degrees of freedom in the system. This procedure leads to an effective action for spins (magnetization) that we are looking for, including the information about the damping, $\mathcal{S}_{eff} = \mathcal{S}_{WZNW} - \hbar \mathrm{Trln}\left[\mathbb{G}^{-1}\right]$, where $\mathbb{G}$ is the total propagator of the conduction electrons. The Wess-Zumino-Novikov-Witten term remains untouched whereas the last term should represent the contribution to the spin dynamics due to interactions with the conduction electrons. When the s-d exchange is weak compared to the Fermi energy, we may introduce the perturbation expansion

$$\mathrm{Trln}\left[\mathbb{G}^{-1}\right] \approx \mathrm{Tr}\ln[G^{-1}] + \mathrm{Tr}[G\mathbb{T}] - \frac{1}{2}\mathrm{Tr}[G\mathbb{T}G\mathbb{T}], \tag{5.13}$$

where the propagator of the free electrons and the bare interaction matrix $\mathbb{T}$ are defined as

$$\begin{aligned} G(\mathbf{k},n) &= \begin{pmatrix} G_\uparrow & 0 \\ 0 & G_\downarrow \end{pmatrix} = \begin{pmatrix} \frac{1}{-i\hbar\omega_n + \xi_{\mathbf{k}\uparrow}} & 0 \\ 0 & \frac{1}{-i\hbar\omega_n + \xi_{\mathbf{k}\downarrow}} \end{pmatrix}, \\ \mathbb{T}(\mathbf{k},\mathbf{k}';n,n') &= -\frac{N_s J\hbar}{V\sqrt{\hbar\beta}} \begin{pmatrix} S_z & S_- \\ S_+ & -S_z \end{pmatrix}_{\mathbf{k},\mathbf{k}';n,n'} . \end{aligned} \tag{5.14}$$

The trace in Eq.(5.13) is taken in momentum space and the Matsubara frequencies have to be summed over. The first term on the right-hand side of Eq. (5.13) gives rise to a constant that is irrelevant in the action. The first order term in $\mathbb{T}$ vanishes in the normal host, but gives rise to an RKKY exchange field when the host material is magnetic, as will be shown in the following sections.

Most of our attention is centered on the second order term in the perturbation expansion, *i.e.* $\frac{1}{2}\mathrm{Tr}\ln[G\mathbb{T}G\mathbb{T}]$, which describes the correlation of spins at different instants, and which eventually still be shown to represent the damping of the magnetization dynamics. In condensed notation, with the indices of momentum and the Matsubara frequencies suppressed, the second order term consists of the correlation functions of the spins in the ferromagnet:

$$\begin{aligned} \frac{1}{2}\mathrm{Tr}[G\mathbb{T}G\mathbb{T}] = \frac{N_s^2 J^2 \hbar}{2\beta V^2} \sum_{\mathbf{k}\mathbf{k}'} \sum_{nn'} & \left(G_\uparrow S_z G_\uparrow S_z + G_\uparrow S_- G_\downarrow S_+ \right. \\ & \left. + G_\downarrow S_+ G_\uparrow S_- + G_\downarrow S_z G_\downarrow S_z \right). \end{aligned} \tag{5.15}$$

The first and the last terms that are related to the longitudinal susceptibility, and with sub-indices indicated explicitly, are given by:

$$\begin{aligned}&\sum_{\mathbf{k}\mathbf{k}'}\sum_{nn'}G_\sigma(\mathbf{k},n)S_z(\mathbf{k}-\mathbf{k}';n-n')G_\sigma(\mathbf{k}',n')S_z(\mathbf{k}'-\mathbf{k};n'-n)\\&=\frac{1}{\hbar}\int_0^{\hbar\beta}d\tau\int_0^{\hbar\beta}d\tau'\sum_{\mathbf{k}\mathbf{q},m}\frac{(f_{\mathbf{k}+\mathbf{q},\sigma}-f_{\mathbf{k}\sigma})e^{i\omega_m(\tau-\tau')}}{i\hbar\omega_m+\xi_{\mathbf{k}+\mathbf{q},\sigma}-\xi_{\mathbf{k}\sigma}}S_z(-\mathbf{q};\tau)S_z(\mathbf{q};\tau'),\end{aligned}\tag{5.16}$$

where we have introduced bosonic frequencies $\omega_m = \omega_n - \omega_{n'}$ and an exchanged momentum $\mathbf{q} = \mathbf{k}' - \mathbf{k}$. The summation over fermionic Matsubara frequencies ω_n has been carried out, leading to Fermi-Dirac distribution functions $f_{\mathbf{k},\sigma}$. For spins confined to the two dimensional film and localized on the lattice sites, it is justified to assume weak momentum dependence, *i.e.* the assumption of elastic scattering of the electrons leads to $S(\pm\mathbf{q},\tau) \approx S(\tau)$. Such an approximation implies neglecting the dispersion of the spin-wave excitations in the sandwiched film, which is also known as the *macro-spin approximation.* Assuming small momentum exchange or a small $|\mathbf{q}|$ compared to the Fermi vector k_F, the distribution function and the energies can be expanded as,

$$\sum_{\mathbf{k}}\frac{f_{\mathbf{k}+\mathbf{q},\sigma}-f_{\mathbf{k}\sigma}}{i\hbar\omega_m+\xi_{\mathbf{k}+\mathbf{q},\sigma}-\xi_{\mathbf{k}\sigma}}\approx\sum_{\mathbf{k}}\frac{\frac{\partial f}{\partial\epsilon_{\mathbf{k}}}\frac{\hbar^2\mathbf{k}\cdot\mathbf{q}}{m}}{i\hbar\omega_m+\frac{\hbar^2\mathbf{k}\cdot\mathbf{q}}{m}}.\tag{5.17}$$

Therefore the expression associated with the correlation function reduces to

$$\begin{aligned}&\sum_{\mathbf{k}\mathbf{k}'}\sum_{nn'}G_\uparrow(\mathbf{k},n)S_z(\mathbf{k}-\mathbf{k}';n-n')G_\uparrow(\mathbf{k}',n')S_z(\mathbf{k}'-\mathbf{k};n'-n)\\&=\frac{1}{\hbar}\int_0^{\hbar\beta}d\tau\int_0^{\hbar\beta}d\tau'\sum_{\mathbf{k}\mathbf{q}}\left(\frac{\partial f}{\partial\epsilon_{\mathbf{k}}}\frac{\hbar^2\mathbf{k}\cdot\mathbf{q}}{m}\right)\sum_m\frac{e^{i\omega_m(\tau-\tau')}}{i\hbar\omega_m+\frac{\hbar^2\mathbf{k}\cdot\mathbf{q}}{m}}S_z(\tau)S_z(\tau').\end{aligned}\tag{5.18}$$

The subtleties in the summation of the Matsubara frequencies ω_m are treated in detail in Appendix 5.8 and we quote only the final results: with a contour integral over variable Ω on the complex frequency plane, which can be reduced to an integration along the real axis, *i.e.* via analytic continuation,

$$\begin{aligned}\sum_m\frac{e^{i\omega_m(\tau-\tau')}}{i\hbar\omega_m+\frac{\hbar^2\mathbf{k}\cdot\mathbf{q}}{m}}=\beta\int_0^{+\infty}d\omega&\left[\delta\left(\omega-\frac{\hbar\mathbf{k}\cdot\mathbf{q}}{m}\right)-\delta\left(\omega+\frac{\hbar\mathbf{k}\cdot\mathbf{q}}{m}\right)\right]\\&\times\frac{\cosh(\hbar\beta\omega/2-\omega|\tau-\tau'|)}{\sinh(\hbar\beta\omega/2)}.\end{aligned}\tag{5.19}$$

Inserted into the expression of the spin-spin correlation function this yields

$$
\begin{aligned}
&\sum_{\mathbf{k}\mathbf{k}'}\sum_{nn'} G_\uparrow(\mathbf{k},n)S_z(\mathbf{k}-\mathbf{k}';n-n')G_\uparrow(\mathbf{k}',n')S_z(\mathbf{k}'-\mathbf{k};n'-n)\\
&=\frac{\beta}{\hbar}\int_0^{\hbar\beta}d\tau\int_0^{\hbar\beta}d\tau'\int_0^{+\infty}d\omega\sum_{\mathbf{k}\mathbf{q}}\left(\frac{\partial f}{\partial\epsilon_{\mathbf{k}}}\frac{\hbar^2\mathbf{k}\cdot\mathbf{q}}{m}\right)S_z(\tau)S_z(\tau')\\
&\times\left[\delta\left(\omega-\frac{\hbar\mathbf{k}\cdot\mathbf{q}}{m}\right)-\delta\left(\omega+\frac{\hbar\mathbf{k}\cdot\mathbf{q}}{m}\right)\right]\frac{\cosh(\hbar\beta\Omega/2-\Omega|\tau-\tau'|)}{\sinh(\hbar\beta\Omega/2)}.
\end{aligned}
\tag{5.20}
$$

The summation of momentum $\mathbf{k}$ together with the Dirac δ-functions is carried out by taking $\sum_{\mathbf{k}}=V\int d^3k/(2\pi)^3$ and working in spherical coordinates, where θ is the angle between $\mathbf{k}$ and $\mathbf{q}$

$$
\begin{aligned}
&\sum_{\mathbf{k}}\left(\frac{\partial f}{\partial\epsilon_{\mathbf{k}}}\frac{\hbar^2\mathbf{k}\cdot\mathbf{q}}{m}\right)\left[\delta\left(\omega-\frac{\hbar\mathbf{k}\cdot\mathbf{q}}{m}\right)-\delta\left(\omega+\frac{\hbar\mathbf{k}\cdot\mathbf{q}}{m}\right)\right]\\
&=-\frac{\omega m^2V}{2q\pi^2\hbar^2}\Theta\left(k_F-\frac{\omega m}{\hbar q}\right)
\end{aligned}
\tag{5.21}
$$

In the last step, a Heaviside step function has been introduced. Physically, this step function defines the lower limit for the momentum $\mathbf{q}$, which reads $q>q_1=\omega m/(\hbar k_F)$. Hence

$$
\begin{aligned}
&\sum_{\mathbf{k}\mathbf{k}'}\sum_{nn'} G_\uparrow(\mathbf{k},n)S_z(\mathbf{k}-\mathbf{k}';n-n')G_\uparrow(\mathbf{k}',n')S_z(\mathbf{k}'-\mathbf{k};n'-n)\\
&=-\frac{\beta V^2m^2}{4\mathcal{A}\pi^3\hbar^3}\int_0^{\hbar\beta}d\tau\int_0^{\hbar\beta}d\tau'\\
&\times\int_0^{+\infty}d\omega\;\omega\;\ln\left(\frac{4\epsilon_F}{\hbar\omega}\right)\frac{\cosh(\hbar\beta\omega/2-\omega|\tau-\tau'|)}{\sinh(\hbar\beta\omega/2)}S_z(\tau)S_z(\tau'),
\end{aligned}
\tag{5.22}
$$

where the summation over momentum $\mathbf{q}$ has been converted to a one-dimensional integration, since the momentum parallel to the magnetic film is always conserved and $\mathbf{q}$ is the momentum perpendicular, *i.e.*

$$
\sum_{\mathbf{q}}\frac{1}{q}\Theta\left(k_F-\frac{\omega m}{\hbar q}\right)=\frac{V}{\mathcal{A}}\int_{q_1}^{q_2}\frac{dq}{2\pi}\frac{1}{q}=\frac{V}{2\pi\mathcal{A}}\ln\left(\frac{q_2}{q_1}\right)=\frac{V}{2\pi\mathcal{A}}\ln\left(\frac{4\epsilon_F}{\hbar\omega}\right).
\tag{5.23}
$$

The upper limit of the above integration is taken as $q_2=2k_F$ [9] and $\mathcal{A}$ is the area of the magnetic film. After insertion of Eq. (5.23) into Eq. (5.22), the energy integral is seen to suffer from an infrared divergence. As noted by Ref.[[9]], we must introduce a low energy cut-off that can be associated with the lower bound for q. To this end the s-d exchange interaction has to be compared to the splitting induced by the non-local exchange field. In the scattering region, the splitting of the electronic energy caused by the $s-d$ exchange (Δ_{sd}) can be estimated as

$$\Delta_{sd} \approx \frac{2J\hbar\hbar}{\mathcal{V}} \approx 4J_{sd}, \tag{5.24}$$

where the relation of J (in the action) with the atomic exchange integral J_{sd} has been assumed to be $J \approx 2J_{sd}\mathcal{V}/\hbar^2$ [9]. This consideration eventually leads to the low momentum cut-off

$$q_1 = m\Delta_{sd}/\hbar^2 k_F. \tag{5.25}$$

The atomic exchange integral is typically $J_{sd} \approx 0.1$ eV in magnitude [9].

Based on the above discussion, the correlation functions are found to be

$$\begin{aligned}
&\sum_{\mathbf{k}\mathbf{k}'}\sum_{nn'} G_\uparrow(\mathbf{k},n)S_z(\mathbf{k}-\mathbf{k}';n-n')G_\uparrow(\mathbf{k}',n')S_z(\mathbf{k}'-\mathbf{k};n'-n)\\
&= -\frac{\beta V^2 m^2}{4\mathcal{A}\pi^3\hbar^3}\ln\left(\frac{\epsilon_F}{J_{sd}}\right)\int_0^{\hbar\beta} d\tau \int_0^{\hbar\beta} d\tau' \\
&\qquad \times \int_0^{+\infty} d\omega\omega \frac{\cosh(\hbar\beta\omega/2-\omega|\tau-\tau'|)}{\sinh(\hbar\beta\omega/2)} S_z(\tau)S_z(\tau').
\end{aligned} \tag{5.26}$$

As far as the normal host is concerned, there is no spin splitting for conduction electrons in the bulk, and therefore no difference between $G_\uparrow$ and $G_\downarrow$. This leads to the final expression for the second order perturbation:

$$\begin{aligned}
\frac{1}{2}\mathrm{Tr}[G\mathbb{T}G\mathbb{T}] = &-\frac{N_s^2 J^2 m^2}{4\mathcal{A}\hbar^2\pi^3}\ln\left(\frac{\epsilon_F}{J_{sd}}\right)\int_0^{\hbar\beta} d\tau \int_0^{\hbar\beta} d\tau' \\
&\times \int_0^{+\infty} d\omega\, \omega\, \frac{\cosh(\hbar\beta\omega/2-\omega|\tau-\tau'|)}{\sinh(\hbar\beta\omega/2)} \mathbf{S}(\tau)\cdot\mathbf{S}(\tau').
\end{aligned} \tag{5.27}$$

After the above derivations, a total effective action for the magnetization emerges as

$$\begin{aligned}
\mathcal{S}_{eff} = \mathcal{S}_{WZNW} + \mathcal{S}_{con} &- \frac{N_s^2 J^2 m^2}{4\mathcal{A}\hbar\pi^3}\ln\left(\frac{\epsilon_F}{J_{sd}}\right)\int_0^{\hbar\beta} d\tau \int_0^{\hbar\beta} d\tau' \\
&\times \int_0^{+\infty} d\omega\, \omega\, \frac{\cosh(\hbar\beta\omega/2-\omega|\tau-\tau'|)}{\sinh(\hbar\beta\omega/2)} \mathbf{S}(\tau)\cdot\mathbf{S}(\tau'),
\end{aligned} \tag{5.28}$$

where $\mathcal{S}_{con}$ induces the magnetization dynamics. The last term ($\mathcal{S}_{dis}$) containing spins at different times that essentially causes the damping, according to the Caldeira-Leggett formalism [13], which can be obtained by evaluating the equation of motion for the spin system. Employing periodic boundary condition $\mathbf{S}(\tau + \hbar\beta) = \mathbf{S}(\tau)$, one integrand over imaginary times can be extended from $[0, \hbar\beta]$ to $[-\infty, +\infty]$, and the dissipative action can be divided into contributions that are local and non-local in time, *i.e.* $\mathcal{S}_{dis} = \mathcal{S}_l + \mathcal{S}_{nl}$. As detailed in the appendix, only the non-local action contributes to the equation of motion. After integrating over frequency ω, the non-local part reads

$$\mathcal{S}_{nl} = \frac{N_s^2 J^2 m^2}{8\mathcal{A}\hbar\pi^3} \ln\left(\frac{\epsilon_F}{J_{sd}}\right) \int_0^{\hbar\beta} d\tau \int_{-\infty}^{+\infty} d\tau' \frac{[\mathbf{S}(\tau) - \mathbf{S}(\tau')]^2}{(\tau - \tau')^2}. \tag{5.29}$$

The desired effective action of the magnetization therefore reads

$$\begin{aligned}\mathcal{S}_{eff} =& \mathcal{S}_{WZNW} + \mathcal{S}_{con} \\ &+ \frac{N_s^2 J^2 m^2}{8\mathcal{A}\hbar\pi^3} \ln\left(\frac{\epsilon_F}{J_{sd}}\right) \int_0^{\hbar\beta} d\tau \int_{-\infty}^{+\infty} d\tau' \frac{[\mathbf{S}(\tau) - \mathbf{S}(\tau')]^2}{(\tau - \tau')^2}.\end{aligned} \tag{5.30}$$

In the last term, the relevant time scale of the present system is governed by external magnetic or anisotropy fields, which also determines the cut-off for the time integral.

5.4 Equation of motion and damping parameter

The Euler-Lagrange principle is now applied to the spin variables with the associated effective Lagrangian $\mathcal{L}_{eff}$ defined by $\mathcal{S}_{eff} = \int_0^{\hbar\beta} d\tau \, \mathcal{L}_{eff}$. Focusing on the non-local term, this approach leads to:

$$\begin{aligned}\frac{\partial}{\partial \mathbf{S}(\tau)} \int_{-\infty}^{+\infty} d\tau' \frac{[\mathbf{S}(\tau) - \mathbf{S}(\tau')]^2}{(\tau - \tau')^2} &= 2 \int_{-\infty}^{+\infty} d\tau' \frac{\mathbf{S}(\tau) - \mathbf{S}(\tau')}{(\tau - \tau')} \frac{1}{(\tau - \tau')} \\ &= 2 \int_{-\infty}^{+\infty} d\tau' \frac{d\mathbf{S}(\tau')}{d\tau'} \left[\mathcal{P}\frac{1}{(\tau - \tau')} - i\pi\delta(\tau - \tau')\right] \\ &= -2i\pi \frac{d\mathbf{S}(\tau)}{d\tau}.\end{aligned} \tag{5.31}$$

In the last step the integral over the Cauchy principle value vanishes because the integrations over τ' from both sides cancel when approaching τ. This last step is valid as long as the time scale we are interested is the characteristic time scale of the magnetization response [13]. Performing a Wick rotation to real time t, *i.e.* $\tau \to it$, the equation of motion is obtained by setting $\partial\mathcal{S}/\partial\mathbf{S} = 0$, as

$$-\frac{\mathcal{N}_s}{S^2}\mathbf{S} \times \frac{d\mathbf{S}(t)}{dt} + \gamma\mathcal{N}_s\mathbf{H}_{ex} - \frac{N_s^2 J^2 m^2}{4\mathcal{A}\hbar\pi^2}\ln\left(\frac{\epsilon_F}{J_{sd}}\right)\frac{d\mathbf{S}(t)}{dt} = 0. \tag{5.32}$$

By taking the cross product of both sides with $\mathbf{S}\times$, the above equation can be recast as:

$$\frac{d\mathbf{S}(t)}{dt} = -\gamma\mathbf{S} \times \mathbf{H}_{ex} + \frac{N_s^2 J^2 m^2}{4\mathcal{A}\mathcal{N}_s\hbar\pi^2}\ln\left(\frac{\epsilon_F}{J_{sd}}\right)\mathbf{S} \times \frac{d\mathbf{S}(t)}{dt} = 0. \tag{5.33}$$

Converting the spins into a magnetization vector using the relation $\mathbf{S} = \mathcal{V}\mathbf{M}/\gamma$, a Landau-Lifshitz-Gilbert like equation is recovered:

$$\frac{1}{\gamma}\frac{d\mathbf{M}}{dt} = -\mathbf{M} \times \mathbf{H}_{ex} + \underbrace{\frac{N_s^2 J^2 m^2 M_s^2 \mathcal{V}}{4\mathcal{A}\mathcal{N}_s\hbar\pi^2}\ln\left(\frac{\epsilon_F}{J_{sd}}\right)}_{G}\frac{1}{\gamma^2 M_s^2}\mathbf{M} \times \frac{d\mathbf{M}}{dt}. \tag{5.34}$$

Taking a simple cubic structure with lattice constant a for the magnetic film, and a thickness d for the film, the total number of spins is $\mathcal{N}_s = \mathcal{A}d/a^3$. Inserting these relations into the expression for the damping parameter G, we obtain

$$G = \frac{(JM_s am)^2}{4\hbar\pi^2 d}\ln\left(\frac{\epsilon_F}{J_{sd}}\right). \tag{5.35}$$

The damping parameter derived as in Eq. (5.35) can be directly compared with the results of Eq. (30) in Ref. [9].

5.5 Magnetic film sandwiched by ferromagnetic host

We generalize the previous discussions of a normal metal host to a ferromagnetic one The s-d exchange is assumed to be the dominate interaction between magnetization of the magnetic film and spins of the conduction electrons. The total Hamiltonian is similar to that in the previous section, but with the host metal described by a Stoner model. For conduction electrons, the splitting between different spin bands is denoted by U. The spin quantization direction is chosen as the orientation of the magnetization of the host metal. Consequently the total Hamiltonian reads

$$\mathcal{H} = \sum_{\mathbf{k},\sigma} \xi_{\mathbf{k},\sigma} \phi^\dagger_{\mathbf{k}\sigma} \phi_{\mathbf{k}\sigma} - \frac{N_s J \hbar}{V} \sum_{\mathbf{k}\mathbf{k}'} \sum_{\sigma\sigma'} \phi^\dagger_{\mathbf{k}\sigma} \mathbf{S}_{\mathbf{k}\mathbf{k}'}(t) \cdot \boldsymbol{\sigma}_{\sigma\sigma'} \phi_{\mathbf{k}'\sigma'}, \tag{5.36}$$

where the energy difference in such a Stoner model is introduced as:

$$\xi_{\mathbf{k}\uparrow} = \epsilon_{\mathbf{k}} - \epsilon_F - \frac{1}{2}U, \quad \xi_{\mathbf{k}\downarrow} = \epsilon_{\mathbf{k}} - \epsilon_F + \frac{1}{2}U. \tag{5.37}$$

The spin-up band is chosen as the majority band, and the energy is measured from the middle of the spin gap. Accordingly, the propagator of the *free* conduction electrons in spin space reads

$$\begin{aligned} G(\mathbf{k}, n) &= \begin{pmatrix} G(\mathbf{k}, n, \uparrow) & 0 \\ 0 & G(\mathbf{k}, n, \downarrow) \end{pmatrix} \\ &= \begin{pmatrix} \frac{1}{-i\hbar\omega_n + \epsilon_{\mathbf{k}} - \epsilon_F - \frac{1}{2}U} & 0 \\ 0 & \frac{1}{-i\hbar\omega_n + \epsilon_{\mathbf{k}} - \epsilon_F + \frac{1}{2}U} \end{pmatrix}. \end{aligned} \tag{5.38}$$

As discussed in the case of a normal metal host, (Gaussian)integrating out the conduction electrons gives rise to the effective action for the magnetization. The first- and second-order terms in the perturbation expansions in terms of the s-d exchange coupling J are:

$$\mathrm{Tr}[G\mathbb{T}] = -\frac{N_s J \hbar}{V\sqrt{\hbar\beta}} \sum_{\mathbf{k}\mathbf{k}'} (G_\uparrow - G_\downarrow) S_z \tag{5.39}$$

$$\begin{aligned} \frac{1}{2}\mathrm{Tr}[G\mathbb{T}G\mathbb{T}] = \frac{N_s^2 J^2 \hbar}{2\beta V^2} \sum_{\mathbf{k}\mathbf{k}'} \sum_{nn'} & (G_\uparrow S_z G_\uparrow S_z + G_\uparrow S_- G_\downarrow S_+ \\ & + G_\downarrow S_+ G_\uparrow S_- + G_\downarrow S_z G_\downarrow S_z) \,. \end{aligned} \tag{5.40}$$

The first-order term is responsible for an exchange field acting on the magnetization of the film, which alters the precession frequency of the magnetization dynamics. But the first-order term does not involve any correlation of magnetization at different instants, *i.e.* no contribution to the damping of magnetization dynamics. In the following we focus on the second-order term that eventually gives rise to damping of magnetization induced by the conduction electrons, as discussed in previous section. Equation (5.40), containing the spin-density–spin-density response function, is divided into two parts, *i.e.* the *longitudinal* and the *transverse* parts. The longitudinal part which correlates the z-component of the magnetization (S_z) is given by:

$$\begin{aligned}
&\frac{N_s^2 J^2 \hbar}{2\beta V^2} \sum_{\mathbf{k}\mathbf{k}'} \sum_{nn'} \left(G_\uparrow S_z G_\uparrow S_z + G_\downarrow S_z G_\downarrow S_z \right) \\
&= -\frac{N_s^2 J^2 m^2}{4\mathcal{A}\pi^3\hbar^2} \int_0^{\hbar\beta} d\tau \int_0^{\hbar\beta} d\tau' \int_0^{+\infty} d\omega\omega \\
&\times \left[\ln \left(\sqrt{\frac{2\hbar^2 k_F k_{F\uparrow}}{\Delta_{sd} m}} \right) + \ln \left(\sqrt{\frac{2\hbar^2 k_F k_{F\downarrow}}{\Delta_{sd} m}} \right) \Theta(\epsilon_F - U) \right] \\
&\times \frac{\cosh(\hbar\beta\omega/2 - \omega|\tau - \tau'|)}{\sinh(\hbar\beta\omega/2)} S_z(\tau) S_z(\tau'),
\end{aligned} \tag{5.41}$$

where the spin-dependent Fermi vectors are defined as $k_{F\uparrow(\downarrow)} = \sqrt{2m\,(\epsilon_F + (-)U/2)}/\hbar$. The step function $\Theta(\epsilon_F - U)$ in Eq.(5.41) reminds us that in the case of a very strong ferromagnet (such as half-metals), modelled by an exchange energy larger than Fermi energy, the minority band can be completely depleted. For the minority band the density of states at the Fermi energy then vanishes, as depicted in panel (c) of Fig. 5.3. In such a situation, $\sum G_\downarrow G_\downarrow = 0$.

The evaluation of the transverse part requires careful manipulation. After summing over the fermionic Matsubara frequencies and with a Fourier transformation back to integrals with respect to imaginary time, we have

$$\begin{aligned}
&\sum_{\mathbf{k}\mathbf{k}'} \sum_{nn'} G_\uparrow S_- G_\downarrow S_+ \\
&= \frac{1}{\hbar} \sum_{\mathbf{q}} \int_0^{\hbar\beta} d\tau \int_0^{\hbar\beta} d\tau' \sum_{\mathbf{k}} \left(f_{\mathbf{k}+\mathbf{q}\downarrow} - f_{\mathbf{k}\uparrow} \right) \sum_m \frac{e^{i\omega_m(\tau-\tau')}}{i\hbar\omega_m + \epsilon_{\mathbf{k}+\mathbf{q}} - \epsilon_{\mathbf{k}} + U} S_-(\tau) S_+(\tau'),
\end{aligned} \tag{5.42}$$

where it is assumed that the d-electrons are localized and thus have negligible momentum dependence. It is instructive to consider the distribution functions in the expansion in more detail. The momentum $\mathbf{q}$ is assumed to be small compared to the Fermi momentum; therefore keeping only the linear term in $\mathbf{q}$ is justified, which

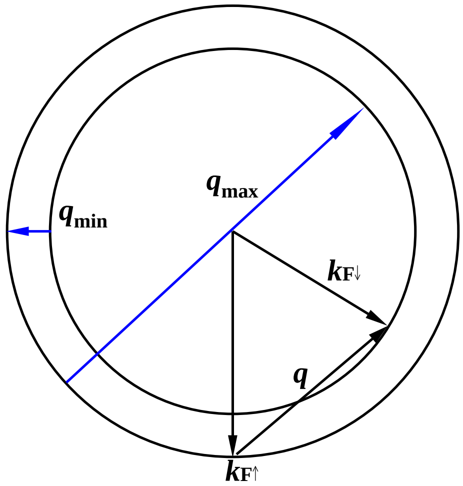

Figure 5.2: Schematic show of the momentum exchange between spin-up and spin-down electrons.

leads to $\epsilon_{\mathbf{k}+\mathbf{q}} - \epsilon_{\mathbf{k}} \approx \hbar^2\mathbf{k}\cdot\mathbf{q}/m < U < \epsilon_F$. The last inequality is certainly not meant to apply to half-metals where the spin gap is seen to be larger than the Fermi energy, which depletes the minority spin band. The situation concerning a half-metal will be discussed later. For the distribution functions the above assumption makes the following approximation valid:

$$f_{\mathbf{k}+\mathbf{q}\downarrow} - f_{\mathbf{k}\uparrow} \approx f_{\mathbf{k}\downarrow} - f_{\mathbf{k}\uparrow} + \frac{\partial f_\downarrow}{\partial \epsilon}\frac{\hbar^2\mathbf{k}\cdot\mathbf{q}}{m} \approx \frac{\partial f}{\partial \epsilon}U + \frac{\partial f_\downarrow}{\partial \epsilon}\frac{\hbar^2\mathbf{k}\cdot\mathbf{q}}{m}, \tag{5.43}$$

where at low temperature, the derivative $\partial f/\partial\epsilon$ simply gives a δ-function with minus sign centered at the Fermi energy ϵ_F. More important are the lower and upper limits of the exchanged momentum q. Since the electrons under consideration are at the Fermi energy, and due to the splitting of Stoner mode, the Fermi sphere effectively splits into two (for different spin bands). As sketched in Fig. 5.2, the minimum of the exchanged momentum is given by $q_{min} = k_{F\uparrow} - k_{F\downarrow}$ and the maximum is given by $q_{max} = k_{F\uparrow} + k_{F\downarrow}$. As such the summation over q is bounded, and carries the function

$$\Lambda_q = \begin{cases} 1, & k_{F\uparrow} - k_{F\downarrow} < q < k_{F\uparrow} + k_{F\downarrow} \\ 0, & \text{otherwise}. \end{cases} \tag{5.44}$$

Having expanded the distribution function and set up the limits for the momentum integration for the magnetic host, the response function of spin-density reads:

$$\begin{aligned}
&\sum_{\mathbf{k}\mathbf{k}'}\sum_{nn'} G_\uparrow S_- G_\downarrow S_+ \\
&= \frac{\beta}{\hbar}\sum_{\mathbf{q}} \Lambda_q \int_0^{\hbar\beta} d\tau \int_0^{\hbar\beta} d\tau' \int_0^{+\infty} d\omega \sum_{\mathbf{k}} \left(\frac{\partial f}{\partial \epsilon} U + \frac{\partial f_\downarrow}{\partial \epsilon}\frac{\hbar^2 \mathbf{k}\cdot\mathbf{q}}{m}\right) \\
&\times \left[\delta\left(\omega - \frac{U}{\hbar} - \frac{\hbar\mathbf{k}\cdot\mathbf{q}}{m}\right) - \delta\left(\omega + \frac{U}{\hbar} + \frac{\hbar\mathbf{k}\cdot\mathbf{q}}{m}\right)\right] \\
&\times \frac{\cosh(\hbar\beta\omega/2 - \omega|\tau-\tau'|)}{\sinh(\hbar\beta\omega/2)} S_-(\tau) S_+(\tau'). \qquad (5.45)
\end{aligned}$$

We introduce spherical coordinates to perform the summation over $\mathbf{k}$, such that

$$\begin{aligned}
&\sum_{\mathbf{k}} \left(\frac{\partial f}{\partial \epsilon} U + \frac{\partial f_\downarrow}{\partial \epsilon}\frac{\hbar^2 \mathbf{k}\cdot\mathbf{q}}{m}\right) \left[\delta\left(\omega - \frac{U}{\hbar} - \frac{\hbar\mathbf{k}\cdot\mathbf{q}}{m}\right) - \delta\left(\omega + \frac{U}{\hbar} + \frac{\hbar\mathbf{k}\cdot\mathbf{q}}{m}\right)\right] \\
&= -\frac{V\omega m^2}{2q\pi^2\hbar^2}\Theta\left[1 - \left(\omega + \frac{U}{\hbar}\right)\frac{m}{\hbar k_{F\downarrow} q}\right]. \qquad (5.46)
\end{aligned}$$

The transverse part of the spin-density–spin-density response function contains the following expressions:

$$\begin{aligned}
\sum_{\mathbf{k}\mathbf{k}'}\sum_{nn'} G_\uparrow S_\mp G_\downarrow S_\pm = &-\frac{V^2\beta m^2}{4\mathcal{A}\pi^3\hbar^3}\ln\left(\frac{k_{F\uparrow}+k_{F\downarrow}}{k_{F\uparrow}-k_{F\downarrow}}\right)\int_0^{\hbar\beta} d\tau \int_0^{\hbar\beta} d\tau' S_\mp(\tau) S_\pm(\tau') \\
&\times \int_0^{+\infty} d\omega\omega \frac{\cosh(\hbar\beta\omega/2 - \omega|\tau-\tau'|)}{\sinh(\hbar\beta\omega/2)}. \qquad (5.47)
\end{aligned}$$

Using the above results, the transverse part of the response function is obtained as

$$\begin{aligned}
&\frac{N_s^2 J^2 \hbar}{2\beta V^2}\sum_{\mathbf{k}\mathbf{k}'}\sum_{nn'} (G_\uparrow S_- G_\downarrow S_+ + G_\downarrow S_+ G_\uparrow S_-) \\
&= -\frac{N_s^2 J^2 m^2}{4\mathcal{A}\pi^3\hbar^2}\ln\left(\frac{k_{F\uparrow}+k_{F\downarrow}}{k_{F\uparrow}-k_{F\downarrow}}\right)\int_0^{\hbar\beta} d\tau \int_0^{\hbar\beta} d\tau' \left(S_x(\tau)S_x(\tau') + S_y(\tau)S_y(\tau')\right) \\
&\times \int_0^{+\infty} d\omega\omega \frac{\cosh(\hbar\beta\omega/2 - \omega|\tau-\tau'|)}{\sinh(\hbar\beta\omega/2)}. \qquad (5.48)
\end{aligned}$$

The effective action for the magnetization after removing the conduction electrons reads

$$\begin{aligned}\mathcal{S}_{eff} =& \mathcal{S}_{WZNW} + \mathcal{S}_{con} \\ & - \frac{N_s^2 J^2 m^2}{4\mathcal{A}\pi^3\hbar} \int_0^{\hbar\beta} d\tau \int_0^{\hbar\beta} d\tau' \int_0^{+\infty} d\omega\omega \frac{\cosh(\hbar\beta\omega/2 - \omega|\tau-\tau'|)}{\sinh(\hbar\beta\omega/2)} \\ & \times \left[\ln\left(\frac{k_{F\uparrow}+k_{F\downarrow}}{k_{F\uparrow}-k_{F\downarrow}}\right)(S_x(\tau)S_x(\tau') + S_y(\tau)S_y(\tau')) + \left(\ln\left(\sqrt{\frac{2\hbar^2 k_F k_{F\uparrow}}{\Delta_{sd} m}}\right)\right.\right. \\ & \left.\left. + \ln\left(\sqrt{\frac{2\hbar^2 k_F k_{F\downarrow}}{\Delta_{sd} m}}\right)\Theta(\epsilon_F - U)\right) S_z(\tau)S_z(\tau')\right], \end{aligned} \tag{5.49}$$

where the correlation functions of the transverse and longitudinal components of the magnetization are different as a result of the polarized host material. When the spin splitting due to Stoner modes vanishes, the above effective action reduces to the case of a normal metal host. According to the Euler-Lagrange principle, the variational method can be employed here to derive the equation of motion for the magnetization, *i.e.* with respect to effective action (Eq. (5.49)). We obtain an equation of motion in the Landau-Lifshitz-Gilbert form, as

$$\frac{1}{\gamma}\frac{d\mathbf{M}}{dt} = -\mathbf{M}\times\mathbf{H}_{ex} + \frac{1}{\gamma^2 M_s^2}\mathbf{M}\times\left[\hat{G}\cdot\frac{d\mathbf{M}}{dt}\right], \tag{5.50}$$

where the damping can no longer be described by a single parameter, but appears as a diagonal matrix (denoted by Diag$[\cdots]$):

$$\begin{aligned}\hat{G} = \frac{(JM_s am)^2}{4\hbar\pi^2 d}\mathrm{Diag}\left[\ln\left(\frac{k_{F\uparrow}+k_{F\downarrow}}{k_{F\uparrow}-k_{F\downarrow}}\right), \ln\left(\frac{k_{F\uparrow}+k_{F\downarrow}}{k_{F\uparrow}-k_{F\downarrow}}\right),\right. \\ \left. \ln\left(\sqrt{\frac{2\hbar^2 k_F k_{F\uparrow}}{\Delta_{sd} m}}\right) + \ln\left(\sqrt{\frac{2\hbar^2 k_F k_{F\downarrow}}{\Delta_{sd} m}}\right)\Theta(\epsilon_F - U)\right]. \end{aligned} \tag{5.51}$$

The anisotropic damping Eq.(5.51) recovers the results in the normal metal host when the spin splitting of conduction electrons is lifted, *i.e.* taking $U = 0$ and thus $k_{F\uparrow} = k_{F\downarrow}$. Upon taking such a limit, attention should be paid to the lower cut-off of the momentum integration over q, which is no longer $k_{F\uparrow} - k_{F\downarrow}$ but $m\Delta_{sd}/(\hbar^2 k_f)$. Thereby the damping parameter Eq.(5.51) reproduces Eq.(5.35) properly when the exchange energy U vanishes.

5.6 Special case: half-metallic host

One of the *extreme* cases of host material is the half-metallic metal, which in our description using a Stoner model is modeled with a spin splitting (U) that is much larger than the Fermi energy, such that the minority band is depleted. This limit corresponds to the polarization p, defined using the density of states at the Fermi energy $p = (N_\uparrow + N_\downarrow)/(N_\uparrow - N_\downarrow)$, being equal to 1. In the half-metallic case, strong magnetism gives rise to $k_{F\downarrow} = 0$ (for the Fermi vector of the minority band), which leads to an interesting damping parameter:

$$\hat{G} = \frac{(JM_s am)^2}{4\hbar\pi^2 d}\mathrm{Diag}\left[0, 0, \ln\left(\sqrt{\frac{2\hbar^2 k_F k_{F\uparrow}}{\Delta_{sd} m}}\right)\right]. \tag{5.52}$$

Here the imaginary part of transverse spin-density response functions vanish, and what remains is the longitudinal one. Since we ascribe the dissipation of the magnetization dynamics to magnetization excitations decaying into particle-hole pairs, in the half-metallic case the inter-band electron-hole excitation is prohibited due to significant energy cost, as depicted in Fig. 5.3.

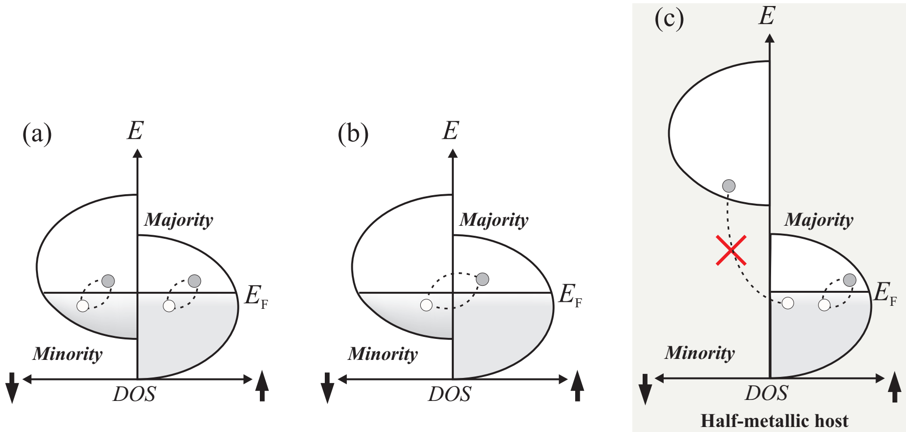

Figure 5.3: Electron-hole excitation that governs the Ohmic dissipation. In all figures, the empty circles are holes and the filled ones electrons. Panel (a), the intra-band electron-hole excitation. Panel (b), the inter-band excitation in a weak ferromagnet. Panel (c), in the half-metallic case, the inter-band excitation is suppressed due to the significant energy cost.

5.7 Conclusion

We have studied the damping of a magnetic film sandwiched by metallic hosts of normal metal and ferromagnet. The interaction between magnetization and the conduction electrons opens a channel for dissipation. In the absence of a bias (*i.e.* the equilibrium situation) the magnetization excitation decays into electron-hole pairs, leading to Ohmic dissipation that appears in the equation of motion in the Landau-Lifshitz-Gilbert form. The damping parameter is directly related to the imaginary part of the spin-density–spin-density response function that governs the dissipation. When the host material is magnetic, damping of the magnetization dynamics of the film can no longer be described by a single parameter, but takes a matrix form (tensor). In the extreme case of a half-metallic host, the inter-band electron-hole excitation is suppressed, and the imaginary part of the transverse spin-density response function vanishes.

5.8 Appendix: Summation of Matsubara frequencies

In this appendix, as a reference, we list several formulae concerning the summation of Matsubara frequencies. These identities can often be found in the textbooks on many-body theory, such as the text by Fetter and Walecka [16]. For fermionic Matsubara frequencies $\omega_n = (2n+1)\pi/\hbar\beta$, and introducing an positive infinitesimal η:

$$\lim_{\eta\to 0}\frac{1}{\beta}\sum_n \frac{e^{i\omega_n \eta}}{i\hbar\omega_n - (\epsilon-\mu)} = \frac{1}{1+e^{\beta(\epsilon-\mu)}}, \tag{5.53}$$

which is exactly the Fermi-Dirac distribution function. For bosonic frequencies $\omega_n = 2n\pi/\hbar\beta$, yielding the similar form

$$\lim_{\eta\to 0}\frac{1}{\beta}\sum_n \frac{e^{i\omega_n \eta}}{i\hbar\omega_n - (\epsilon-\mu)} = -\frac{1}{e^{\beta(\epsilon-\mu)}-1}. \tag{5.54}$$

A Matsubara summation of the following form with bosonic frequencies $\omega_m = 2m\pi/\hbar\beta$ is often encountered:

$$\sum_m \frac{e^{-i\omega_m \tau}}{i\omega_m - x}, \tag{5.55}$$

which is evaluated differently for $\tau > 0$ and $\tau < 0$.

For negative τ, Matsubara summation yields

$$\sum_m \frac{e^{-i\omega_m |\tau|}}{i\omega_m - x}, \tag{5.56}$$

which has poles on the real axis and can be evaluated by the integral [16]:

$$\sum_m \frac{e^{-i\omega_m |\tau|}}{i\omega_m - x} = \hbar\beta \oint_{C'} \frac{d\Omega}{2\pi i}\frac{e^{-\Omega|\tau|}}{e^{\hbar\beta\Omega}-1}\frac{1}{\Omega - x} \tag{5.57}$$

along contour $\mathcal{C}$ as depicted in Fig.5.4. Since the function $1/(e^{\hbar\beta\Omega}-1)$ has simple poles with residues $1/\hbar\beta$ at $\Omega = i2n\pi/\hbar\beta$ on the imaginary axis, the function in the above contour integral converges when $|\Omega| \to \infty$. On the other hand, when $\tau > 0$, in order to make the contour integral converge at $|\Omega| \to \infty$, the function is selected to be:

$$\sum_m \frac{e^{-i\omega_m |\tau|}}{i\omega_m - x} = \hbar\beta \oint_{C'} \frac{d\Omega}{2\pi i}\frac{e^{-\Omega|\tau|}}{1-e^{-\hbar\beta\Omega}}\frac{1}{\Omega - x}\ . \tag{5.58}$$

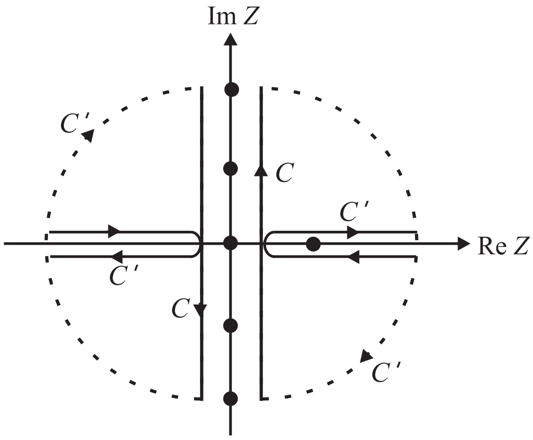

Figure 5.4: The integration contour for the Matsubara summation. The contour $\mathcal{C}$ enclosing imaginary axis can be deformed to the contour $\mathcal{C}'$.

Combining the above two expressions for $\tau > 0$ and $\tau < 0$, we obtain for the summation $\mathcal{I}(\tau)$ the following result:

$$\sum_m \frac{e^{-i\omega_m|\tau|}}{i\omega_m - x} = \hbar\beta \oint_{\mathcal{C}'} \frac{d\Omega}{2\pi i} \frac{1}{\Omega - x} \frac{\cosh(\hbar\beta\Omega/2 - \Omega|\tau|)}{\sinh(\hbar\beta\Omega/2)} \,. \tag{5.59}$$

The integral on the arcs (dotted line) of the contour $\mathcal{C}'$ vanishes when the radius of the contour approaches infinity, and one left with the integral along the real axis. This can be decomposed into four parts by introducing a real frequency $\Omega \to \omega \pm i\varepsilon^+$ (note that care must be taken with the overall minus sign)

$$\begin{aligned} -\frac{1}{\hbar\beta}\sum_m \frac{e^{-i\omega_m|\tau|}}{i\omega_m - x} = & \int_0^{\infty} \frac{d\omega}{2\pi i} \frac{1}{\omega - x + i\varepsilon^+} \frac{\cosh(\hbar\beta\omega/2 - \omega|\tau|)}{\sinh(\hbar\beta\omega/2)} \\ & + \int_{\infty}^{0} \frac{d\omega}{2\pi i} \frac{1}{\omega - x - i\varepsilon^+} \frac{\cosh(\hbar\beta\omega/2 - \omega|\tau|)}{\sinh(\hbar\beta\omega/2)} \\ & + \int_{-\infty}^{0} \frac{d\omega}{2\pi i} \frac{1}{\omega - x + i\varepsilon^+} \frac{\cosh(\hbar\beta\omega/2 - \omega|\tau|)}{\sinh(\hbar\beta\omega/2)} \\ & + \int_{0}^{-\infty} \frac{d\omega}{2\pi i} \frac{1}{\omega - x - i\varepsilon^+} \frac{\cosh(\hbar\beta\omega/2 - \omega|\tau|)}{\sinh(\hbar\beta\omega/2)} \,. \end{aligned} \tag{5.60}$$

The integrals above can all be converted into integrations over ω on the half-line $[0, +\infty]$, which only requires a substitution $\omega \to -\omega$ for the third and fourth integrations, *i.e.*

$$\begin{aligned}\sum_m \frac{e^{-i\omega_m|\tau|}}{i\omega_m - x} =& -\hbar\beta \int_0^\infty \frac{d\omega}{2\pi i}\left[\frac{1}{\omega - x + i\varepsilon^+} - \frac{1}{\omega - x - i\varepsilon^+}\right. \\ & \left. + \frac{1}{\omega + x - i\varepsilon^+} - \frac{1}{\omega + x + i\varepsilon^+}\right]\frac{\cosh(\hbar\beta\omega/2 - \omega|\tau|)}{\sinh(\hbar\beta\omega/2)} \\ =& \hbar\beta \int_0^\infty d\omega[\delta(\omega - x) - \delta(\omega + x)]\frac{\cosh(\hbar\beta\omega/2 - \omega|\tau|)}{\sinh(\hbar\beta\omega/2)},\end{aligned} \tag{5.61}$$

where the following identity has been used:

$$\frac{1}{\omega \pm i\varepsilon^+} = \mathcal{P}\frac{1}{\omega} \mp i\pi\delta(\omega). \tag{5.62}$$

Bibliography

[1] E. M. Lifshitz and L. P. Pitaevskii, *Statistical Mechanics, Part 2* (Butterworth-Heinemann, 1980).

[2] T. Gilbert, Phys. Rev. **100**, 1243(1955); IEEE Trans. Magn. **40**, 3443 (2004).

[3] S. Mizukami, Y. Ando, and T. Miyazaki, J. Appl. Phys., Part 1 **40**, 580 (2001); J. Magn. Magn. Mater. **226**, 1640 (2001); Phys. Rev. B **66**, 104413 (2002).

[4] Y. Tserkovnyak, A. Brataas, and G. E. W. Bauer, Phys. Rev. Lett. **88**, 117601 (2002).

[5] Y. Tserkovnyak, A. Brataas, G. E. W. Bauer, and B. Halperin, Rev. Mod. Phys. **75**, 107001 (2005).

[6] A. Brataas, Y. V. Nazarov, and G. E. W. Bauer, Phys. Rev. Lett. **84**, 2481 (2000).

[7] Ya. M. Blanter and M. Büttiker, Phys. Rep. **336**, 1 (2000).

[8] P. W. Brouwer, Phys. Rev. B **58**, 10135(1998).

[9] E. Simanek and B. Heinrich, Phys. Rev. B **67**, 144418 (2003).

[10] D. L. Mills, Phys. Rev. B **68**, 014419 (2003).

[11] R. A. Duine, A. S. Nunez, J. Sinova, and A. H. MacDonald, Phys. Rev. B **75**, 214420 (2007).

[12] R. P. Feynman and F. L. Vernon, Ann. Phys. **24**, 118 (1963).

[13] A. O. Caldeira and A. J. Leggett, Ann. Phys. **149**, 374 (1984).

[14] E. Fradkin, *Field Theories of Condensed Matter Systems* (Addison-Wesley, Redwood City, 1991).

[15] A. Auerbach, *Interacting Electrons and Quantum Magnetism* (Springer-Verlag, New York, 1994).

[16] A. L. Fetter and J. D. Walecka, *Quantum Theory of Many-Particle Systems* (McGraw-Hill, New York, 1971).

Summary

Manipulation of electronic charge in various kinds of micro-structures and miniature devices has been studied thoroughly for a very long time. Besides the charge degrees of freedom, the spin, as a quantum degree of freedom carried by an electron, has likewise been a subject of scientific research ever since its discovery nearly one-hundred years ago. As a consequence, the ferromagnet, a material already using for thousands of years, is now understood in modern physics as a macroscopic condensate of spins.

Research on transport and potential applications involving spins is a new field that arose rather recently. The discovery of giant-magneto-resistance (GMR) in normal-metal-ferromagnet hetero-structures in the 1980's led to substantial scientific attention and novel technological applications. An excellent example is the hard-disk drive, which plays vital roles in data storage and our daily lives. More recently still a novel field named *spintronics* has emerged.

In the renowned GMR effect, the electrical resistance crucially depends on the relative orientations of the magnetization directions of two ferromagnets separated by a normal metal. The physical mechanism behind this is the electron scattering at spin-sensitive interfaces, *i.e.* at an interface between a normal metal and a ferromagnet, electrons with different spin orientations are scattered differently. As a reverse effect, polarized spins carried by conduction electrons interact with a magnetization, exerting a torque and causing the transfer of angular-momentum. As a result of angular- momentum conservation, the transferred angular momentum can give rise to magnetization dynamics. This leads to the so-called *spin transfer torque* predicted by Slonczewski and Berger, which prediction has been followed by substantial experimental testing and further theoretical investigation.

It is well-known that a magnetic field can induce magnetization dynamics, such as precession or more complicated trajectories. The spin-transfer torque can act as an alternative mechanism for switching the magnetization in nano-devices without resorting to heavy magnetic fields. The mechanism itself is of scientific interest as well. Developed based on deep insight into electron scattering, the *magneto-electronic circuit theory* treats spin transport and spin-transfer torques in nano-structures in an elegant and concise way.

This thesis is dedicated to the study of magnetization dynamics driven by electrical and spin currents, or spin-transfer torques and related effects. The magneto-electronic circuit theory is the major tool employed here. In Chapter 1 of this thesis, we briefly reviewed the current physical understanding of ferromagnetism and important issues such as spin injection, spin detection, and spin-transfer torques in nano-structures. The Landauer-Büttiker formalism for electron transport has been introduced in order to further appreciate the magneto-electronic circuit theory.

In Chapter 2 and 3, a new lateral device called a spin-flip transistor was introduced. We focused on the *dc*-current-driven magnetization dynamics with different source-drain magnetizations. The studies in these two chapters suggested that the details of the spin-transfer torque must be analysed according to the specific configuration of a setup. Spin-flip scattering and spin-pumping effects also played important roles in determining critical switching current. In Chapter 2 we found a tunable steady-state precession of the base magnetization. While in Chapter 3, a tunable two-state behavior of the magnetization was found as a result of a different configuration of source-drain magnetizations.

Another interesting phenomenon associated with magnetization dynamics is so-called spin pumping: a precessing magnetization (*e.g.* under ferromagnetic resonance) pumps spin current into the adjacent normal metal, losing angular momentum and at the same time building up a non-equilibrium spin accumulation. In Chapter 4, we proposed a mechanism to convert the spin signal due to spin pumping to a voltage across the ferromagnet-normal metal interface. To achieve this, we noticed that a strong exchange field in the ferromagnet allows only the parallel (to the magnetization direction) component of the back-flow spin current (generated by a spin accumulation in the normal metal) to penetrate the ferromagnetic layer. But this penetration leads to spin accumulation inside the ferromagnet. The spin-flip scattering and the difference in conductivities between electrons with different spin then create a potential difference across the interface: a *dc* voltage. The beautiful experiments done by Prof. van Wees's group of Groningen University confirmed these predictions.

The damping parameters of magnetization dynamics are important physical quantities, since they are closely related to dissipation in a magnetic system. One of the dominant effects caused by spin pumping, as noted above, is the enhancement of the damping parameter in the Landau-Lifshitz-Gilbert (LLG) equation (the equation of motion of magnetization dynamics), as a result of losing (dissipating) angular momentum into the adjacent material.

In Chapter 5, we investigated the damping parameter of a thin magnetic film embedded in a normal metal (host) from a different perspective. The conduction electrons form a dissipative environment for the magnetization via the s-d exchange coupling. According to the celebrated Caldeira-Leggett formalism, the dissipation that is responsible for the damping of the spin dynamics can be obtained by analysing the *non-local-in-time* part of an action for the magnetisation dynamics. To do so, we set up an imaginary-time path integral for the s-d exchange model. By removing the conduction electron degrees of freedom, we obtained an effective action for the magnetization.

The dissipation channel is the decay of the magnetization excitations into electron-hole pairs, and we derived a LLG-like equation for the dynamics. In the case of a normal-metal host the damping is captured by a single parameter, but when the host becomes ferromagnetic, the damping parameters are described by a tensor-like quantity in the LLG equation. Future studies should address spin-wave excitations in the ferromagnetic host, since in the spirit of the Caldeira-Leggett formalism, in such situations magnons behave as an environment that give rise to more interesting magnetization dynamics.

Samenvatting

Manipulatie van elektrische lading in verschillende soorten microstructuren en geminiaturiseerde apparatuur is al geruime tijd uitgebreid bestudeerd. Naast de ladingsvrijheidsgraden, is de spin, als kwantumvrijheidsgraad, evenzo het onderwerp van wetenschappelijk onderzoek geweest sinds de ontdekking ervan bijna honderd jaar geleden. Als gevolg wordt de ferromagneet, een materiaal wat al duizenden jaren in gebruik is door de mensheid, in de moderne fysica inmiddels begrepen als een macroscopisch condensaat van spin.

Onderzoek naar transport en mogelijke toepassingen van spin, integendeel, is een onderzoeksgebied waar men pas recent aan is begonnen. De ontdekking van giant-magneto-resistance (GMR) in metaal-ferromagneet heterostructuren in de jaren ’80 leidde tot aanzienlijke wetenschappelijke aandacht en ingenieuze technologische toepassingen. Een uitstekend voorbeeld hiervan is de harde schijf, welke een vitale rol speelt in zowel de technologie van data-opslag, als in ons dagelijks leven. Inmiddels is er zelfs een nog nieuwer onderzoeksgebied bijgekomen: de *spintronica*.

In het befaamde GMR effect hangt de elektrische weerstand cruciaal af van de relatieve orintaties van de magnetisatie-richtingen van twee ferromagneten die van elkaar gescheiden zijn door een stuk normaal metaal. Het achterliggend fysisch mechanisme is de verstrooiing van elektronen aan spingevoelige grensvlakken, *d.w.z.* doordat aan een grensvlak tussen een normaal metaal en een ferromagneet elektronen met verschillende spinrichting anders verstrooid worden. Het omgekeerde effect bestaat ook: gepolariseerde spins van geleidingselektronen staan in wisselwerking met de magnetisatie, waardoor ze een moment uitoefenen en zorgen voor de overdracht van impulsmoment. Als gevolg van het behoud van impulsmoment kan deze overdracht voor magnetisatie-dynamica zorgen. Dit leidt tot de zogeheten

spin-transfer torque voorspeld door Slonczewski en Berger.

Het is alom bekend dat een magnetisch veld magnetisatie-dynamica kan opwekken, zoals precessie of ingewikkeldere trajectorin van de magnetisatie. De spin-transfer torque kan daardoor gebruikt worden als een alternatief mechanisme voor het schakelen van de magnetisatie in nanoapparatuur, zonder tussenkomst van sterke magnetische velden. Het mechanisme zelf is ook wetenschappelijk interessant. Ontwikkeld op basis van diepe inzichten in elektronenverstrooiing, zorgt de magneto-electronische circuit theorie voor een elegante en beknopte beschrijving van spin-transport en spin-transfer torques.

Dit proefschrift is gewijd aan het bestuderen van magnetisatie-dynamica opgewekt door elektrische- en spinstromen, ofwel spin-transfer torques en gerelateerde verschijnselen. De magneto-electronische circuit theorie is het voornaamste theoretische gereedschap wat hierin gebruikt is. In hoofdstuk 1 hebben wij een kort overzicht gegeven van het gangbare fysische model van ferromagnetisme en belangrijke onderwerpen zoals spininjectie, spindetectie en spin-transfer torques in nanostructuren. et Landauer-Bttiker formalisme voor elektronentransport is gentroduceerd om hiermee de magneto-elektronische circuit theorie op te kunnen bouwen.

In hoofdstuk 2 en 3 is een nieuwe laterale structuur gentroduceerd, een zogeheten spin-flip transistor. We hebben gekeken naar magnetisatie-dynamica aangedreven door een gelijkstroom, bij verschillende magnetisaties van plus- en minpool. De beschouwingen van deze twee hoofdstukken suggereerden dat de details van de spin-transfer torques geanalyseerd moeten worden aan de hand van de specifieke geometrie van een (experimentele) opstelling. Spin-flip verstrooiing en spin-pump verschijnselen speelden ook een belangrijke rol in het bepalen van de kritische schakelstroom. In hoofdstuk II vonden we een stembare stationaire precessie van de basis-magnetisatie, terwijl in hoofdstuk III een stembare 2-toestandsgedrag van de magnetisatie werd gevonden, als gevolg van een andere configuratie van de magnetisaties van plus- en minpool.

Een ander interessant verschijnsel dat met magnetisatie-dynamica te maken heeft is het zogeheten 'spin-pumping:' een tollende magnetisatie (bijvoorbeeld onder ferromagnetische resonantie) pompt een spinstroom in het aangrenzende normale metaal, en verliest zodoende impulsmoment tegelijk het een niet-evenwicht spinaccumulatie opbouwt. In hoofdstuk 4 stelden wij een elektrische meting voor om het spinsignaal ten gevolge van spin-pumping om te zetten in een spanning over het metaal-ferromagneet grensvlak. Om dit te bereiken, merkten we op dat een sterke exchange veld in de ferromagneet ervoor zou zorgen dat alleen de component van de back-flow spinstroom (opgewekt door spinaccumulatie in het normale metaal) die parallel staat aan de magnetisatierichting de ferromagneet in kan dringen. Dit binnendringen zorgt op zijn beurt weer voor een spinaccumulatie in de ferromagnetische laag. De spin-flip verstrooiing en het verschil in conductiviteit tussen elektronen met verschillende spins veroorzaken vervolgens een potentiaalverschil over het grensvlak: een gelijkspanning. De bijzonder mooie experimenten uitgevoerd in de groep van professor van Wees aan de Universiteit Groningen bevestigden deze voorspellingen.

De dempingparameters van de magnetisatie-dynamica zijn belangrijke fysische grootheden, aangezien zij nauw samenhangen met de dissipatie in een magnetisch systeem. Een van de dominante effecten van spin-pumping is het vergroten van de dempingparameter in de Landau-Lifshitz-Gilbert (LLG) vergelijking (de bewegingsvergelijking van de magnetisatie-dynamica), als gevolg van het verlies van impulsmoment aan het aangrenzende materiaal.

In hoofdstuk 5 hebben we vanuit een ander perspectief onderzoek gedaan naar de dempingparameter van een dunne magnetische film, ingebed in een stuk normaal metaal. De geleidingselektronen vormen een dissipatieve omgeving voor de magnetisatie middels de s-d exchange koppeling. Volgens het welbekende Caldeira-Leggett formalisme kan de dissipatie die verantwoordelijk is voor de demping van de spindynamica verkregen worden uit een analyse van het *niet-lokaal-in-tijd* zijnde deel van een action voor de magnetisatie-dynamica. Om dit te doen hebben wij een padintegraal in imaginaire tijd geconstrueerd voor het s-d exchange model. Door de vrijheidsgraden van de geleidingselektronen te verwijderen kwamen wij vervolgens uit op een effectieve action voor de magnetisatie.

Dit dissipatie-kanaal is het verval van magnetisatie-excitaties in electron-gat paren, en wij hebben een LLG-achtige vergelijking voor de dynamica afgeleid. In het geval van een normaal metaal wordt de demping gevat in n parameter, maar wanneer dit vervangen wordt door een ferromagneet, blijken de dempingparameters door een tensor-achtige grootheid in de LLG vergelijking beschreven te worden. Toekomstig onderzoek zou zich kunnen richten op spingolf excitaties in de ferromagneet, aangezien in de geest van het Caldeira-Leggett formalisme, magnonen in dergelijke situaties een omgeving vormen die bijzonder interessante magnetisatie-dynamica kan opleveren.

Publication List

Voltage generation by ferromagnetic resonance at a nonmagnet to ferromagnet contact,
X. Wang, G. E. W. Bauer, B. J. van Wees, A. Brataas, and Y. Tserkovnyak,
Phys. Rev. Lett. **97**, 216602 (2006).

Current-controlled magnetization dynamics in the spin-flip transistors,
X. Wang, G. E. W. Bauer, and T. Ono,
Jpn. J. Appl. Phys. **45**, 3863 (2006).

Dynamics of thin-film spin-flip transistors with perpendicular source-drain magnetizations,
X. Wang, G. E. W. Bauer, and A. Hoffmann,
Phys. Rev. B **73**, 054436 (2006).

Curriculum Vitae

Born on 25 June 1979, in Chongqing, China.

September 1992 to July 1998: *Bashu High School*, Chongqing, China. He obtained various prizes in the *National Olympiad of Physics/Mathematics/Chemistry* for high school students. But none of them was the first prize. Consequently he decided to pursue more science.

September 1998 to July 2002: *Nanjing University*, Nanjing, China. He obtained the *Bachelor of Science* in the specialization of theoretical physics with thesis titled *Coexistence of Superconductivity and Magnetism in metals,* under the supervision of Prof. Jun Li in the group led by Prof. Changde Gong. He was the recipient of *People Scholarship* in 1999 and 2001, and the *Excellent Graduate Award* in 2002. Meanwhile, he was a cofounder of a student society, *Pivot*, which just celebrated the 10th anniversary.

September 2002 to September 2004: *Institute for Theoretical Physics, Utrehct University*, the Netherlands. He obtained the *Master of Science* degree with thesis *BEC-BCS Crossover in an Atomic Fermi Gas* under the direct supervision of Prof. Henk T. C. Stoof and Dr. Giovanni Maria Falco. In August 2003, he participated the *Advanced Summer School of Mathematical Physics* at *Bogoliubov Laboratory of Theoretical Physics* in Dubna (Russia).

September 2004 to September 2008: *Kavli Institute of Nanoscience, Technische Universiteit Delft*, the Netherlands. He was a PhD candidate under the supervision of Prof. Gerrit E. W. Bauer, in the group of theoretical physics. He attended lots of conference and workshops worldwide, including the *MMM* conference at San Jose in 2005 and the *International Conference of Magnetism* at Kyoto in 2006.